Université de Montréal

Morphologic Evaluation of Ruptured Abdominal Aortic Aneurysm by 3D Modeling

par

An Tang, MD

Département de radiologie

Faculté de médecine

Mémoire présenté à la Faculté de médecine
en vue de l'obtention du grade de maîtrise en sciences biomédicales
option recherche clinique biomédicale

Août 2012

Université de Montréal
Faculté des études supérieures et postdoctorales

Ce mémoire intitulé :

Morphologic Evaluation of Ruptured Abdominal Aortic Aneurysm by 3D Modeling

Présenté par :
An Tang

a été évalué par un jury composé des personnes suivantes :

Isabelle Trop, MD, MPH, président-rapporteur
Gilles Soulez, MD, MSc, directeur de recherche
Claude Kauffmann, PhD, co-directeur
Rafik Ghali, MD, membre du jury

Résumé

Un anévrysme de l'aorte abdominale (AAA) est défini par une dilatation de plus de 50% par rapport au diamètre normal. La méthode standard et largement répandue pour mesurer la dimension d'un AAA consiste à mesurer le diamètre maximal (Dmax). Présentement, les principaux prédicteurs de risque de rupture sont le Dmax, le sexe et le taux d'expansion d'un anévrysme.

Toutefois, le Dmax a certaines limitations. Des AAAs de formes très différentes peuvent avoir le même diamètre maximal. Le Dmax manque de sensibilité pour détecter le risque de rupture, en particulier pour les petits anévrysmes. Par conséquent, il y a un besoin d'évaluer de manière spécifique et individuelle la susceptibilité de rupture d'un AAA.

Nous présentons le concept et le flux de travail d'un logiciel de segmentation des AAAs développé à notre institution. Nous décrivons les étapes antérieures de validation: évaluation de la reproductibilité du Dmax manuel, comparaison de Dmax par logiciel avec Dmax manuel, validation de la reproductibilité du Dmax et volume par logiciel dans des études transversale et longitudinale pour la détection de croissance et évaluation de la reproductibilité de mesures sur angiographie par tomodensitométrie et en présence d'endoprothèse.

En vue d'identifier de nouveaux paramètres géométrique associés avec le risque de rupture, nous avons réalisé une étude cas-témoin comparant 63 cas avec AAA rompu ou symptomatique et 94 contrôles avec AAA asymptomatique. Une analyse de régression logistique univariée a identifié 14 indices géométriques associés avec une rupture de AAA. Dans l'analyse de régression logistique multivariée, en ajustant pour le Dmax et le sexe, les AAA avec un bombement plus haut situé et une surface moyenne plus élevée étaient associés à une rupture.

Nos résultats préliminaires suggèrent que l'inclusion d'indices géométriques obtenus par segmentation de tomodensitométrie tend à améliorer la classification de AAA avec un risque de rupture par rapport à un modèle traditionnel seulement basé sur le Dmax et le sexe.

De plus larges études longitudinales sont requises pour vérifier la validité du modèle proposé. Des simulations de flux et biomécaniques devraient être envisagées pour améliorer la prédiction du risque de rupture basée sur la modélisation d'anévrysmes.

Mots-clés : Aorte, Anévrysme de l'aorte abdominale, analyse quantitative, diamètre, volume, imagerie tridimensionnelle, segmentation, angiographie par tomodensitométrie, humains

Abstract

Abdominal aortic aneurysm (AAA) is defined as a dilatation of the abdominal aorta exceeding the normal diameter by more than 50%. The standard and widely used approach to assess AAA size is by measuring the maximal diameter (Dmax). Currently, the main predictors of rupture risk are the Dmax, sex, and the expansion rate of the aneurysm.

Yet, Dmax has some limitations. AAAs of vastly different shapes may have the same maximal diameter. Dmax lacks sensitivity for rupture risk, especially among smaller AAAs. Thus, there is a need to evaluate the susceptibility of a given AAA to rupture on a patient-specific basis.

We present the design concept and workflow of the AAA segmentation software developed at our institution. We describe the previous validation steps in which we evaluated the reproducibility of manual Dmax, compared software Dmax against manual Dmax, validated reproducibility of software Dmax and volume in cross-sectional and longitudinal studies for detection of AAA growth, and evaluated the reproducibility of software measurements in unenhanced computed tomographic angiography (CTA) and in the presence of stent-graft.

In order to define new geometric features associated with rupture, we performed a case-control study in which we compared 63 cases with ruptured or symptomatic AAA and 94 controls with asymptomatic AAA. Univariate logistic regression analysis revealed 14 geometric indices associated with AAA rupture. In the multivariate logistic regression analysis, adjusting for Dmax and sex, the AAA with a higher bulge location and higher mean averaged surface area were associated with AAA rupture.

Our preliminary results suggest that incorporating geometrical indices obtained by segmentation of CT shows a trend toward improvement of the classification accuracy of AAA with high rupture risk at CT over a traditional model based on Dmax and sex alone.

Larger longitudinal studies are needed to verify the validity of the proposed model. Addition of flow and biomechanical simulations should be investigated to improve rupture risk prediction based on AAA modeling.

Keywords : Aorta, Aortic Rupture, Abdominal Aortic Aneurysm, Quantitative Analysis, Diameter, Volume, Three-Dimensional Imaging, Segmentation, CT angiography, Humans

Table of Contents

Résumé i
Abstract iii
Table of Contents v
List of Tables viii
List of Figures ix
List of Appendix xi
List of Abbreviations and Symbols xii
Dedication xiii
Acknowledgements xiv

1 Introduction 1

1.1 The Size Problem in Vascular Surgery 2
1.2 Trends in Abdominal Aortic Aneurysm Treatment 5
1.3 3D Modeling 7
1.4 Thesis Structure 10

2 Abdominal Aortic Aneurysms 12

2.1 Definition 12
2.2 Epidemiology 13
2.3 Growth 14
2.4 Rupture Risk and Outcome 16
2.5 Screening and Surveillance 18
2.6 Diagnosis of unruptured and ruptured AAA 21
2.7 Management of AAA 26
2.7.1 Current Thresholds for Treatment 27
2.7.2 Medical Treatment 27
2.7.3 Surgical Treatment 27
2.7.4 Endovascular Aortic Repair 29
2.7.5 Results of Randomized Controlled Trials 33

2.8 3D Modeling 37
2.8.1 Geometrical parameters 37
2.8.2 Biomechanical Simulations 39
2.8.3 Mechanical properties 42

3 Segmentation Software 43
3.1 Software Concept 44
3.2 Segmentation Workflow 51
3.3 Software Validation Strategy 55
3.4 Reproducibility of Manual Dmax Measurements 56
3.5 Clinical Validation of Software vs. Manual Dmax Measurements 61
3.6 Reproducibility and Accuracy of Software Dmax and Volume Growth Measurements 65
3.7 Impact of Contrast Injection and Stent-graft Implantation on Volume Reproducibility 69
3.8 Geometrical Indices 72
3.9 Potential Clinical Applications of Segmentation Software 73

4 Morphologic Evaluation of Ruptured and Unruptured AAA by 3D Modeling 74
4.1 Abstract 74
4.2 Introduction 75
4.1.1 Hypothesis 76
4.1.2 Aim 76
4.3 Materials and Methods 76
4.3.1 Study Design 76
4.3.2 Study Population 77
4.3.3 Data Collection 78
4.3.4 CT Imaging Techniques 78
4.3.5 Segmentation Methods 79
4.3.6 Size and Shape Indices 81
4.3.7 Statistical analysis 81
4.4 Results 82
4.4.1 Clinical Characteristics 82

4.4.2 Geometric Characteristics 84
4.4.3 Results of Univariate Logistic Regression Analysis 85
4.4.4 Results of Multivariable Logistic Regression Analysis 85
4.4.5 Classification Accuracy 86
4.4.6 ROC Curve Analysis 87
4.5 Discussion 87
4.5.1 Main Findings 87
4.5.2 Interpretation of Results 89
4.5.3 Clinical Implications 90
4.5.4 Limitations 90
4.5.6 Conclusion 91

5 Conclusion **92**
5.1 Closing Words 92
5.2 Future Work 94

Bibliography **95**

Appendix **cix**

List of Tables

Table 1.1: Summary of imaging findings on CT indicating completed, impending or contained AAA rupture. 22

Table 2.1: Summary of randomized trials comparing AAA treatment: endovascular aortic repair (EVAR), open aortic repair (OAR), or surveillance. 35

Table 2.2: Features expected from a modern AAA segmentation solution 44

Table 3.1: Intraclass correlation coefficient by diameter measurement method at baseline and follow-up (102). 59

Table 3.2: Inter-observer reproducibility of manual Dmax measurements (36). 62

Table 3.3: Intra-observer reproducibility of software and manual Dmax measurements (36). 62

Table 3.4: Intra- and inter-observer reproducibility Dmax and volume growth measurements (36). 66

Table 4.1: Patient characteristics in case and control groups (157 subjects) 83

Table 4.2: Geometric characteristics of AAA in case and control groups (157 subjects) ... 84

Table 4.3: Results of multivariate logistic regression analysis 85

Table A.1: One-dimensional size indices cxi

Table A.2: Two-dimensional size indices cxii

Table A.3: Three-dimensional size indices cxii

Table A.4: Three-dimensional shape indices cxii

Table A.5: Second order curvature-based indices cxiii

List of Figures

Figure 1.1: Qualitative description of normal aorta and AAA shapes. 2
Figure 1.2: Discrepancies between diameter and volume growth in two AAAs. 4
Figure 1.3: Comparison of 2 AAAs with similar maximal diameter. 5
Figure 1.4: Color-coded parametric maps overlaid on AAA outer wall mesh. 8
Figure 1.5: Roadmap. 10
Figure 2.1: 3D model of an AAA in a 79-year-old female. 13
Figure 2.2: Three-dimensional mesh rendering of AAA at baseline and follow-up. 15
Figure 2.3: Before/after rupture comparison in 78-year-old woman with AAA. 16
Figure 2.4: AAA surveillance on abdominal ultrasound. 19
Figure 2.5: AAA rupture diagnosis on axial CT angiography. 23
Figure 2.6: Signs of AAA rupture on CT in different patients. 25
Figure 2.7: AAA measurements for stent graft sizing. 26
Figure 2.8: Schematic of open surgical repair. 28
Figure 2.9: Schematic of endovascular aortic repair (EVAR). 29
Figure 2.10: Fenestrated endovascular aortic repair (FEVAR). 32
Figure 2.11: Finite volume analysis (FVA). 41
Figure 2.12: 3D rendering showing AAA wall shear stress simulation at peak velocity. Flow direction is indicated by a white arrow. (Image courtesy of Florian Joly. Generated in Fluent, Ansys). 42
Figure 3.1: Manual segmentation workflow on axial images. 43
Figure 3.2: Axial unenhanced CT showing low contrast situation. 48
Figure 3.3: AAA model in a 72-year-old man with a Dmax of 6.97 cm. 50
Figure 3.4: Overview of software interaction. 51
Figure 3.5: Radial and longitudinal stretch views for segmentation. 53
Figure 3.6: AAA model in a 72-year-old man with a Dmax of 6.97 cm. 54
Figure 3.7: Sequential approach to double-oblique (DO) reformation method. 58
Figure 3.8: Inter-reader agreement. 63
Figure 3.9: 3D representation of AAA growth over time. 66

Figure 3.10: Inter-reader agreement for volume measurements. 67
Figure 3.11: 3D renderings of AAA models. 70
Figure 4.1: Study Flowchart. 78
Figure 4.2: 3D volume rendering with parametric maps on model overlay based on a contrast-enhanced CT in a patient with ruptured AAA. 80
Figure 4.3: ROC analysis. 87
Figure A.1. Definition of 1 D geometrical indices, modified from Martufi *et al*. (91). cx

List of Appendices

Appendix 1. Mathematical definitions of geometric indices cix

Appendix 2. Manuscript 1: Reproducibility of AAA diameter measurement and growth. cxiv

Appendix 3. Manuscript 2: Clinical validation of a software for quantitative follow-up of AAA maximal diameter and growth by CTA. cxxiv

Appendix 4. Manuscript 3: Measurements and detection of abdominal aortic aneurysm growth: Accuracy and reproducibility of a segmentation software. cxxxii

List of Abbreviations and Symbols

3D	=	Three-dimensional
AAA	=	Abdominal aortic aneurysm
AAVS	=	American Association for Vascular Surgery
ANOVA	=	Analysis of variance
AUC	=	Area under the ROC curve
CHUM	=	Centre Hospitalier de l'Université de Montréal
CI	=	Confidence interval
CSD	=	Computational fluid dynamics
CT	=	Computed tomography
CTA	=	Computed tomography angiography
Dmax	=	Maximal diameter
EVAR	=	Endovascular aortic repair
eEVAR	=	Emergency endovascular aortic repair
FEA	=	Finite element analysis
FEVAR	=	Fenestrated endovascular aortic repair
FSI	=	Fluid structure interaction
ICC	=	Intraclass correlation coefficient
ILT	=	Intraluminal thrombus
MDCT	=	Multidetector computed tomography
NPV	=	Negative predictive value
OR	=	Odds ratio
PPV	=	Positive predictive value
PWS	=	Peak wall stress
ROC	=	Receiver operating characteristic
SD	=	Standard deviation
SVS	=	Society for Vascular Surgery

For my father and mother
who made so many sacrifices for me

Acknowledgments

I feel tremendously privileged to have had the opportunity to work with Dr. Gilles Soulez and Dr. Claude Kauffmann on this research program. I would like to thank Gilles, whose generosity in time and experience is only exceeded by his kindness, and who has been my mentor for the past ten years. He showed me the way by taking time to review my manuscripts and research proposals despite his numerous commitments. He is leading by example and always cheerfully planning the next study.

I am grateful to Dr. Claude Kauffmann for developing the software and conceptual tools necessary to perform these studies together. Claude has always had a vision of preserving the richness of anatomical information from multiplanar imaging. Also, he was always eager to immerse himself in the technical intricacies of the segmentation process. Without his help, this study would not have been possible. The majority of renderings in these pages are the result of his artistry. These diagrams also mirror the passion we share for visual display of quantitative information.

I would like to acknowledge the essential contribution of Dr. Stéphane Elkouri, vascular surgeon at CHUM, and Dr. Oren Steinmetz, vascular surgeon at McGill, who identified the AAA surgical candidates eligible for this study.

I am grateful to Dr. Trop and Dr. Ghali for serving as jury members to my Master's thesis.

Attending the courses on the university campus for my formal training required support from my abdominal section chief. Special thanks to Dr. Jean-Sébastien Billiard for outstanding support and for allowing me to balance the requirements of a master's degree with those of a full clinical workload.

I addition, I would like to thank Dr. Miguel Chagnon, biostatistician at University of Montreal, for his expertise and judgment.

I would like to thank four wonderful residents and medical students: Sophie Tremblay-Paquet, Laurie Cloutier-Gill, Stéphanie Lam, and Florence Morin-Roy for their precious help in data collection and in AAA segmentation. They were very generous with their time and commitment.

Finally, I would like to thank my parents, Tang Quoc Kiet and Nguyen Thi Hon, for their love and support. Three decades ago, my parents made the bold move to leave Vietnam as boat people, hoping for a better future for their son. In the following years, they have made countless sacrifices for me, and have provided me with support and encouragement. This dissertation is dedicated to them.

1 Introduction

This dissertation introduces a new software approach to describe the morphology of abdominal aortic aneurysms (AAA). Modern multiplanar imaging methods such as computed tomography angiography (CTA) provide a vast data set depicting human anatomy with high resolution. Once loaded in post-processing workstations, this data set can be viewed in orthogonal, oblique or curved planes, displayed as maximum intensity projections, or volume rendered with realistic color palettes, surface shading and lighting.

Despite the sophistication of modern imaging techniques, the geometry of AAA is often summarized qualitatively in reports according to its shape ("fusiform" or "saccular"), its superior extension above or below renal arteries, and its inferior extension to the iliac arteries. The maximum diameter (Dmax) is often the only objective quantitative measurement reported. For surgical planning, additional length, diameter and angle measurements are also reported.

The root of the problem is not missing data acquisition or insufficient visualization capabilities. Instead, the problem is access to existing, but unreported information. To accurately describe the morphology of AAA in terms of objective metrics, an intermediate step must first be accomplished: the boundaries of its outer wall and its lumen must first be delineated. This process is called segmentation. The price to pay is additional work to collect geometric information. In the process, we will generate a three-dimensional model representing the AAA wall, thrombus, and lumen.

Of course simply tracing the contour of AAA wall and lumen on each individual image is not a complete solution to the modeling problem. A manual approach may be feasible for a proof of concept on a limited number of cases. However, to scale this method to a large database of AAA cases either for research purpose or eventually for clinical purpose, segmentation automation is an essential ingredient. The idea is to find the right balance between user interaction, automated software tasks and graphic display to complete the task in a reasonable time.

1.1 The Size Problem in Vascular Surgery

The aorta is the largest artery coursing from the thorax and extending down to the abdomen, where it bifurcates into the common iliac arteries. The normal diameter of the aorta is approximately 2 cm (1). An abdominal aortic aneurysm (AAA) is defined as a dilatation of the aorta by a diameter of 3 cm or more (2). While AAAs may affect any segment of the aorta, most involve the segment below the renal arteries. AAAs may be qualitatively described as *fusiform* if they maintain a cylindrical shape or *saccular* if they are spherical in shape (Figure 1.1).

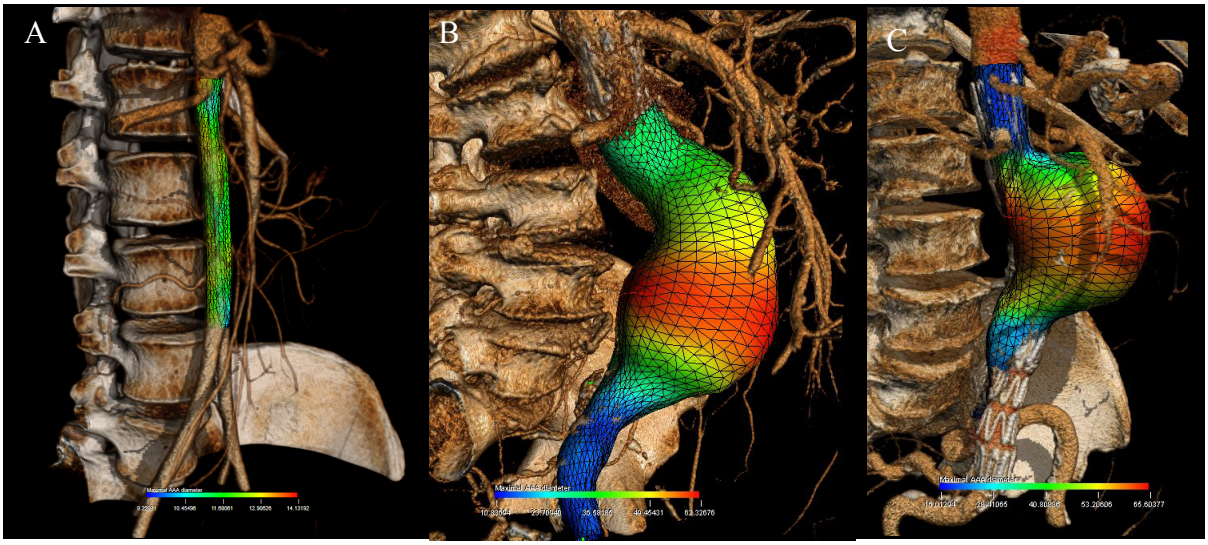

Figure 1.1: Qualitative description of normal aorta and AAA shapes.
(A) Normal aorta. (B) Fusiform AAA. (C) Saccular AAA.

The majority of AAAs are true aneurysms that involve all three layers of the arterial wall (intima, media, and adventitia). Pseudoaneurysms (or false aneurysms) may also occur, which are characterized by a discontinuity in the inner layers of the arterial wall and is only contained by the adventitia or surrounding soft tissues.

AAAs of vastly different shapes may have the same maximal diameter. Furthermore, although growth occurs in three dimensions, it is a well-entrenched practice to report the maximal diameter (Dmax), a one-dimensional measure, as a surrogate measure of AAA

size. The main predictors of rupture risk are the maximal diameter (Dmax) and the expansion rate of the aneurysm.

This practice of categorizing AAAs according to their Dmax has been widely used in randomized controlled trials. For instance, to address the uncertainty about whether prophylactic repair is the best management for smaller symptomless aneurysms of 4.0 - 5.9 cm in diameter, the United Kingdom Small Aneurysm Trial randomly assigned 1090 patients to undergo early elective open surgery or ultrasonographic surveillance and followed them for a mean of 4.6 years (3). The results did not support a policy of open surgical repair for AAAs of this size range.

Whereas studies support watchful surveillance of small AAAs (<5.5 cm), randomized clinical trials suggest that the risk of AAA rupture warrants intervention when the maximal diameter reaches 5.5 cm (4, 5).

Based on the rupture risk, mortality rate in elective procedure and life expectancy of the patient, the American Association for Vascular Surgery (AAVS) in association with the Society for Vascular Surgery (SVS) have issued recommendations regarding AAA treatment (6). The main indications for a procedure are Dmax ≥ 5.5 cm in men, ≥ 4.5-5.0 cm in women, rapid expansion > 1cm/year, or symptomatic AAA. The different size threshold for men and women reflect the higher risk of rupture among women.

For larger AAAs, the annual rupture risk of 6 to 7 cm aneurysm is 10 to 20% (7).

There are several advantages to using Dmax. First, it is practical: Dmax is widely used, validated, and can be measured and compared with different imaging modalities (ultrasound, computed tomography, magnetic resonance imaging). Second, it is useful: in a large prospective observational study of large AAAs at least 5.5 cm in diameter, Dmax was the strongest predictor of rupture (8).

Yet, Dmax has a major limitation: its lack of sensitivity for rupture risk, especially among smaller AAAs (9). The rupture rate of AAAs < 5 cm was 12.8% (34/265) according to an autopsy study by Darling *et al*. (10). However, the mean risk of rupture of aneurysms of 4.0 - 5.5 cm in diameter was deemed to be lower, in the range of 1.0% per year, according to the United Kingdom Small Aneurysm Trial, in which study participants were randomised to early elective surgery or ultrasonographic surveillance (3). This estimate was

supported by a population-based study of patients with AAAs followed by ultrasound, which found an estimated rupture risk of 0% per year (95% confidence interval [CI], 0%-5%) when less than 4.00 cm, 1.0% per year (95% CI, 0%-5%) when 4.00 to 4.99 cm, and 11% per year (95% CI, 1%-21%) when 5.00 to 5.99 cm (11).

Clearly, these numbers indicate a limitation to a "one-size-fits-all" approach to selecting patients at higher risk for rupture and highlight the need for evaluating the susceptibility of a given AAA to rupture on a patient-specific basis (Figure 1.2). The goal of a custom-tailored approach would be to improve the clinical management of these patients.

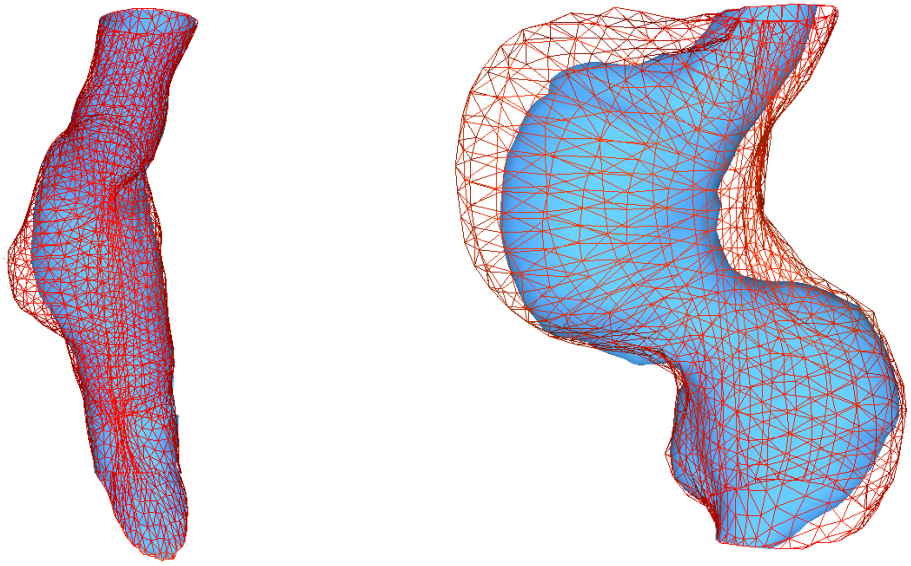

Figure 1.2: Discrepancies between diameter and volume growth in two AAAs.
Baseline mesh is delineated in blue and follow-up mesh in red. (A) Diameter grows by 18% due to focal bulge, but volume grows by only 5%. (B) In a different patient, the diameter also increases by 18%, but this is accompanied by a 45% volume increase due to global growth.

In addition, two AAAs may have a similar Dmax, but markedly different geometries (Figure 1.3). The implied observation is that these aneurysms may have different rupture risks by virtue of different volumes, shapes, thrombus thickness and presumably different wall stress.

In summary, Dmax is a tried and true method for predicting rupture risk. Dmax thresholds have been used to determine rupture risk in clinical trials and are widely used in clinical practice to stratify patient risk. However, Dmax should not be seen as an end in itself, but as a surrogate measure.

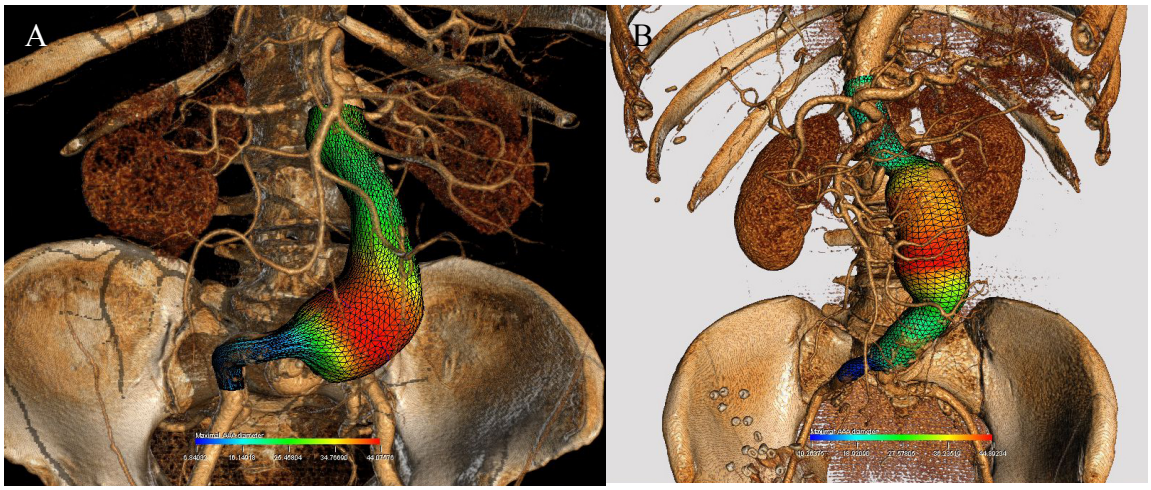

Figure 1.3: Comparison of 2 AAAs with similar maximal diameter.
(A) Asymmetrical, saccular, and curved AAA. (B) Relatively symmetrical, fusiform, and angulated AAA.

1.2 Trends in Abdominal Aortic Aneurysm Treatment

AAA open surgical repair was first performed in 1951 by Dubost *et al*. (12). In 1952, Michael de Bakey and Denton Cooley were the first to use a homograft in repairing a large aneurysm of the thoraco-abdominal aorta (13). With the aid of textile engineers, surgical innovators experimented with synthetic tube grafts. Eventually, Dacron polyester proved superior to other fabrics (14). Open surgical repair is performed by a vascular surgeon and requires a laparotomy. The aorta is clamped and a graft is sewn to act as a bridge for blood flow, thus preventing arterial pressure to further expand the native AAA wall.

Minimally invasive endovascular aneurysm repair was first reported in 1986 (15). The concept is to reline, rather than to remove, the diseased portion of the aorta to achieve a more physiological repair. By preserving the integrity of the aneurysmal wall, blood loss and trauma to surrounding tissues are minimized. An interventional radiologist and/or a vascular surgeon perform this procedure. Incisions are first made at the groin to insert catheters via the femoral arteries to the AAA. Using fluoroscopy, catheters and guide wires are positioned in the aorta and a stent graft made of a metallic stent covered with a prosthetic fabric is deployed in the AAA. Endovascular aortic repair (EVAR) eliminates the need to perform a laparotomy and clamp the aorta during the procedure. This reduces the hemodynamic stress and is most commonly considered in patients at increased surgical risk.

Technical success of more than 95% and perioperative mortality rates between 1 and 2% are reported (16, 17). In randomized studies, lower perioperative mortality and morbidity rates have been reported after EVAR as compared with open surgical repair (2.1-4 versus 5.7-7%) (18, 19) even though mid term and long term survival rate following EVAR and open repair are not different (17, 20, 21). The main limitations of EVAR are the durability of aneurysm exclusion and the occurrence of endoleaks (leakage of blood between the graft and AAA) (22).

In the setting of ruptured AAAs, emergency EVAR (eEVAR) has been proposed by Yusuf *et al*. (23). Its application requires overcoming additional practical and logistical barriers: the patient must be stable during the anatomical CT imaging required prior to EVAR and the hospital must provide coverage of interventional radiology and vascular surgery services (24).

EVAR cannot be performed on everyone. The patient's anatomy must fit the graft. Ideal characteristics of an AAA for EVAR require a complete seal at the proximal (infra-renal aorta) and distal (iliac arteries) landing zones of the stent graft. The proximal neck, defined as the healthy aortic portion (neck) between the lower renal artery and the aneurysm, should not be dilated, have a minimal length (10-15 mm), low angulation and minimal thrombus infiltration (25). Regarding iliac arteries, high angulation should also be avoided and have a minimal diameter to accommodate the delivery device. The distal

portion of the graft is preferentially deployed in the common iliac artery if there is a landing zone above the origin of the internal iliac arteries. If not, the internal iliac artery can be covered or embolized and the stent extended into the external iliac artery. Recently, more complex EVAR procedures with short or angulated neck involving the preservation of renal or digestive arteries by fenestrated stent grafts or internal iliac arteries by branched iliac stent grafts were performed (26-28).

In summary, open surgical repair and EVAR are two treatment options to large AAA (≥5.5 cm in diameter). Open surgical requires an abdominal incision. EVAR is less invasive, has lower perioperative mortality and morbidity rates, but no mid term and long term improvement in survival rate. To determine anatomical suitability to EVAR, a CT-scan must be performed to evaluate the candidate's arterial anatomy.

1.3 3D Modeling

Our proposed solution to the size problem in vascular surgery exploits the need to perform a CT-scan for surgical planning of patients' anatomy. Nowadays, data is acquired with high resolution and nearly isotropic voxels suitable for multiplanar reconstructions.

With modern post-processing methods, it is possible to perform AAA segmentation. In addition to exquisite 3D rendering, segmentation allows calculation of AAA volumetry. Given the three-dimensional nature of AAA growth, Prinssen *et al*. have shown that volumetric assessment was more sensitive than diameter measurement in the detection of changes in aneurysm size (29).

Recently, using a semiautomated segmentation method, we have confirmed that volume measurements were more sensitive than Dmax to detect AAA growth while providing an equivalent and high reproducibility (30).

An indirect benefit of performing segmentation for volumetry is the ability to generate a model of the AAA outer wall, thrombus, and lumen. From a clinical perspective, this allows visual depiction of the geometric diversity of AAAs and reveals the anatomical relationship with renal and iliac vessels that are critical for EVAR planning. From a

research perspective, the AAA mesh is a prerequisite for extracting geometric parameters and performing biomechanical simulations.

Potential discrepancies may exist between Dmax and volume progression. A diameter increase is necessarily accompanied by a volume increase, but the converse is not true. Figure 1.2 shows that a volume increase can theoretically occur with minimal diameter increase. This highlights the potential need to report both diameter and volume growth.

The main limitation of AAA volumetry is the absence of an absolute gold standard for the measurement of the aneurysm sac volume. Additional limitations include the time-consuming nature of segmentation methods and the current inability to co-register interval studies.

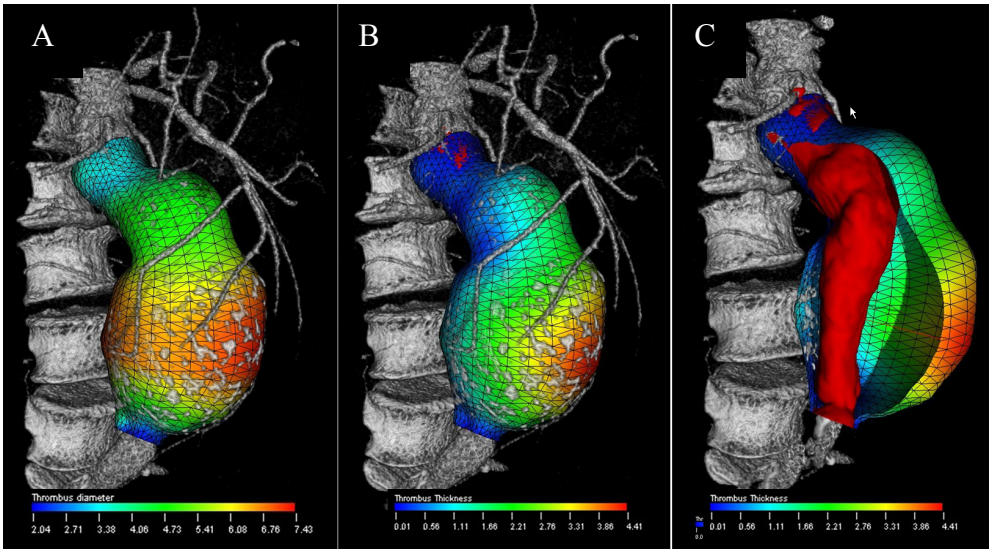

Figure 1.4: Color-coded parametric maps overlaid on AAA outer wall mesh.
(A) AAA surface model with color-coded Dmax values at each location of the AAA wall. (B) Color-coded thrombus thickness map, (C) illustration of the thrombus thickness computed as the closest distance between the outer aneurysm wall and the lumen represented in red (31).

Once the AAA is segmented and the outer wall mesh generated to compute the aneurysmal volume, this surface can also be used to display color-coded geometric parameters such as the local diameter (mm) (Figure 1.4). Thus, Dmax can be visually depicted as a surrogate measure of rupture risk.

Additional morphological features have been proposed to predict the rupture risk. Stenbaek *et al*. suggested that thrombus growth may be a better predictor of AAA rupture than increase in maximal diameter (32). While the effect of intraluminal thrombus on rupture risk remains controversial (33), there is no doubt that the segmentation of a thrombus remains essential to simulate the peak wall stress.

Ultimately, rupture occurs when the mechanical stresses (expressed in force/unit area) exceed wall strength or reaches wall failure threshold. Thus, a rupture prediction index may be mapped on the AAA outer wall to indicate areas with higher wall stress/strength ratio (9). The basic principles in terms of computational modeling of AAA will be discussed later in this thesis.

In summary, the high resolution, nearly isotropic voxels, and volumetric nature of CT data is suitable for multi-planar and three-dimensional reconstructions of AAA anatomy. With modern post-processing methods, it is possible to perform AAA segmentation. This may become clinically useful since volume is emerging as a more sensitive measure of growth than Dmax. While outer wall and thrombus segmentation require additional work to generate a 3D model, this is rewarded by the possibility of extracting quantitative geometric information and performing wall stress simulations to estimate an individual rupture risk.

1.4 Thesis Structure

I have written this master's thesis in a manner that will be accessible to a broad range of readers, including medical students, general radiologists, vascular surgeons, software engineers and computer graphics researchers.

Figure 1.5 is a roadmap of the territory covered in the various chapters. Medical students should read this document sequentially. Radiologists will be most interested in the images and 3D renderings throughout the text, and may begin their exploration by approaching this master's thesis like a photography book. Vascular surgeons and interventional radiologists with intimate knowledge of AAA may wish to jump directly to Chapter 3. The collaborators to our previous papers may focus on Chapter 4 and 5.

Finally, the mathematically inclined will be most interested in Appendix 1, which provide the definitions for the 1D, 2D and 3D size indices and the 3D shape indices used in the study described in Chapter 4.

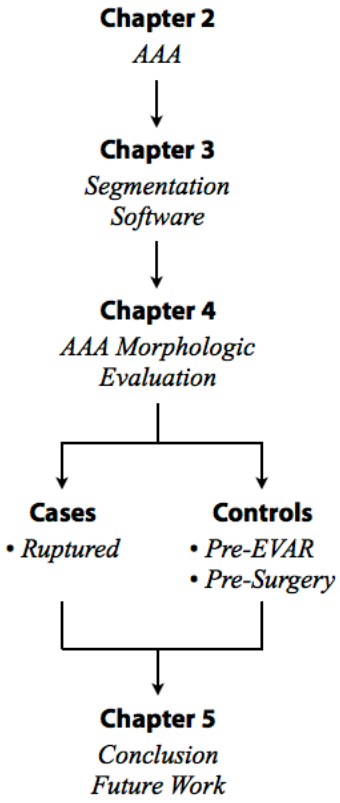

Figure 1.5: Roadmap.

Chapters Descriptions

• Chapter 2 introduces abdominal aortic aneurysms and reviews the epidemiology, rupture risk, imaging methods, rationale for treatment and treatment options. It contains a succinct overview of computational fluid dynamics methods that require 3D modeling as a prerequisite to perform simulations.

• Chapter 3 presents the design concept and workflow of the AAA segmentation software developed at our institution. It also describes the orderly validation steps completed over the past 3 years, from reproducibility of manual maximal diameter (Dmax) measurements, validation of software Dmax against the manual reference standard, reproducibility of software Dmax and volume measurements in a cross-sectional study, in a longitudinal study for detection of AAA growth, reproducibility of software measurements in unenhanced CTA and in the presence of stent-graft. The last section describes the geometric indices that can be computed and the potential clinical benefits from this software.

• Chapter 4 applies segmentation and geometrical indices developed previously to a case-control study that compares ruptured and unruptured AAAs. This study is the result of collaborative work between radiologists and vascular surgeons from two universities: Université de Montréal and McGill University.

• Chapter 5 summarizes the lessons learned, the challenges ahead and points to future research directions.

2 Abdominal Aortic Aneurysms

2.1 Definition

The normal aortic diameter varies depending on age and sex. According to Ouriel *et al*. (1), the mean diameter of normal aorta, as measured by abdominal CT, was 2.1 ± 0.05 cm at the infra-renal level, and 2.5 ± 0.05 cm at the supra-celiac level. These values varied according to sex: 2.3 ± 0.1 cm and 2.6 ± 0.1 cm respectively for men, and 1.9 ± 0.1 cm and 2.3 ± 0.1 cm for women. The diameter increased with age at a rate of 0.1 mm/year for both sexes.

Abdominal aortic "ectasia" is defined as a focal dilatation less than 50% the normal diameter, whereas an abdominal aortic aneurysm is defined as a permanent dilatation more than 50% above the expected normal diameter (2) (Figure 2.1).

Small AAA is defined as <5.5 cm in diameter because the risk of rupture is low (3, 34, 35).

AAA morphology is characterized by loss of parallelism of the outer walls, either saccular (20%), or more frequently fusiform (80%).

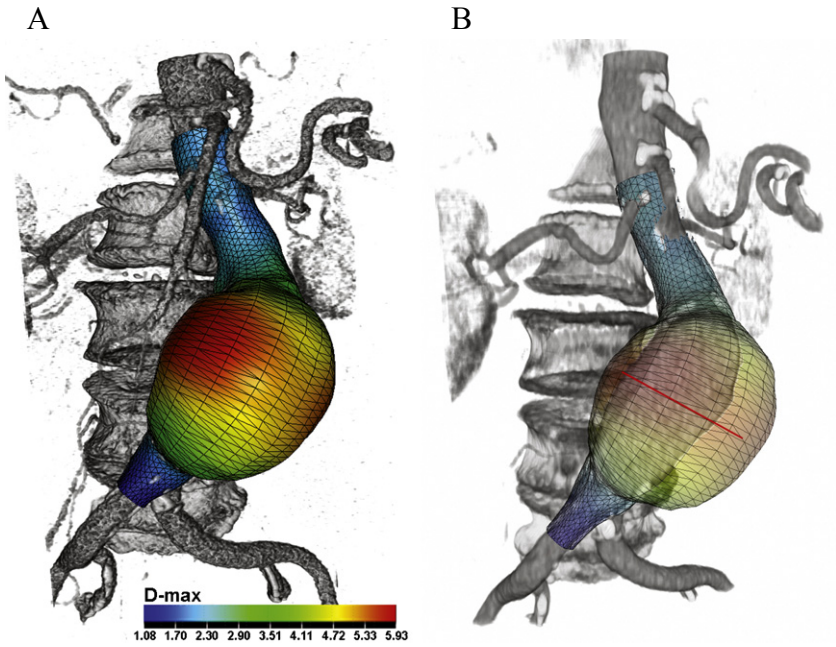

Figure 2.1: 3D model of an AAA in a 79-year-old female.
(A) 3D volume rendering with color-coded diameters: the smallest diameters are represented in blue and the largest in red. (B) The outer wall mesh is semi-translucent and the lumen mesh is revealed underneath. The automatically calculated Dmax is displayed as a red line (36).

2.2 Epidemiology

The prevalence of AAA is three times higher among men than women. The age-related increase in diameter of the infrarenal aorta is more marked in men than in women. The prevalence of aneurysms increases by about 6 percent by decade. Clinically relevant aneurysms (> 4 cm in diameter) are found in about 1 percent of men 55 to 64 years of age, and the prevalence increases by 2 to 4 percent per decade afterwards (37, 38).

Smoking is the strongest independent risk factor: 90 percent of patients with aneurysms have smoked (38). As compared with those who have never smoked, the incidence of aneurysm is increased by a factor of six among those who have smoked for more than 40 years and by a factor of seven among those who have smoked more than 20 cigarettes per day (39).

Additional risk factors include: male sex, age > 75 years, Caucasian race, hypertension, family history, and hyperlipidemia (40).

An etiologic classification of arterial aneurysms is important (2). AAAs are most commonly arteriosclerotic aneurysms. Alternatively, aneurysms may develop as a result of an arterial dissection, and may be associated with cystic medial necrosis, a pathologic process characterized by an accumulation of basophilic substance in the media with cyst-like lesions, which occur in connective tissue disease such as Marfan's syndrome, and Ehlers-Danlos type IV. Inflammatory aneurysms occur in younger patients and may result from retroperitoneal fibrosis, collagen disease, fibromuscular dysplasia, or autoimmune diseases such as rheumatoid arthritis, lupus, Behçet's disease and giant cell arteritis. Infected (mycotic) pseudoaneurysms may result from hematogenous seeding or direct spread from an adjacent vertebral ostemyelitis or from retroperitoneal abscesses.

False aneurysms may result from a trauma. In patients with a history of aortic surgery, an anastomotic aneurysm may result from an infection, arterial wall failure, suture failure, or graft failure.

2.3 Growth

The natural history of AAA growth has been evaluated with serial ultrasound or CT in patients who were not surgical candidates, either because of small size, high surgical risk, or patient refusal (41).

Growth has been studied in terms of Dmax (Figure 2.2), the most commonly used measurement to establish growth rate, rupture risk, and treatment indication. AAA growth in diameter results from forces applied on the arterial wall according to Laplace's law and gradual wall weakening due to decreased elastin concentration, increased metalloproteinase (MMP) and action of proteolytic enzymes produced by macrophages (9).

Two patterns of AAA growth have been observed: accelerating or linear expansion expansion (40, 42). Accelerating (triphasic) growth is characterized by a quiescent phase of long duration, an inflexion where Dmax reaches a threshold (between 45 and 55 mm),

followed by an accelerated growth as the aneurysm enlarges. Linear growth, which is less common, occurs without acceleration.

In addition to a Dmax > 5.5 cm, a "rapid" growth characterized by an expansion rate of 1.0 cm or more within 6 months is often used as an indication for surgery.

Figure 2.2: Three-dimensional mesh rendering of AAA at baseline and follow-up.
The lumen (red), outer wall at baseline (green), and 3 years follow-up (blue) are shown in a 69-year-old man. The Dmax was 58.5 mm at baseline and 74.3 mm at follow-up (27% relative growth). The volume was 202.9 ml at baseline and 327.3 ml at follow-up (61% relative growth). 3D-3D co-registration of baseline and follow-up examinations allow instantaneous volume comparison on the same dataset (30).

2.4 Rupture Risk and Outcome

AAA rupture can be manifested along a continuum extending from impending rupture, contained rupture, intramural hemorrhage, to uncontained retroperitoneal or intraperitoneal blood extravasation (Figure 2.3).

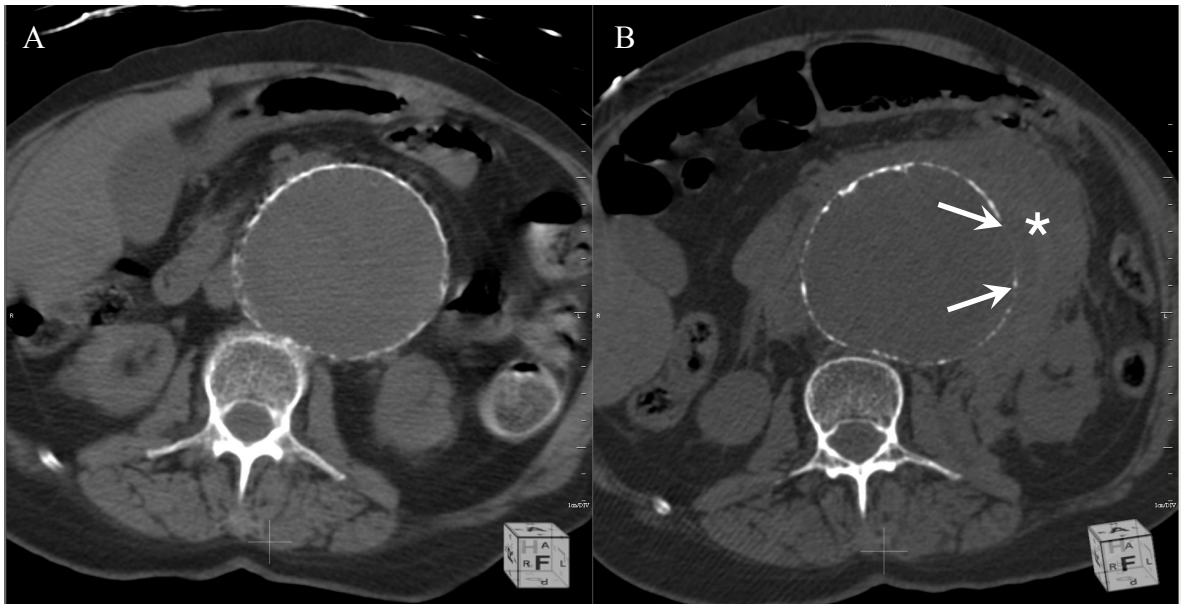

Figure 2.3: Before/after rupture comparison in 78-year-old woman with AAA.
(A) Large unruptured AAA. (B) The same patient presented 5 days later, with signs of AAA rupture: focal gap and displacement of mural calcifications (two arrows) and retroperitoneal hematoma adjacent to the rupture site (asterisk).

The rupture risk of small aneurysms is low, but the natural history of an untreated aneurysm is one of progressive expansion (43). The risk of rupture increases markedly when the Dmax exceeds 5.5 cm. AAA tend to rupture at a lower diameter in women than men, hence the lower threshold (4.5 - 5.0 cm) for treatment.

Among patients with AAA, few die from a ruptured aneurysm; most (66%) will die from another cardiovascular cause (34). However, a ruptured AAA has a grim prognosis, with a 90% mortality rate (9, 44). Death may occur before arrival to the hospital, during

surgical repair or after surgical repair. Since only 10-15% of patients survive an AAA rupture, there is a need to identify predictors of rupture risk (45).

AAA rupture risk increases with larger diameters. A prospective cohort study performed in 47 Veterans Affairs medical centers on 198 patients revealed a 1-year incidence of rupture of 9.4% for AAA 5.5 to 5.9 cm, 10.2% for AAA of 6.0 to 6.9 cm (19.1% for the subgroup of 6.5-6.9 cm), and 32.5% for AAA of 7.0 cm or more (8). The cumulative incidence of probable rupture, stratified by initial AAA diameter, revealed that the proportion of patients with AAA rupture in the ≥ 7.0 cm stratum was significantly higher than the other two strata (both p <0.01).

Similar results were found by Powell *et al*. in their meta-analysis of large AAA not considered for open repair, stratified by size < 6.0 and > 6.0 cm, and sex (46). The pooled rupture rates for the endovascular aneurysm repair unfit for open repair of AAA (EVAR 2) study was 9.7 per 100 person-years for AAA < 6.0 cm and 17.4 per 100 person-years for AAA ≥ 6.0 cm.

It has been suggested that the presence of thrombus within an AAA may increase the risk of rupture (47). Since this initial publication, the effect of intraluminal thrombus on rupture risk remained controversial and debated. The proponents of thrombus as a risk factor of rupture argue that intraluminal thrombus reduces oxygen supply to AAA wall, which leads to cell dysfunction, extracellular matrix degrading factors, and wall weakening (48, 49). Stenbaek *et al*. reported that a rapid increase of thrombus area may be a better predictor of AAA rupture than increase in maximal diameter in a cohort of 67 patients who underwent at least 2 CT examinations (32).

The proponents of a protective role hypothesize that thrombus may reduce and redistribute the stresses in the aortic wall (50), that the incompressibility and isotropic nature of this tissue has a mechanical cushioning effect (51) and reduces peak wall stress (52). Using a numerical method based on fluid solver for flow and solid solver for intraluminal thrombus and wall, Bluestein *et al*. suggested that a well-oriented thrombus generates a channel like geometry with streamlined flow patterns and appears to reduce the stress in the AAA wall significantly (33).

A recent study comparing the geometry of 10 ruptured and 66 unruptured aneurysms favored a protective role for thrombus since they identified lower ratios of intraluminal thrombus volume to aneurysm volume among their ruptured AAA than among unruptured AAA (53).

2.5 Screening and Surveillance

AAAs are not always symptomatic and may be difficult to detect on physical examination. Abdominal palpation does not have the sensitivity nor the specificity of ultrasound in screening for aneurysm (54). Two studies suggest that one-time ultrasound screening of men, at the age of 65, is sufficient to identify nearly all those who are at risk (55, 56). A trial involving 67 800 men in the United Kingdom demonstrated that screening halves the rate of aneurysm-related death within four years, but did not reduce overall mortality (4).

Ultrasound

Once aneurysms are identified, follow-up surveillance with ultrasound is indicated to monitor growth beyond diameter thresholds for surgery (34). In the United Kingdom Small Aneurysm Trial, the proposed screening intervals were 24 months for aneurysms AAA with diameters of 3.5 cm at baseline, 12 months for 4.0 cm, and 6 months for 5.0 cm (3).

Using an abdominal ultrasound probe (curved probe with a frequency range of 3 to 5 MHz) on a fasting patient lying in dorsal decubitus allows detection and measurement of AAA. An anterior approach allows the acquisition of longitudinal and transverse images of the aorta. Even when the aorta is obscured by intra-luminal gas in bowel structures, a left lateral approach may be used to record coronal and transverse images of the aorta. B-mode grayscale images allow detection of mural thrombus and calcifications (Figure 2.4). A color Doppler mode may help improve delineation of the thrombus and lumen. In addition, the pulsed Doppler mode allows assessment of patency of the main arterial branches originating from the aorta (renal arteries, celiac trunk, superior mesenteric artery, inferior mesenteric artery, and common iliac arteries).

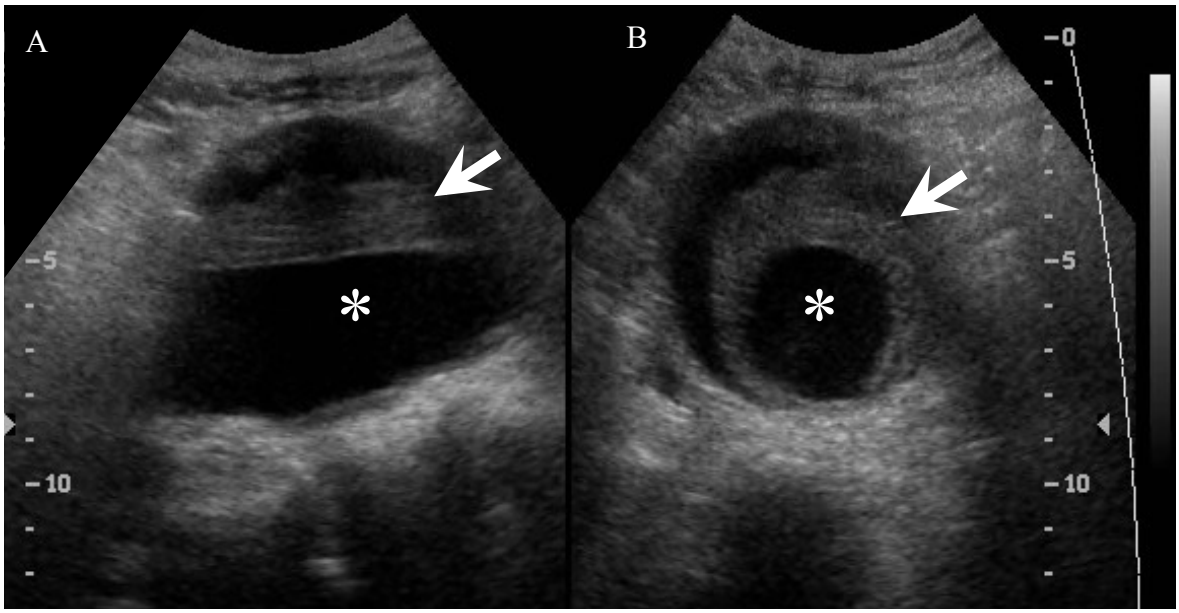

Figure 2.4: AAA surveillance on abdominal ultrasound.
(A) Midline sagittal and (B) transverse images. Lumen is indicated by asterisks and thrombus by arrows.

In a screening setting, ultrasound is the preferred modality due to its non-invasive nature, the absence of radiation, low cost, wide availability, and high patient acceptance. The Canadian Society for Vascular Surgery has issued the following guidelines for screening patients for AAA (57): population based screening program recommended for men 65 to 75 years of age who are candidates for surgery and are willing to participate, individualized investigation with ultrasound of women >65 years old with multiple risk factors for AAA (smoking history, cerebrovascular disease, family history of AAA), yearly abdominal ultrasound recommended for individuals with aneurysm 3.0 to 4.4 cm.

The precision of aortic diameter measurements by ultrasound is considered good. In a study performed on 112 patients by 4 different observers, the inter-observer variability on the measurement of the infra-renal aortic diameter was < 4 mm, and variability was similar for measurements in the antero-posterior and transverse planes (58). Variability was greater for measurements at the renal level than at the aortic bifurcation.

Limitations of ultrasound include its operator-dependence, need for an unobscured acoustic window, and limited utility for identifying an impending rupture or a contained rupture in an acute clinical setting.

Ultrasound vs. Computed Tomography

The accuracy of screening for AAA by ultrasound has been compared with CT. In a study performed on 64 patients with AAA larger than 4.5 cm, the mean difference between ultrasound and CT measurements was 4 mm and the limit of variability was 12 mm (59). More importantly, no false negative ultrasound scans were found using a threshold of 3 cm as abnormal, which justified the use of this modality as a screening and surveillance tool.

However, in the follow-up of patients after endovascular aortic repair (EVAR), CT is the preferred modality. In a retrospective study performed on 125 patients with AAA treated by EVAR who underwent serial ultrasound and CT, the sensitivity and specificity of ultrasound compared to that of CT was 25% and 89% for endoleak detection (60). Considering the significant disagreement in AAA diameter change between the two modalities, CT remains the primary imaging study for endoleak surveillance post-EVAR.

Computed Tomography

In the setting of screening and surveillance of AAA, CT is considered a second-line modality given its higher cost and associated radiation. First-line evaluation of AAAs may occur occasionally in the setting of indicental discovery on CTs performed for other clinical indications, such as CT urography performed for evaluation of hematuria or CT colonography for detection of colorectal polyps (61).

However, in the setting of acute aortic syndrome, CT is the preferred modality for evaluation of a suspected or known AAA and is used to detect signs of rupture and surgical planning. This modality is favored for evaluation of acute aortic syndrome due to its widespread availability, proximity to emergency departments, rapid acquisition, ease of interpretation, and volumetric nature of the dataset that allows multi-planar reconstructions (62).

Magnetic Resonance Imaging

The advent of fast gradient-recalled echo (GRE) sequences allowed rapid acquisition of images during gadolinium bolus injection, similar to CT in quality. However, the longer acquisition time, additional contra-indications, and high cost reduce the availability and convenience of this imaging modality. Therefore, MR imaging is seldom used for evaluation of AAA and only reserved for patients who have a contraindication to CT such as iodinated contrast allergy or renal failure (63).

Computed Tomography vs. Magnetic Resonance Imaging

In a study comparing the accuracy and reliability of AAA diameter measurement based on multidetector CT and magnetic resonance angiography, the intermodality agreement was good to excellent (intraclass correlation coefficient of 0.62 to 0.98) with small differences between methods (range of agreement from -4.1 to 2.1 mm by Bland-Altman analysis) (64).

2.6 Diagnosis of unruptured and ruptured AAA

Symptoms and signs of unruptured AAA

Patients with unruptured abdominal aneurysms may be symptomatic and present with back pain, abdominal pain, and intermittent claudication. Physical examination may reveal a pulsatile abdominal mass, tenderness on aortic palpation, or groin pain (65).

Symptoms of ruptured AAA

Patients with ruptured AAA may present with the triad of hypotension (45%), abdominal pain (72%), and a pulsatile abdominal mass (83%) (66). Additional signs may include hypovolemia or shock due to hemorrhage.

Imaging findings in ruptured AAA

Table 1.1 lists the spectrum of imaging findings that may be observed in completed, impending or contained AAA rupture.

Table 1.1: Summary of imaging findings on CT indicating completed, impending or contained AAA rupture.

Location	Imaging findings	Completed rupture	Impending or contained rupture
Extra-luminal	Contrast extravasation	+++	-
	Retroperitoneal hematoma	++	-
	Intraperitoneal hematoma	++	-
	Periaortic stranding	-	+
Wall	Focal wall discontinuity	+	+
	Intramural hematoma	-	+
	Increased aneurysm size	-	+
	Rapid enlargement rate (≥ 1.0 cm per year)	-	+
	Thrombus fissuration	-	+
	Draped aorta sign	-	+
Luminal	Aortoenteric fistula	-	+
	Aortocaval fistula	-	+

Legend: +++ very specific, ++ specific, + suggestive

The most specific sign of rupture is the demonstration of contrast extravasation beyond the AAA outer wall (Figure 2.5 and 2.6.a). Examples of the most common signs of AAA rupture seen on CT are shown in Figure 2.6.

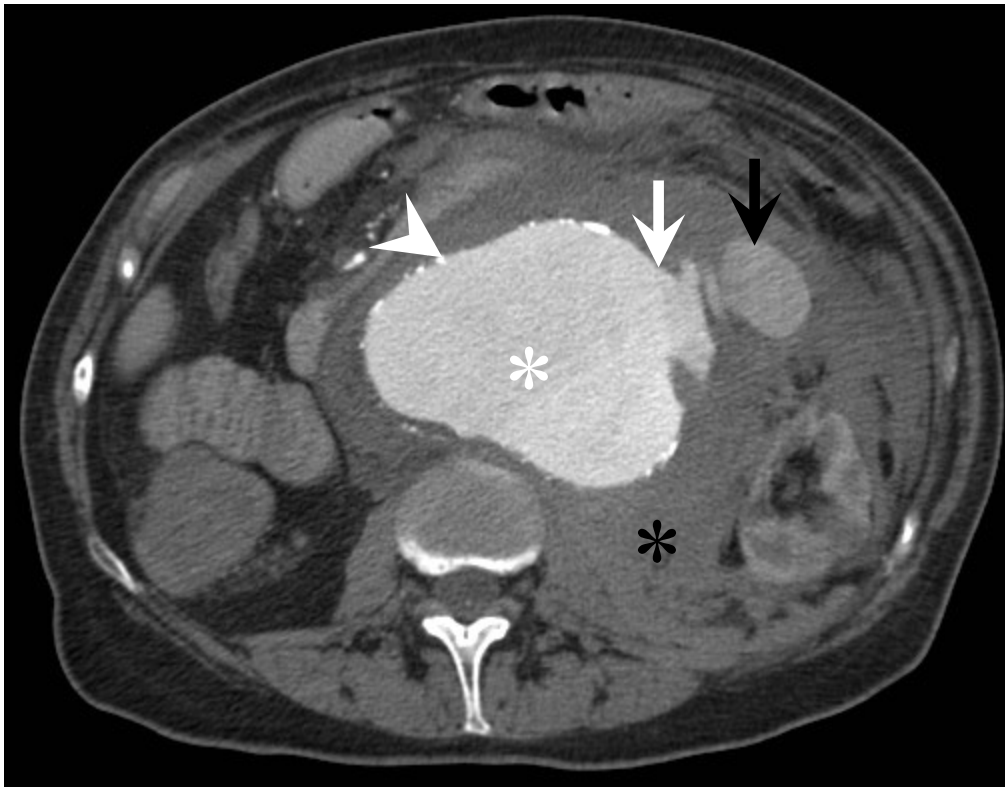

Figure 2.5: AAA rupture diagnosis on axial CT angiography.
Contrast-enhanced lumen is indicated by white asterisk, luminal calcification by arrowhead, rupture site by white arrow, contrast extravasation by black arrow, and retroperitoneal hematoma by black asterisk.

Since injection of iodinated contrast agent is often contraindicated in patients presenting with AAA due to uncertain history of allergy or acute renal failure, unenhanced CT may help depict several other signs of rupture. The most common sign is the demonstration of a retroperitoneal hematoma adjacent to an AAA (Figure 2.6.b). Blood may be found in the perirenal space, posterior pararenal space along the psoas, or anterior pararenal space. In severe bleeding, intraperitoneal blood (Figure 2.6.c) may also be seen along the mesenteric folds, paracolic gutters, perihepatic space, rectouterine, or rectovesical recesses.

Impending rupture may also be manifested by thrombus fissuration (Figure 2.6.d). This represents internal dissection of blood into the mural thrombus and may evolve toward an intramural hematoma, manifested by a hyperattenuating crescent sign (Figure 2.6.e).

Appearance of a new focal discontinuity in circumferential wall calcifications and focal bulge may indicate an unstable or ruptured aneurysm (Figure 2.6.f) (67, 68). A very large (>7 cm) aneurysm and an enlargement rate of ≥1.0 cm per year indicate a high likelihood of rupture. Another imaging sign that indicates impending or contained rupture is the "draped aorta sign" (Figure 2.6.g). This sign is considered present when the posterior wall of the aorta molds the contour of adjacent vertebral bodies and becomes indistinct from adjacent structures (62).

Inflammatory aneurysms, caused by retroperitoneal fibrosis or autoimmune diseases such as rheumatoid arthritis, lupus, and giant cell arteritis, may reveal periaortic stranding (Figure 2.6.h). Similarly, infected (mycotic) pseudoaneurysms that result from hematogenous seeding or direct spread from an adjacent vertebral ostemyelitis or from retroperitoneal abscesses may show periaortic stranding, periaortic gas, and abscess.

Although very rare, an AAA may erode into adjacent structures and fistulize. A primary aortoenteric fistula represents a complication of atherosclerotic AAA, and secondary a complication of AAA surgery. Aortoenteric fistulas most commonly involve the duodenum in its third and fourth portions. They will show periaortic gas (Figure 2.6.i). An aortoenteric fistula presents clinically with abdominal pain and gastrointestinal tract bleeding. Exceptionally, an AAA may erode into the inferior vena cava and result in an aortocaval fistula (not shown).

Figure 2.6: Signs of AAA rupture on CT in different patients.

(A) Contrast extravasation. (B) Retroperitoneal hematoma. (C) Intraperitoneal hematoma. (D) Thrombus fissuration. (E) Intramural hematoma. (F) Focal wall discontinuity (arrow) and focal bulge (arrowhead). (G) Draped aorta sign. (H) Periaortic stranding. (I) Periaortic gas secondary to an aortoenteric fistula.

2.7 Management of AAA

Patients with large aneurysms should be referred to vascular specialists for optimization of medical treatment and evaluation for surgical repair or AAA suitability for EVAR (Figure 2.7).

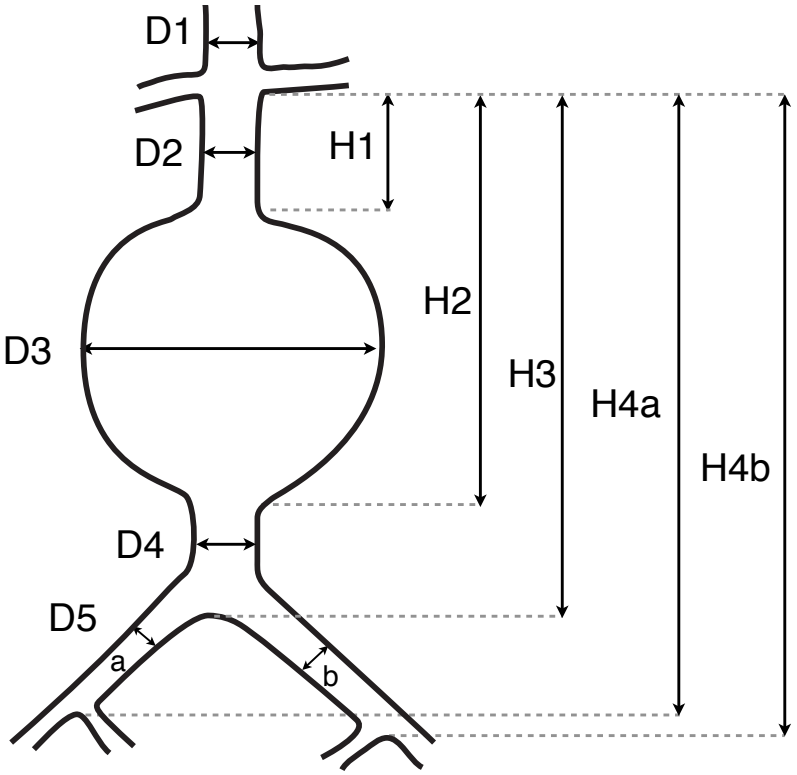

Figure 2.7: AAA measurements for stent graft sizing.
Schematic of the diameters and lengths AAA model. D1 = diameter of supra-renal aorta, D2 = diameter of aortic neck, D3 = maximum diameter of AAA, D4 = diameter of infra-renal aorta, D5 = diameter of common iliac artery (a, right; b, left), H1 = length of aortic neck, H2 = length from lowest renal artery to end of AAA, H3 = length from lowest renal artery to aortic bifurcation, H4 = length from lowest renal artery to iliac bifurcation (a, right; b, left).

2.7.1 Current Thresholds for Treatment

The American Association for Vascular Surgery (AAVS) in association with the Society for Vascular Surgery (SVS) have issued recommendations regarding AAA treatment (6). Current criteria to determine AAA treatment eligibility include: Dmax ≥ 5.5 cm in men, ≥ 4.5-5.0 cm in women, rapid expansion rate > 1 cm/year, or symptomatic AAA. These indications should be adapted to patient rupture risk, estimated mortality rate during an elective procedure, and life expectancy of patients.

2.7.2 Medical Treatment

The goal of medical therapy is to prevent small aneurysms below the treatment thresholds from reaching sizes at which rupture risk is high.

Smoking has been shown to be a risk factor of development and growth of AAA (39, 42). In a longitudinal study performed on 1743 patients, aneurysms had a higher growth rate in current smokers than in former smokers. The risk of rupture and death attributable to rupture were higher among current than former smokers and patients who never smoked. The corollary is that smoking cessation aims to reduce the growth rate and rupture risk of AAA.

There is limited or conflicting evidence on the impact of drug treatment on AAA growth rate. Several studies have explored the role of antihypertensive (angiotensin converting enzyme inhibitors, ß-blockers), statins, low dose aspirin, antioxidants, and antibiotics (doxycycline) in the reduction of AAA growth rate or peri/postoperative cardiovascular morbidity and mortality.

2.7.3 Surgical Treatment

Open aneurysm repair was first described by Charles Dubost in 1951 (12) when he first treated an aortic aneurysm with a homograft to prevent rupture.

Open aneurysm repair, the standard treatment, requires general anesthesia, a large incision, and extensive operative dissection of the retroperitoneal space to suture a Dacron graft to the aorta above and below the aneurysm (Figure 2.8). The perioperative mortality is high. The best centers perform open surgical repair at aneurysm-related mortality rates <5%, although the risk of death can be >10% in patients with poor renal function or comorbidities (34, 69, 70).

In addition to mortality directly related to open surgical repair, secondary surgical procedures required to treat complications may also contribute to mortality (69).

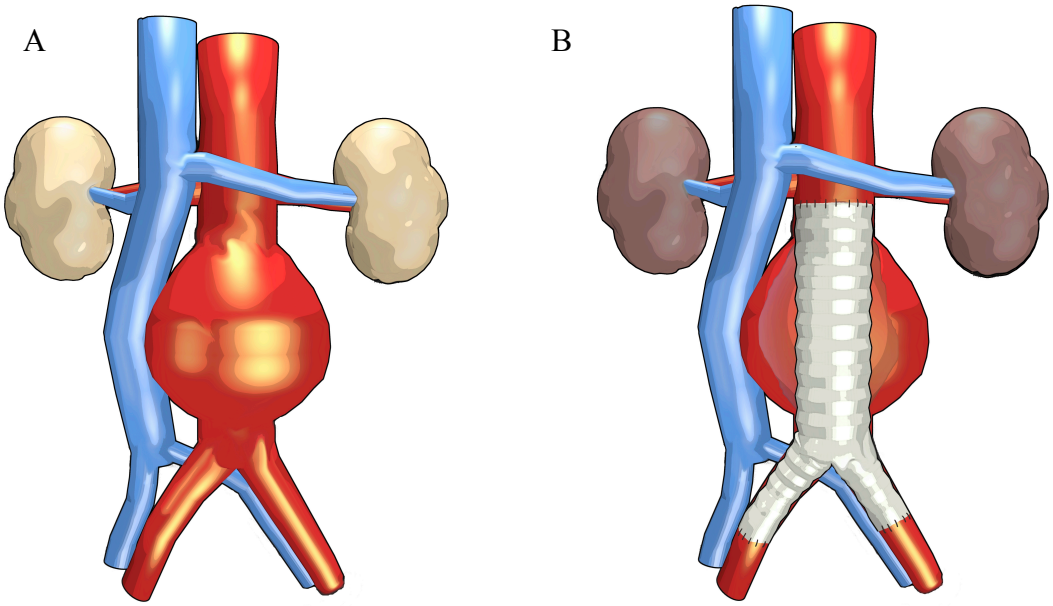

Figure 2.8: Schematic of open surgical repair.
(A) Schematic of infrarenal AAA before, and (B) after open surgical repair with aorto-biiliac graft. (Medical illustrations by Ivan Dominguez for An Tang)

Postoperative complications may be related to aortic cross-clamping or a hypovolemic state (renal insufficiency, ureteral necrosis), the patient condition (pulmonary complications, myocardial ischemia), the surgical procedure (anastomotic pseudo-aneurysms, anastomotic stenosis, graft thrombosis, graft infection), or delayed complications (recurrent aneurysms, peri-prosthetic effusion).

2.7.4 Endovascular Aortic Repair

Endovascular aneurysm repair (EVAR) involves relining the aorta with a stent graft, composed of a metallic stent with a textile lining, under fluoroscopic guidance through the femoral arteries (Figure 2.9). The stent graft must completely seal the proximal (infra-renal aorta) and distal (common iliac arteries) landing zones to prevent blood circulation in the excluded segment.

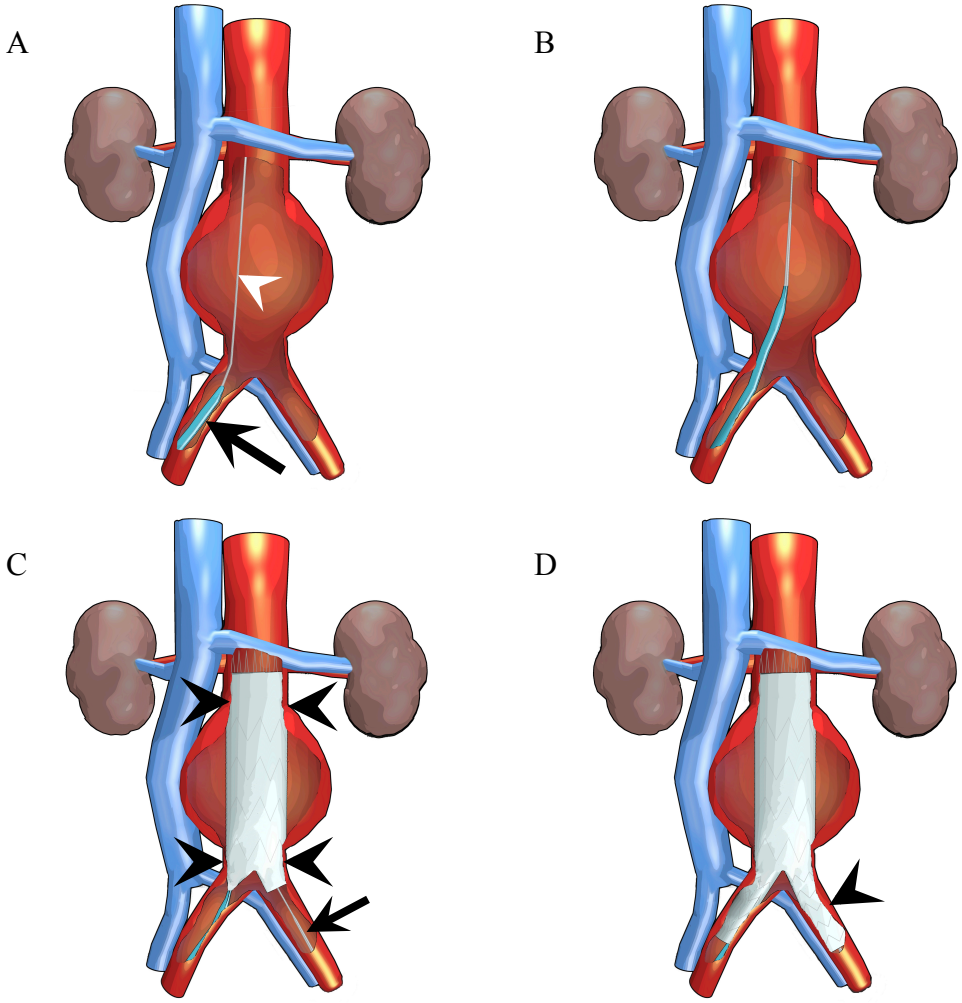

Figure 2.9: Schematic of endovascular aortic repair (EVAR).
(A) A transfemoral metallic guidewire (white arrowhead) is positioned in the lumen of the AAA through a sheath (black arrow). (B) The main body of the stent-graft is introduced up to the level of the renal arteries and (C) the stent-graft (black arrowheads) deployed by retrieval of the sheath and by balloon angioplasty (not shown). A second guide wire is

introduced via the contralateral femoral artery (black arrow) to deploy the (D) left iliac component (black arrowhead). (Medical illustrations by Ivan Dominguez for An Tang)

The potential advantages of the EVAR approach demonstrated in randomized trials include a reduction in perioperative mortality, morbidity, blood loss, hospital stay, duration of intensive care unit stay, and discomfort (18, 21, 24)

Although recovery is faster with this minimally invasive procedure, EVAR may not be cost-effective due to the high cost of the stent graft, need for close surveillance early after repair, long-term follow-up afterwards, and delayed complications (endoleaks), which may occur years after the procedure. The increased rates of graft-related complications and reinterventions contribute to higher overall cost (21). In addition, no significant differences were observed in aneurysm-related or in total mortality between patients randomized to either treatment group in the long term.

Anatomical suitability

Not all patients are eligible for EVAR due to their AAA anatomy. While exact values may vary, the following numbers provide an indication of AAA anatomical suitability. The proximal neck, from the renal arteries to the beginning of the AAA should have a minimal length (≥ 15 mm), should have low angulation (<60°), should not be dilated (≤ 30 mm), and should not be cone shaped (i.e. neck diameter increased by >20% over 15 mm) (71). The stent graft should not cover the superior mesenteric artery and renal arteries. The distal landing zone should not be too tortuous and should have a diameter of ≥ 7 mm to permit stent graft deployment, but < 23 mm to permit adequate seal (72).

Five types of AAA morphology have been described in the Eurostar classification (73): type A: aneurysm confined to abdominal aorta which ends ≥ 15 mm above aortic bifurcation; type B: aneurysm that involves aortic bifurcation, with normal iliac arteries; type C: aneurysm that involves both proximal common iliac arteries; type D: aneurysm that extends into one iliac bifurcation; type E : aneurysm that extends into both iliac bifurcations.

Emergency endovascular aneurysm repair

In light of the minimally invasive nature of EVAR and reduction in peri-operative morbidity and mortality, this technique has also been considered in the management of acutely symptomatic or ruptured AAAs. The feasibility of emergency endovascular aneurysm repair (eEVAR) has been demonstrated by Yusuf *et al*. in a case report in 1994 (23). This treatment strategy poses an additional logistical challenge by requiring that a team, composed of an interventional radiologist and a fully trained vascular surgeon competent in endovascular and open techniques, must be available around the clock to evaluate the anatomical suitability to EVAR in emergency settings (74).

A meta-analysis of eEVAR, which included 23 pooled studies and 7040 patients, of which 730 underwent eEVAR, found a significant reduction in mortality (pooled odds ratio 0.624), reduction by 4 days of ICU stay, reduction by 8.6 days of hospital stay, reduction of blood loss and procedure time (24, 74).

Fenestrated endovascular aneurysm repair

To expand the AAA anatomy eligible for EVAR, fenestrated endovascular aneurysm repair (FEVAR) was developed (75). FEVAR includes fenestrations (holes) in the graft to provide access to visceral arteries (Figure 2.10). This allows extension of the proximal landing zone above the visceral arteries (typically the renal arteries and superior mesenteric artery), thus overcoming the traditional requirement for a proximal aortic neck of at least 10-15 mm. The design of these fenestrated stent grafts is rapidly evolving to facilitate cannulation of visceral arteries (28).

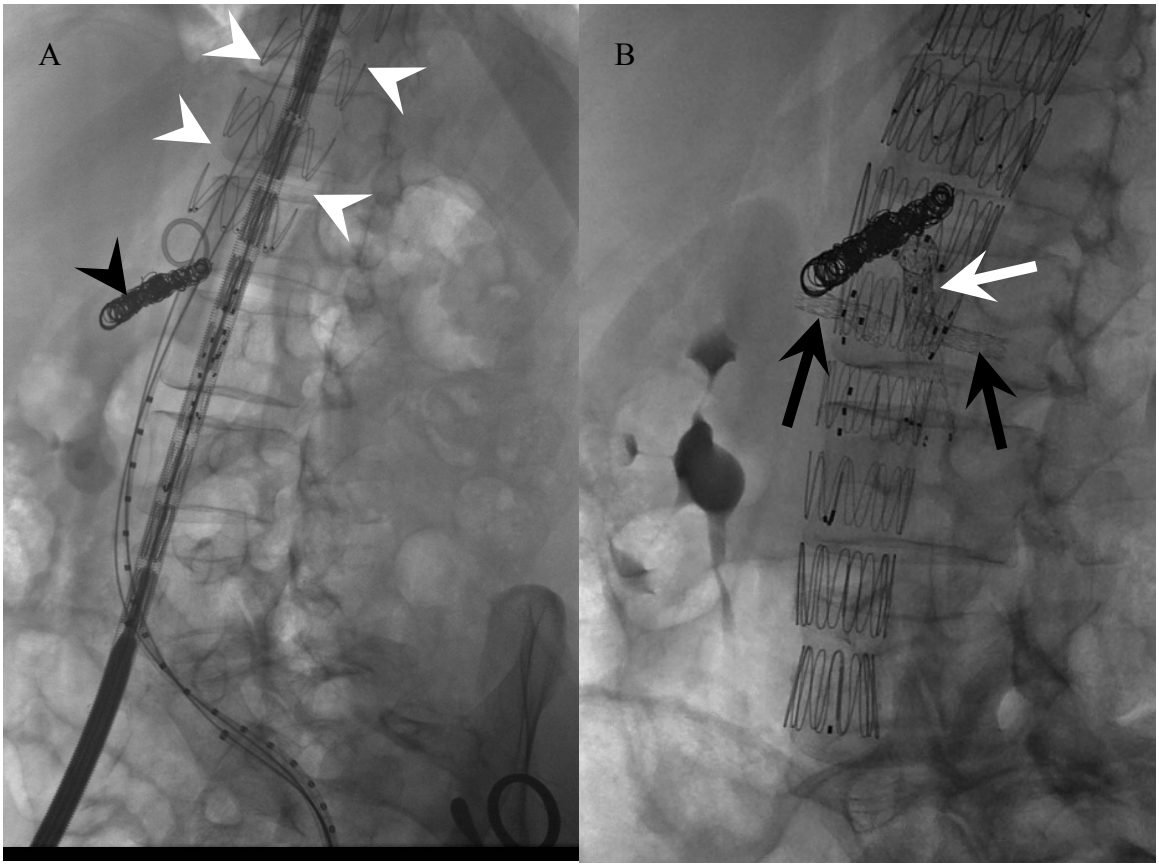

Figure 2.10: Fenestrated endovascular aortic repair (FEVAR).
(A) A stent graft (white arrowheads) is partially deployed in a thoraco-abdominal aortic aneurysm above the visceral arteries. The celiac trunk (black arrowhead) was previously embolized with coils to exclude an aneurysm. (B) A final image at the end of the procedure shows positioning of individual stents in the superior mesenteric artery (white arrow) and both renal arteries (black arrows) across the fenestrated stent graft.

EVAR complications

Complications related to EVAR, either endoleaks or mechanical failure, occur in 15 to 52% of cases (76-78). Endoleaks are defined as blood flow external to the stent-graft, but internal to the aneurysm sac. There are 5 types of endoleaks. Type I endoleak result from a proximal (Ia) or distal (Ib) coverage defect and lead to a direct communication between the systematic circulation and the aneurysm sac. Type II endoleak results from a retrograde blood flow coming from aortic branch vessels (typically lumbar or inferior mesenteric arteries). Type III results from a structural failure of the stent-graft (disconnection between

prosthetic modules or fabric tear). Type IV results from Dacron porosity. Type V endoleak, also called endotension, refers to aneurysm expansion in the absence of imaging signs of type I-IV endoleaks and is thought to result from ultrafiltration of blood across the stent-graft or pressure transmission through the thrombus (79).

Additional complications may result from infection, accidental coverage of the ostium of renal arteries, endograft deformation and fracture.

To detect early and long-term complications, follow-up contrast-enhanced with delayed phase CT imaging is recommended at an interval of 3, 6, 12, 24 months, and annually thereafter.

2.7.5 Results of Randomized Controlled Trials

Randomized controlled trials (RCTs) provide the highest level of evidence because they are least susceptible to bias (both known and unknown causes). Furthermore, several confirmed (as opposed to single) randomized controlled trials provide strong evidence for evidence-based medicine.

Endpoints in Randomized Controlled Trials

Primary endpoints listed in RCT either include overall rate of death from any cause, or rate of death related to rupture or aneurysm related death. To determine whether deaths are related to AAA, they are typically defined as death caused directly or indirectly by rupture or repair, preoperative evaluation, late graft failure or complication, or AAA or pseudoaneurysm after grafting or any death occurring ≤ 30 days after aneurysm repair or ≤ 30 days after randomization of patients in the surveillance group. Mortality analyses are performed on an intent-to-treat basis.

Secondary endpoints listed in RCT may include aneurysm related death, aneurysm rupture, procedure failure, perioperative or late complications (vascular complications at the femoral entry site, prosthesis infection, wound infections, cardiovascular, pulmonary complications, endograft migrations), secondary interventions (graft limb occlusion,

endoleaks, conversion to open repair after attempted endovascular graft implantation, graft-related, wound-related), AAA growth rates, and health related quality of life.

Occasionally, the primary end point may be a composite of the endpoints listed above. For instance, this was the case in the Dutch Randomized Endovascular Aneurysm Management (DREAM) trial, in which the short-term primary endpoint was a composite of operative mortality and moderate or severe complications (19, 80), and the long-term primary endpoint was the rate of death from any cause and reintervention (20).

Main Findings of Randomized Controlled Trials

It is widely accepted that the rupture risk increases substantially as AAA diameter increases from 5 cm to 6 cm. This is supported by a population-based study by Nevitt *et al*. (7), more recent analysis of this data by Reed *et al*. (11), and similar estimates from the United Kingdom Small Aneurysm Trial (UKSAT) (3). Instead, RCTs investigated the equipoise of intervention over surveillance in small AAAs or compared the outcomes of endovascular and open repair of AAA.

Two trials, the Aneurysm Detection and Management (ADAM) and the UKSAT examined the benefits of early open aortic repair on small AAAs (4.0 - 5.4 cm) and reported no improvement in survival in comparison with surveillance (3, 5).

Given the lower perioperative morbidity and mortality of EVAR, there was a sound rationale to seek a survival benefit with EVAR in small AAAs. Two trials, Positive Impact of Endovascular Options for Treating Aneurysms Early (PIVOTAL) (81) and Comparison of surveillance vs. Aortic Endografting for Small Aneurysms Repair study (CAESAR) (35, 82), compared EVAR to surveillance and found no significant difference in aneurysm-related or all cause of mortality between the two groups.

Four trials compared the outcomes of endovascular and open repair of AAAs $\geq$ 5.5 cm: Endovascular Aneurysm Repair (EVAR) (18, 21, 83), Dutch Randomized Endovascular Aneurysm Management (DREAM) (19, 20, 80), or $\geq$ 5.0 cm: Open Versus Endovascular Repair (OVER) (84), and Anévrysme de l'aorte abdominale: Chirurgie versus Endoprothese (ACE) (17). In essence, these trials found lower in-hospital perioperative mortality and

mortality for elective EVAR as compared with open aortic repair, but no significant difference in long-term mortality after 2 years.

Only one trial compared emergency EVAR (eEVAR) with open aortic repair in acute ruptured AAA (85). The authors demonstrated the feasibility of an eEVAR trial. However, this study was interrupted due to logistical obstacles. Interim results were reported for the 32 patients recruited to the study. On an intention to treat basis, the 30-day mortality rate was similar: 53% in the EVAR group and 53% in the open aortic repair group. The rate of moderate or severe operative complications was also similar: 77% in the EVAR group and 80% in the open surgical repair group.

Table 2.1 lists the RCTs comparing different treatments, or intervention with surveillance, and summarizes their key findings.

Table 2.1: Summary of randomized trials comparing AAA treatment: endovascular aortic repair (EVAR), open aortic repair (OAR), or surveillance.

Comparison	Study	n	Summary
OAR vs. Surveillance	ADAM (5)	1136	-Inclusion: 4.0 - 5.4 cm AAA -Key findings: No significant difference in rate of AAA-related mortality (3.0% vs. 2.6%). -AAA-related hospitalization was 39% lower in the surveillance group -Similar operative mortality rate (2.1% after early open repair and 1.8% after open repair in surveillance arm) within 30 days
	UKSAT (3)	1090	-Inclusion: 4.0 - 5.5 cm AAA -Key finding: No significant difference in mortality between groups (5.7% vs. 6.6%) at 5 years
EVAR vs. surveillance	PIVOTAL (81)	728	-Inclusion: 4.0 - 5.0 cm AAA -Key findings: No significant difference in aneurysm related mortality or all cause mortality between the two groups
	CAESAR (35, 82)	360	-Inclusion: 4.1-5.4 cm AAA -Key findings: No significant difference in all cause mortality, aneurysm related mortality, aneurysm rupture, or major morbidity at a mid-term median follow-up of 32 months.
EVAR vs.	EVAR	1082	-Inclusion: ≥ 5.5 cm

Comparison	Study	n	Summary
OAR	(18, 21, 83)		-Key Findings: lower in-hospital and operative mortality for EVAR vs. open repair (1.7% vs. 4.7%, $p<0.001$) -Similar all-cause mortality at 4 years (26% vs. 29, $p=0.46$)
EVAR vs. OAR (continued)	DREAM (19, 20, 80)	351	-Inclusion: ≥ 5.5 cm -Key Findings: Lower in-hospital and operative mortality for EVAR vs. open repair (1.2% vs. 4.6%, $p=0.10$) -Similar survival rates at 2 years (89.7 vs. 89.6% $p=0.86$) and 6 years (68.9% vs. 69.9%, $p=0.97$) -Lower rate of freedom from secondary interventions for EVAR vs. open repair after 6 years (70.4% vs. 81.9%, $p=0.03$)
	OVER (84)	881	-Inclusion: ≥ 5.0 cm -Key findings: lower perioperative mortality for EVAR vs. open repair (0.5% vs. 3.0%, $p=.004$) -No significant difference in mortality at 2 years (7.0% vs. 9.8%, $p=0.13$) -Reduced procedure time, blood loss, transfusion requirement, duration of mechanical ventilation, hospital stay, and ICU stay in EVAR group.
	ACE (17)	316	-Inclusion: ≥ 5.0 cm -Key findings: No significant difference between EVAR vs. open repair in survival free of death and major adverse events at one year (93.2% vs. 95.5%), and three years (82.4% vs. 85.1%, $p=0.09$), in-hospital mortality (1.3% vs. 0.6%, $p=1.0$), survival, and percentage of minor complications. -Higher percentage of reintervention in EVAR group (16% vs. 2.4%, $p<0.0001$)
eEVAR vs. OAR	Hinchliffe *et al*. (85)	32	-Inclusion: suspected ruptured AAA. -Key findings: Suspended study, interim analysis reported. Logistical feasibility of eEVAR vs. open repair. Comparable 30-day mortality (53% vs. 53%), moderate or severe operative complications (77% vs. 80%).

In summary, open surgical repair and EVAR are two treatment options for large AAA (≥5.5 cm in diameter). In the setting of randomized trials, EVAR was associated with lower operative mortality and shorter hospitalization than open surgical repair. The rates of graft-related complications and reinterventions are higher with EVAR, and delayed

complications contribute to higher overall cost (21). However, no study has demonstrated a long term survival advantage to either treatment (18, 19). Non operable (high risk) patients do not benefit from EVAR as compared with observation (18). Currently, the favored candidates for EVAR are intermediate-risk patients with suitable anatomy.

2.8 3D Modeling

Due to the limited sensitivity of Dmax for assessment of rupture risk, especially among smaller AAAs, several authors explored alternative strategies to allow for patient-specific rupture risk assessment.

These approaches fall into two categories: identification of geometrical parameters and biomechanical simulations. The latter can be further divided in three types of simulations: finite element analysis (FEA), computational fluid dynamics (CFD), and fluid structure interaction (FSI).

A detailed discussion of these simulation methods is beyond the scope of this master's thesis. The following section provides an overview of the underlying concepts.

2.8.1 Geometrical parameters

As an alternative to the maximal diameter of the outer wall, it has been suggested that the thrombus or the AAA morphology could represent surrogate markers of rupture risk.

Intraluminal Thrombus

The presence of a thrombus as a protective effect, a risk factor, or a neutral effect on rupture remains controversial.

Some studies suggested a protective effect of the thrombus against rupture based on peak wall stress reduction, either using computer simulation (68) or by evaluating geometric surface or volume ratios (52).

Conversely, some suggested that the thrombus predisposes to rupture based on increased thrombus load associated with expansion and subsequent rupture observed on patients with at least two consecutive CT scans (32, 86).

Finally, maximum thrombus thickness and circumference was found to be similar in ruptured and intact groups in a larger case-control study (87). While ruptured AAAs tend to be larger in diameter and have a greater volume of thrombus compared with intact AAAs, no difference was observed in the ratio of thrombus volume to aneurysm volume in ruptured or intact aneurysms (88). This highlights the importance of normalizing the size of a thrombus over that of the aneurysm.

Quantitative parameters

A benefit of performing AAA segmentation lies in the ability of generating a 3D model of the aneurysm. With prior knowledge of the aneurysm geometry, it is possible to extract various quantitative geometrical parameters.

Using a noninvasive computational approach, and assumptions on mechanical properties of the AAA wall, it is possible to explore geometrical parameters that may be better indicators of AAA rupture. Thus, it has been suggested in a proof-of-concept study that the peak wall stress was best correlated with the mean centerline curvature, the maximum centerline curvature, and the maximum centerline torsion (89).

Expanding on the idea of using three-dimensional data obtained by aneurysm segmentation, a quantitative tortuosity index has been developed to classify aneurysm shape beyond the standard adjectives "fusiform" or "saccular" typically used to describe an aneurysm shape (90). The aneurysm tortuosity was defined as the deviation of the AAA center axis from the centerline.

The logical extension of this work was to collect a set of global geometrical indices describing the size and shape of the aneurysm sac. This comprehensive work was recently performed by Martufi *et al*. (91). As a proof-of-concept, the geometry of nine AAA subjects treated for elective repair were characterized with the geometrical indices listed.

In a follow-up paper, the same team implemented their AAA size and shape evaluation approach to a retrospective dataset of 10 ruptured and 66 unruptured aneurysms (53). They also proposed a decision tree algorithm with 4 decision branches to discriminate ruptured from unruptured AAA. The average prediction accuracy of the decision tree model was 86.6%, whereas a Dmax of 5.0 cm as the sole predictive variable resulted in an accuracy of 38.2% in their dataset.

Our most recent work is built on the semi-automated segmentation software developed at our institution over the past 6 years and incorporates the geometrical indices proposed by Martufi *et al*. and Shum *et al*. (53, 91).

2.8.2 Biomechanical Simulations

An up to date review of computational modeling of AAA was recently published by Roy *et al*. (92), a member of our team. The key elements required for patient-specific geometries and hemodynamics simulations are summarized below.

AAA rupture occurs when the local stresses on the aortic wall exceed its mechanical strength. Hence, the motivation to do research in vascular biomechanics to predict aneurysmal growth and vessel behavior. This approach requires simulating the physical properties of blood vessels, blood flow, and grafted implants. As a prerequisite step, physicians must become familiar with concepts of rheology, mechanical engineering, and material science.

Definitions and concepts

Stiffness or *elasticity*, also known as *Young's modulus*, is the measure of the resistance offered by a material to perpendicular deformation. Mathematically, it represents the slope of a stress-strain curve.

Shear modulus is similar to *Young's modulus*, except that it is a measure of the resistance offered by a material to tangential deformation.

A *stress* is a force applied over a surface area. A shear stress is a force applied tangential to a vessel and may either act on the thickness of the vessel ("structural shear stress") or result from blood flow ("flow shear stress").

For a material, such as a vessel, that is submitted to tensile loads along 3 directions, *von Mises* stress determines strength beyond which the material yields. The *von Mises* stress combines tensile and shear stress.

When a material is stretched, *Poisson's ratio* describes the ratio of the transverse contraction to the extension. Biological tissues, which are mostly constituted of water, are incompressible by nature and given a Poisson's ratio of 0.5.

Viscosity is a measure of the resistance to flow.

Fluids may be classified as *Newtonian* (such as water) or *non-Newtonian* (such as paint). For *Newtonian* fluids, the viscosity remains constant regardless of the shear rate, whereas *non-Newtonian* fluids observe a decrease in viscosity as the shear rate increases.

The *Navier-Stokes* equations provide a full description of mass, momentum and energy conservation in fluid mechanics.

The *Windkessel* effect refers to the storage of elastic energy during systole due to vessel compliance, and release of elastic energy during diastole.

Discretization or *segmentation* refers to a common process used in medical imaging of cutting a complex structure into small and simple elements. Typically, surfaces are represented with small triangular or tetrahedral surfaces to form a *mesh* (Figure 2.11).

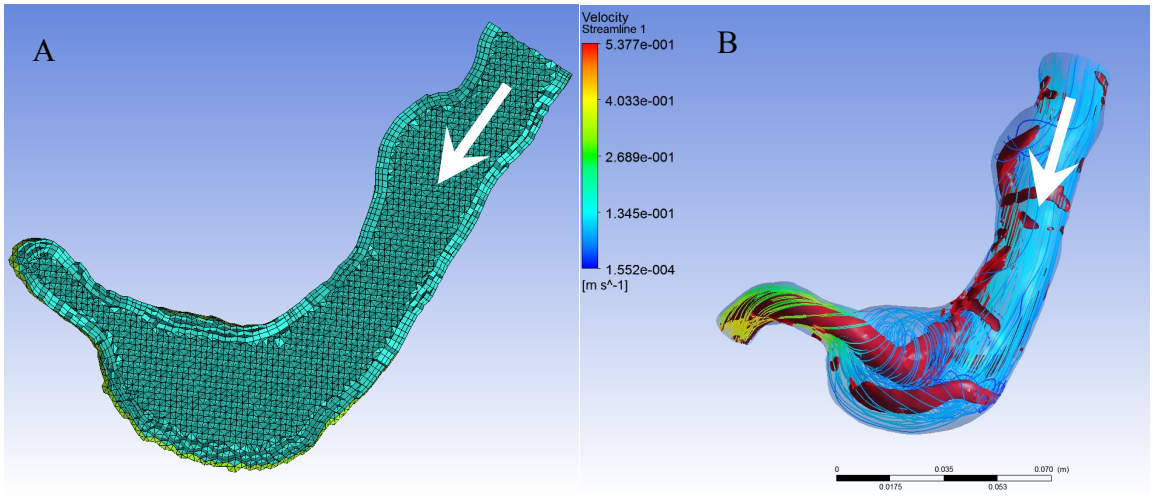

Figure 2.11: Finite volume analysis (FVA).
(A) Mesh used for the finite volume analysis which contains 214 000 tetrahedral elements with prism layers to capture the wall effects (generated in ICEM, Ansys). Flow direction is indicated by white arrows. (B) Visualization of the flow in an AAA. The streamlines are colored by the fluid velocity. The vortex cores are shown in red (Image courtesy of Florian Joly. Generated in Fluent, Ansys).

Finite element analysis (FEA) refers to a method of numerical simulation based on geometrical and mathematical *discretization* of the AAA shape. This is required because AAAs have a complex non cylindrical shape that greatly affects the stress map.

Finite element modeling (FEM) refers to the assembly of finite elements into a continuous mesh, which provides an approximation of the solution to complex problems.

FEA can be further subdivided into two types: *computational fluid dynamics* (CFD) and *fluid-structure interaction* (FSI).

CFD involves the study of velocity and pressure evolution in flows, assuming a rigid vessel.

FSI is identical to CFD, but also accounts for the real stiffness of vessels and the mutual interaction of flow and wall mechanics on each other.

2.8.3 Mechanical properties

Based on *ex vivo* biomechanical testing, the stress-strain curves of healthy aortas and AAAs are known (93). These curves are *non-linear*, meaning that the stiffness varies over a range of strain (or elongation).

Isotropy refers to identical mechanical properties (such as vascular stiffness) in axial and circumferential directions, as opposed to *anisotropy*. Isotropic models are appropriate as a first approximation, but anisotropic models are favored for more accurate results.

Using CT scans or magnetic resonance imaging (MRI), the *in vivo* arterial geometry can be extracted to perform patient-specific 3D modeling and rupture risk assessment(9). An example of shear wall stress simulation at peak systolic velocity is provided for one of our patients in Figure 2.12.

Future research directions include stent graft modeling and virtual stent graft planning.

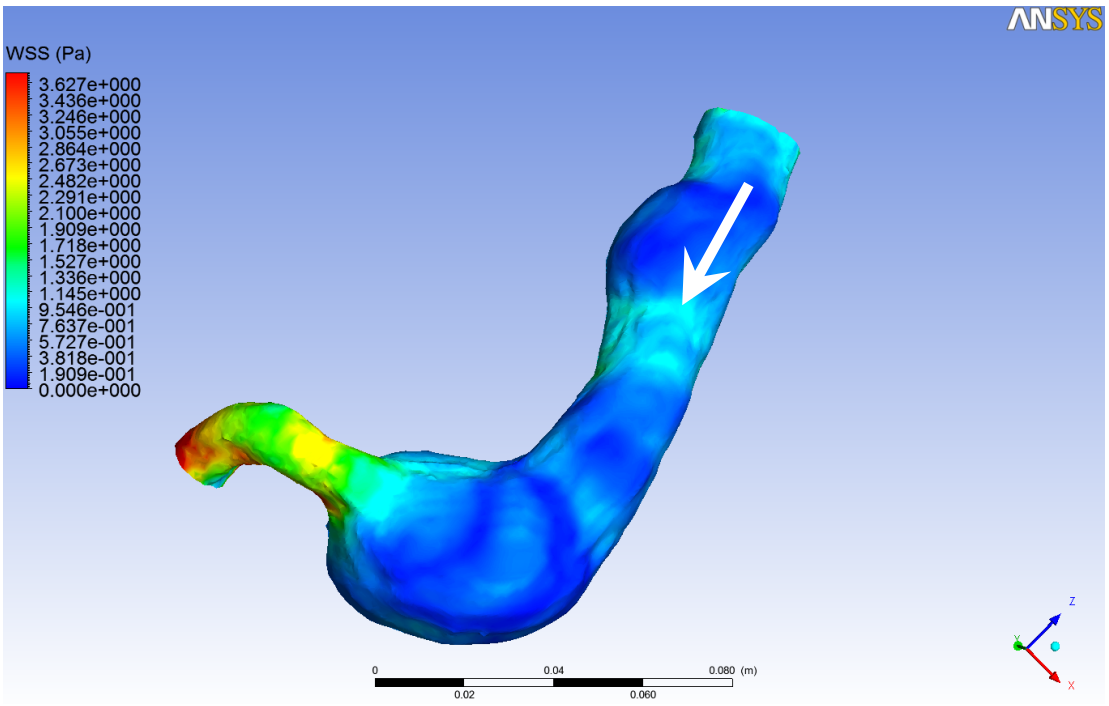

Figure 2.12: 3D rendering showing AAA wall shear stress simulation at peak velocity. Flow direction is indicated by a white arrow. (Image courtesy of Florian Joly. Generated in Fluent, Ansys).

3 Segmentation Software

In order to perform morphologic evaluation of AAA and wall stress simulations, an intermediate step must first be accomplished: delineation of the boundaries of the outer wall and lumen. This process, known as segmentation, is required to render a three-dimensional model representing the AAA wall, thrombus, and lumen.

Some previous studies relied on manual segmentation (89, 90) or a semiautomated process that required considerable human intervention on the order of 2 to 4 hours (94, 95) in addition to computational time also in the range of 2 to 4 hours. Over time, segmentation time was reduced to 45 minutes (96, 97) or less than 20 minutes. Recently, the average segmentation time for a semi-automated method was 15 minutes (98).

Manual segmentation, which required tracing the contour of the AAA wall and lumen on each individual image is exceedingly time-consuming, repetitive, and tedious (Figure 3.1). Given its mind-numbing nature, this approach is only realistic as a proof of concept or for a limited number of studies. Furthermore, with the increasingly thinner slices now achievable with multidetector CT, such an approach is no longer sustainable nor realistic.

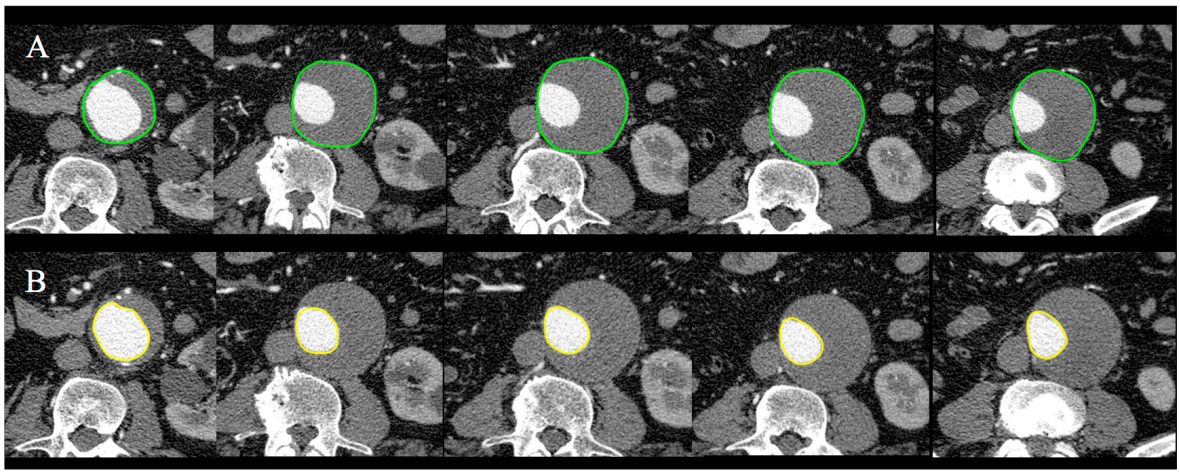

Figure 3.1: Manual segmentation workflow on axial images.
The process of delineating (A) wall and (B) lumen must be repeated for hundreds of images.

3.1 Software Concept

Based on our experience in AAA segmentation and software development, our team — composed of radiologists, image analysts, software engineers, students— determined a list of features required from a modern AAA segmentation solution. These needs are organized in categories, summarized in Table 2.2, and expounded in further detail below.

Table 2.2: Features expected from a modern AAA segmentation solution

Categories	Needs
Clinical needs	-Efficient clinical workflow -User-friendly interface -Segmentation can be delegated to technologist/image analyst -Accurate -Reproducible -Interactive (allows correction) -Fast (<5 minutes/case) -Optimized for CTA examinations -Works on unenhanced studies -Separate meshes for AAA wall and lumen -Allows registration of different studies for longitudinal follow-up
Quantitative output	-Can compute Dmax -Can report AAA, thrombus, and lumen volume -Can extract geometric parameters -Can export results to a database
Technical challenges	-Low contrast between AAA and adjacent soft tissues -Patient position changes during follow-up -Measurement of Dmax and volume must be measured on the same aorta section on different examinations
Mathematical definitions	-Variety of mathematical definitions of Dmax -Fluid dynamics and geometrical definitions of Dmax differ
Volume segmentation	-Challenges related to volume segmentation: -Choice of section plane (axial, coronal, sagittal, curved radial) -Choice of iliac vessel for centerline (right or left) -Choice of markers for AAA follow-up
Output	-Must export meshes that are subsequently usable for mechanical simulations

Clinical needs

Ultimately, AAA segmentation solutions are developed to address current and future needs of the target clinical audience (vascular surgeons and interventional radiologists) and research community (biomedical engineers). However, it is unrealistic to expect these users to perform AAA segmentation on a daily basis. Instead, to optimize the clinical workflow and save time for clinicians who must treat patients, the current practice in 3D imaging laboratories is to delegate the segmentation task to image analysts, radiology technologists, or trainees. The graphic user interface should be sufficiently intuitive and friendly to allow users with variable levels of training to understand the anatomy and image projections. Furthermore, the software should be designed in such a way to permit quality control (i.e. validation and correction) of the segmentation result by the clinician, if needed.

The accuracy, reproducibility (precision), and robustness (imperviousness to technical variations) of the software segmentation solution should also be validated against a reference standard. Since it is impossible to compare the maximal diameter or volume of a AAA derived by segmentation with an *ex vivo* specimen (the aorta would collapse in the absence of blood flow), this validation must be performed *in vivo* against an imaging method that serves as a surrogate reference standard, such as Dmax measured or volume determined from manual segmentation by an expert.

While full automation may appear ideal, it entails additional problems. A fully automated method is highly desirable to shorten segmentation time. However, if the segmentation result is not perfect, it may require corrections that may be very time consuming. Inevitably, automated methods generate errors due to unforeseeable anatomical variants or technical challenges.

Instead, a semi-automated method may provide a good trade-off between fully automated and entirely manual segmentation methods. Such a hybrid method incorporates input from the user who has high-level image understanding and automation of repetitive steps best performed by software. Human feedback can therefore be provided at critical steps during the segmentation process to avoid error propagation.

A total interaction time of less than 5-10 minutes would be ideal for practical and psychological reasons. In a clinical environment, radiologists are often interrupted to

provide their opinion on clinical matters and must consult other imaging examinations on their workstations. Any task that requires a long period of uninterrupted work is therefore very difficult to sustain in the field. The possibility to save a session and restart at the last step is a reasonable solution to that problem. Yet, a total interaction time much longer than 10 minutes generates boredom, because these tasks must be repeated on each new case. Furthermore, sample size required to obtain sufficient power to test hypotheses in clinical studies can be more than a hundred patients. Therefore, time is of the essence for building scaling segmentation methods. In our experience, a segmentation method that requires 5-10 minutes of total interaction time should offer the right balance of user feedback and software automation.

Segmentation methods should be optimized for computed tomography angiography (CTA). As discussed previously, ultrasound is the preferred imaging modality for screening or surveillance, but CTA is largely favored for pre-operative assessment of AAA anatomy due to its resolution, robustness and speed. MR is seldom used for pre-operative assessment, except in patients with contra-indications such as iodinated contrast allergy and renal failure.

Thanks to the injection of an iodinated contrast agent, CTA delineates the aortic lumen. This permits separate segmentation of the patent lumen and the outer AAA wall. The difference between the two resulting meshes should correspond to the thrombus, sometimes termed intra-luminal thrombus (ILT). Injection of a contrast agent is not always possible. In patients with acute or chronic renal failure, there is a concern for potential nephrotoxicity of iodinated contrast agents. Therefore, a robust AAA segmentation method should also be feasible on an unenhanced study. The downside is that only the outer wall can be segmented since there is insufficient density difference between the aortic lumen and thrombus.

An integrated segmentation solution should perform well on a single (cross-sectional) study, but should also allow growth comparison of several consecutive (longitudinal) studies. This is most important in the monitoring of patients post-EVAR because volume growth may indicate an endoleak, and need for reintervention, even when contrast opacification is not demonstrated. Further, studies have shown that volume measurements

may be more sensitive and depict aneurysm enlargement 18 months earlier than standard diameter measurements (99, 100). This highlights the need for co-registration of fiduciary markers on sequential examinations so that measurements can be performed at the same level and in the same plane.

Quantitative output

Current treatment indications or based on Dmax and diameter growth (6). Increased sensitivity of volume over diameter measurements have been reported and suggest that this parameter may be used for monitoring AAA growth (29, 96, 101). At a minimum, a segmentation solution should be able to calculate Dmax automatically since this biomarker represents the current standard of care. Further quantitative output should include thrombus, lumen, and AAA volume. The next logical step is to extract geometrical parameters that describe AAA morphology quantitatively. Finally, all the data derived from segmentation should be exportable to a database.

Technical challenges

AAA segmentation can be challenging for humans and software because the density of the peripheral thrombus can be similar to surrounding tissues. The low contrast between aorta and surrounding soft tissues is worse on unenhanced studies (Figure 3.2). In such situations, identification of wall calcifications can be helpful in delineating the aortic wall and may be incorporated into the segmentation method.

Patient position may change between different examinations. Hence, rigid registration using anatomical fiduciary markers such as vertebral spine and iliac bones may be used to co-register different examinations.

For stent planning simulations, elastic co-registration may be eventually required to simulate the deformity of iliac vessels due to stiff guide wires or delivery device.

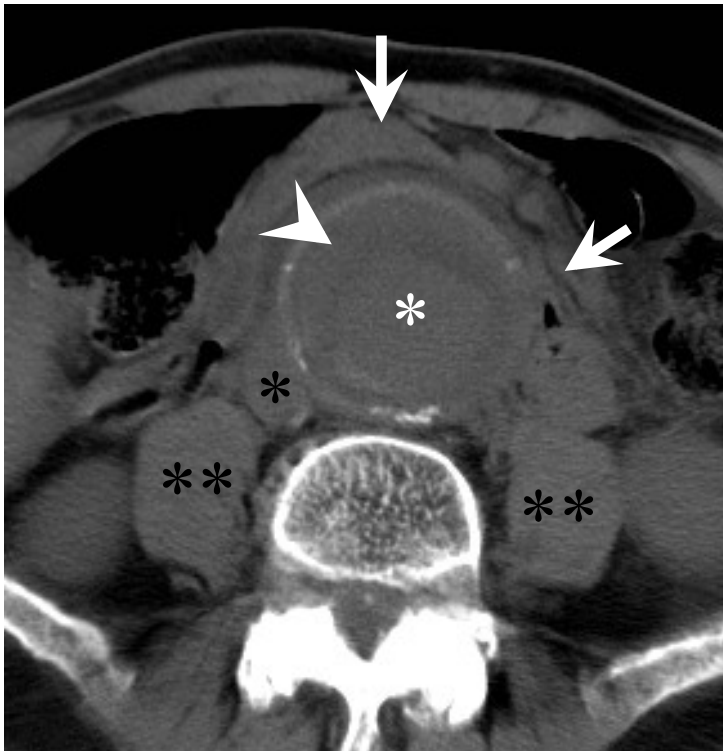

Figure 3.2: Axial unenhanced CT showing low contrast situation.
The densities of the aortic lumen (white asterisk) and thrombus (white arrowhead) are similar to that of the adjacent inferior vena cava (black asterisk), adjacent small bowels (white arrows), and nearby psoas muscles (double black asterisks). The delineation of the aortic contour is facilitated by the presence of wall calcifications (white rim).

Mathematical definitions

To add to the complexity, different measurement methods may exist for the same parameter. For example, some investigators advocate manually measuring Dmax on axial slices, others propose measuring the diameter perpendicular to axial Dmax, the anteroposterior diameter, the transverse diameter, the diameter perpendicular to the estimated central line on axial slices or to the orthogonal multiplanar reconstructions (102). The differences in measurement method contribute to inter-observer variability.

Thus, there is a need for formal mathematical definitions that eliminate inter-observer variability. Yet, even this proposition is challenging because there are at least four different mathematical definitions of Dmax: a) the greater distance included in the contour (91); b)

the greater distance included in the contour defined on the plane perpendicular to the center line; c) the fluid mechanics definition for hydraulic diameter (Dmax = 4*Area/Perimeter), which correspond to the diameter equivalent to a circle that has the same flow as the area of the ellipse studied; c) the fluid mechanics definition for hydraulic diameter defined on the plane perpendicular to the centerline. To our knowledge, the discrepancies between these mathematical definitions of Dmax have not been addressed systematically. The discussion is beyond the scope of this master's thesis, and should be examined in the future.

Recently, mathematical definitions have also been proposed for the description of additional geometrical indices such as tortuosity, asymmetry, and curvature (53, 91). However, the repeatability and predictive ability of these indices have not yet been evaluated. Furthermore, they have not been validated outside of the centers where they were first described.

Volume segmentation

Traditionally, manual segmentation was performed on axial images, the plane in which images are acquired. With the advent of multidetector CT and isometric voxels, it is now possible to view multiplanar reconstructions with a resolution comparable to native axial images. In theory, segmenting an AAA in a plane parallel to the long axis of the AAA (i.e. coronal, sagittal, or oblique longitudinal planes) should be faster because the number of slices to cover would be much smaller than in the axial plane. However, partial volume averaging effects may blur the margins of the aorta on the first and last images in these planes. Segmentation in radial planes (i.e. revolving around the z-axis) may partially solve this phenomenon since the images would almost be perpendicular to the AAA outer wall as long as the aneurysm is straight. Better still, curved radial planes (i.e. revolving around the centerline of the aorta) would display images almost perpendicular to the AAA outer wall even in tortuous AAA (31, 36). An illustration of a stretched longitudinal view and perpendicular axial view is shown in Figure 3.3.

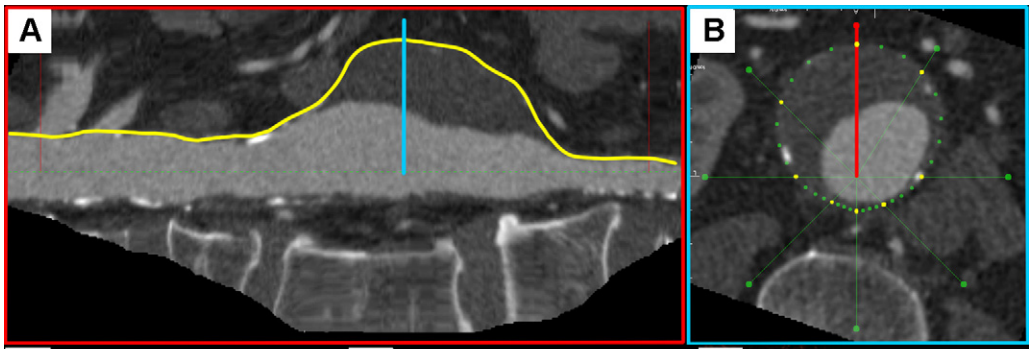

Figure 3.3: AAA model in a 72-year-old man with a Dmax of 6.97 cm.
(A) Stretched longitudinal view of the path-based image. This path may be edited, if needed. The blue line represents the corresponding axial view. (B) Axial view shows AAA optimized path obtained by automated segmentation of aneurysm wall. The green lines represent the radial planes that can be edited in the orthogonal views. The red line represents the active stretched longitudinal view.

Since the aorta bifurcates, one of the two common iliac arteries (right or left) must be chosen for centerline. The curved radial planes will then revolve around the centerline drawn at the center of the aorta and the chosen iliac artery.

Fiduciary markers must be selected for co-registration of different examinations. Instead of bone markers discussed above, markers can be positioned in the aorta itself. For example, fiduciary markers could be positioned between the renal arteries and at the aortic bifurcation for co-registration of different AAA meshes over time and calculation of volume changes.

Output

Once the wall and lumen segmentations are completed, the segmented envelope should be exported and saved as a mesh that can be read by other software. Given the amount of work that goes into segmentation, there is an inherent benefit to use the resulting meshes for wall stress simulations.

3.2 Segmentation Workflow

From 2006 until 2012, our team has developed a semi-automated segmentation software that addresses the vast majority of segmentation needs discussed above.

The main steps of our method are illustrated in Figure 3.4 and discussed below.

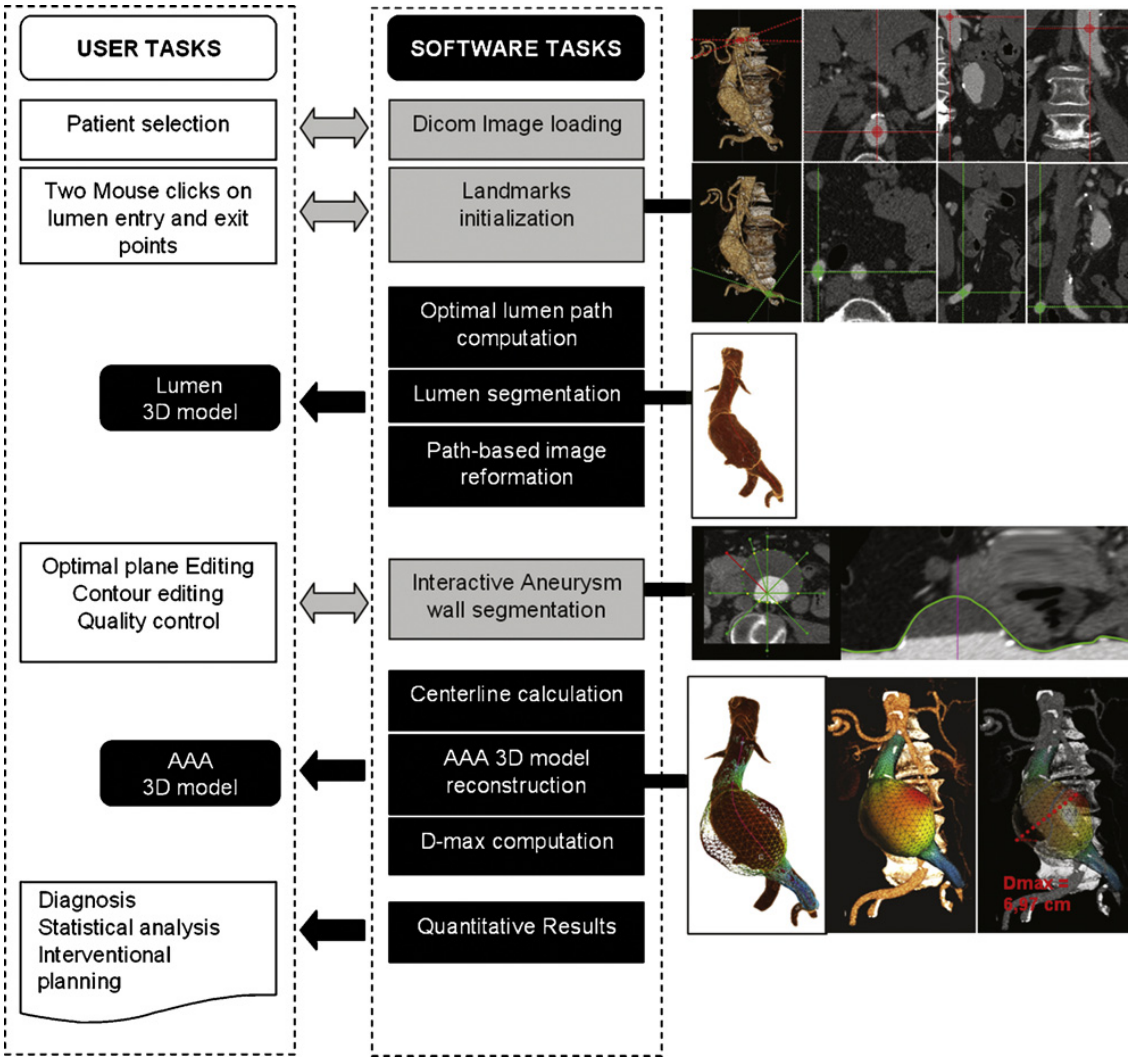

Figure 3.4: Overview of software interaction.
User tasks, software tasks and graphic display are illustrated in the left, middle and right columns, respectively (36).

After loading the CT dataset in DICOM format, the interactive method consists of the following steps:

1) The user clicks on two anatomical landmarks: an entry point on the supra-renal aortic lumen at the level of the celiac trunk and an exit point on one of the common iliac arteries. It is preferable to select the iliac artery that is best aligned with the aortic centerline to prevent distorsions of the stretched longitudinal view of the path-based image.

2) The software will then compute the optimal lumen path and automatically segment the 3D lumen using an hybrid central processing unit (CPU)-graphics processing unit (GPU) implementation of the Dijkstra's and Bellman-Ford's shortest paths algorithm (31). Alternatively, if the CT study is unenhanced, it is possible to create a manual path by creating a centerline from several clicks (approximately seven) from the celiac trunk to one of the iliac arteries.

3) The software will compute a smooth luminal path and GPU-based image reformation. These images are radial reformations passing through the lumen centerline straightened in the middle of the image. If this path has reconstruction artifacts, it can be corrected manually. Otherwise, the user proceeds to the next step.

4) The user performs semi-automated aneurysm wall segmentation on 4 to 8 radial image reformations along the path axis with an active contour process. With this reconstruction plane, it is easier to delineate the AAA wall even when the mural thrombus and adjacent soft tissues have similar densities (Hounsfield units).

5) A key feature is that the software interpolates the aortic contours between the radial image reformations, which dramatically shortens the segmentation time. The user may interactively validate the contour and perform editing, but only if needed (Figure 3.5).

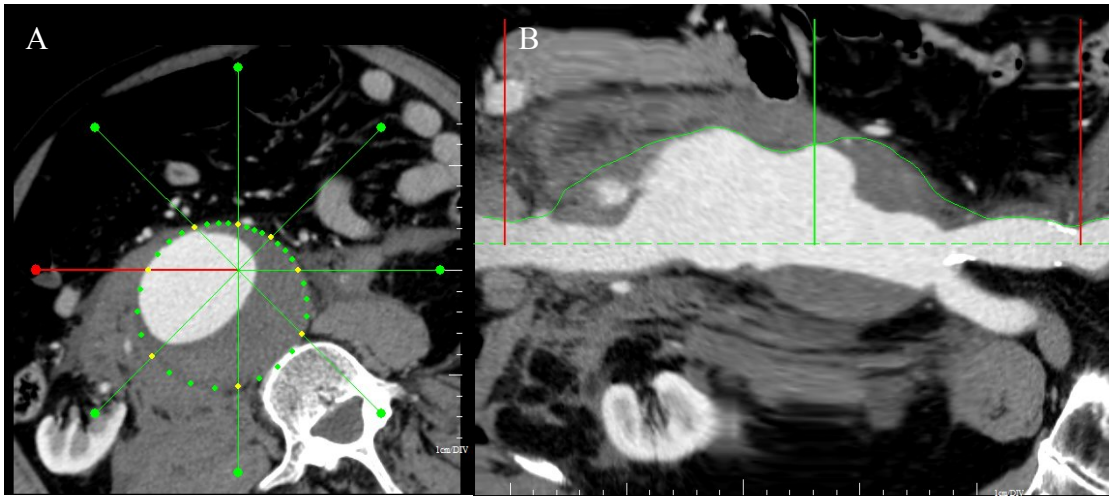

Figure 3.5: Radial and longitudinal stretch views for segmentation.
(A) Radial image reformation. This image is perpendicular to the centerline and displays 8 radial lines. (B) Longitudinal stretched view. This image corresponds to the radial plane highlighted in red in the first image. The user corrects the segmentation by modifying the outer wall contour (green line). Interactive navigation between radial planes facilitates delineation of the outer wall, even when the thrombus density is remarkably similar to the adjacent soft tissues.

6) Once the user approves the segmentation, the software computes a centerline based on the outer wall of the AAA and displays a 3D mathematical model of the AAA with distinct thrombus and lumen reconstructions.

7) Finally, the software performs automated calculation of the Dmax perpendicular to the new central line was processed (Figure 3.6). Thrombus, lumen, and whole AAA volumes are also computed. The work session can be saved at any time in extensible markup language (XML) format.

The success of this interactive or supervised method lies in the complementarity between user and software tasks. The details of the mathematical method are provided in the following reference by Kauffmann *et al*. (31). A patent was filed for this method on June 11, 2008 and issued on Oct 18, 2011 for this invention (103).

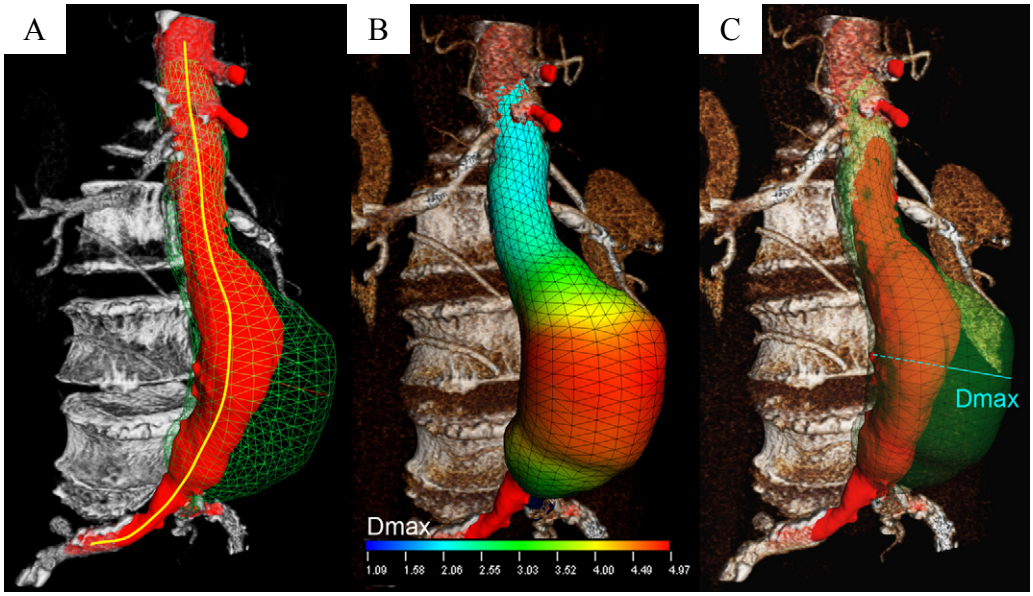

Figure 3.6: AAA model in a 72-year-old man with a Dmax of 6.97 cm.
(A) AAA surface model with optimized path (yellow line), lumen (red) and outer-wall mesh (green) of the AAA. (B) Dmax values are color-coded at each location: the smallest diameters are represented in blue and the largest in red. (C) The automatically calculated Dmax is highlighted by the blue dashed line (30).

Optimization

To shorten the computing time, some tasks were implemented and executed on the GPU. This hybrid CPU-GPU approach leverages the rapid increase in GPU programmability and capability in recent years. Computationally demanding, complex problems are mapped to the GPU. In our implementation, two algorithms are GPU-based: the automatic lumen segmentation and the curved image reformation. In a recent publication by our team, the average segmentation time was 3.0 min ± 1.1 min per case (30).

3D modeling

The 3D mathematical model (mesh) generated by this method can be exported in VRML format and read by a modeling software or interactive programming environment

such as MatLab to perform separate Dmax and volume analysis, comparison between baseline and follow-up examinations, extraction of geometrical parameters (such as size, topology, shape asymmetry and tissue anisotropy). By extension, the lumen and wall meshes can be exported to a mechanical simulation software for wall stress and rupture risk assessment.

Graphical user interface

Over time, additional tools were added in MatLab for rapid quality control, such as ability to select groups of patients (contrast-enhanced vs. unenhanced, with or without stent-graft, with or without rupture, etc.), display patient metadata, display results in table format for multiple reading sessions and observers, extract geometrical parameters, automatically calculate commonly performed statistics to detect outliers (intra- and inter-observer reproducibility by intra-class correlation-coefficient, coefficient of variability, Bland-Altman plots), record comments to improve error traceability, ability to export figures as PDF for publication.

3.3 Software Validation Strategy

As part of our research program, we devised a strategy to validate our AAA segmentation software. Since it is impossible to validate the maximal diameter or volume of an AAA obtained by segmentation with *ex vivo specimen* due to aorta collapse, the validation must instead be performed *in vivo* against a surrogate reference standard.

As a first step, we evaluated the reproducibility of different manual Dmax measurement methods reported in the literature to identify the most reproducible method that would subsequently be used as our Dmax reference standard. This will be described in Section 3.4, which will summarize the findings of the paper published by Dugas *et al*. (102).

As a second step, we compared the cross-sectional reproducibility and accuracy of Dmax measurements using segmentation software against double-oblique MPR manual

measurements as reference standard. This will be described in Section 3.5, which will summarize the findings of the paper published by Kauffmann *et al*. (36).

As a third step, we assessed the longitudinal reproducibility of software-determined diameter, volume, and growth over time. This will be described in Section 3.6, which will summarize the findings of another paper published by Kauffmann *et al*. (30).

As a fourth step, we assessed the impact of contrast injection and stent-graft implantation on volume reproducibility. This will be described in Section 3.7, which summarizes the findings of a study performed by Morin-Roy *et al*. (104).

As a fifth step, we examined geometrical indices reported in the literature, implemented these in our segmentation software. This is will be described in Section 3.8. We will summarize the clinical benefits of our segmentation software in Section 3.9.

Finally, we performed a pilot case-control study in which we compared the geometrical indices of symptomatic or ruptured AAA vs. control subjects prior to elective EVAR or open surgical repair. This will be described in Section 4.0.

3.4 Reproducibility of Manual Dmax Measurements

In this section, we summarize the findings of the paper published by Dugas *et al*. (102), entitled "Reproducibility of Abdominal Aortic Aneurysm Diameter Measurement and Growth Evaluation on Axial and Multiplanar Computed Tomography Reformations".

Introduction

Indications to treat patients with AAA rely, for the most part, on the maximal diameter. Assessment of growth also relies on Dmax difference between baseline and follow-up studies. Hence, the precise measurement of Dmax is critical for appropriate patient management.

Yet, numerous different ways of measuring Dmax have been reported in the literature. Despite the numerous approaches reported in the literature, no study previously compared the reproducibility of these different ways of measuring AAA Dmax.

Therefore, the primary aim of this study was to assess the cross-sectional inter- and intra-observer reproducibility of all previously reported methods for measuring Dmax. The secondary aim was to evaluate the longitudinal reproducibility of these methods over time. The underlying rationale was that the identification of the most reproducible method would subsequently serve as the reference standard for Dmax calculation in cross-sectional and longitudinal studies.

Materials and Methods

We performed a retrospective study of 40 patients with AAA > 3.5 cm who previously underwent at least 2 multidetector CTs at least 6 months apart. Three observers (one senior resident and two vascular interventional radiologists with >10 years of experience), blinded to previous radiological reports and to each other, measured the Dmax on each of the 80 studies (2 x 40) on a workstation.

The seven different Dmax measurement methods reported in the literature and evaluated in this study included: antero-posterior diameter, transverse diameter, maximal diameter in the axial plane, diameter perpendicular to axial Dmax, diameter perpendicular to the long axis on coronal MPR, diameter perpendicular to the long axis on sagittal MPR, and diameter perpendicular to the long axis on double-oblique (orthogonal) reformation (Figure 3.7).

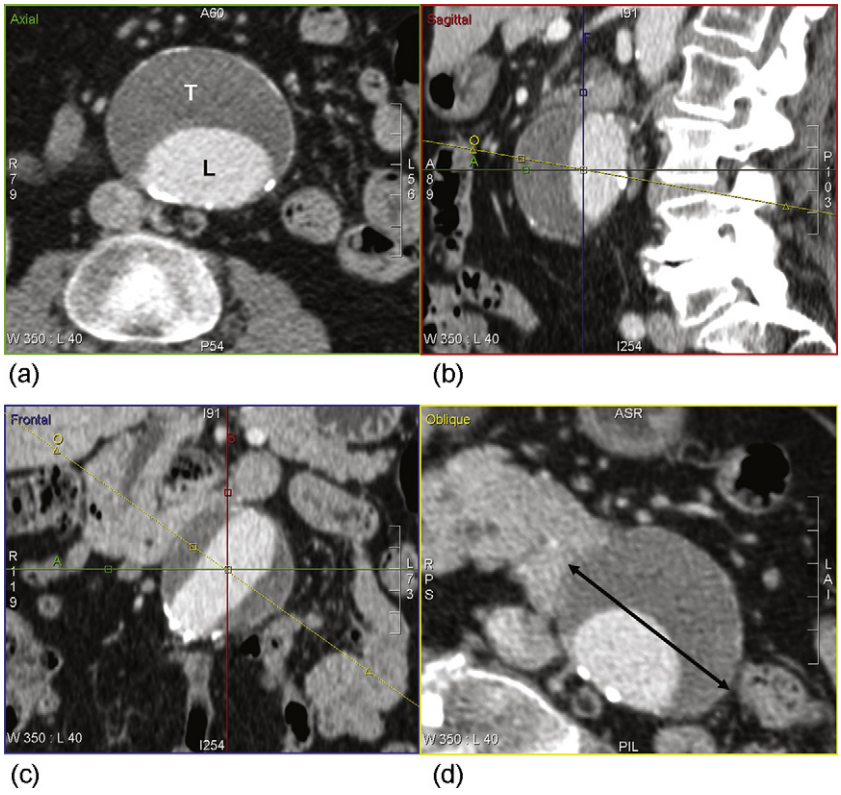

Figure 3.7: Sequential approach to double-oblique (DO) reformation method.
(A) Axial contrast-enhanced CT in arterial phase shows abdominal aortic aneurysm. Lumen (L) is opacified by IV contrast. Large mural thrombus (T) fills part of the aneurysm. (b) and (c) MPR views of the aneurysm. Red line represents sagittal plane (b); blue line, coronal plane, green line, axial plane and yellow line, the user-defined DO plane (d), which is perpendicular to aneurysm wall in sagittal and coronal planes. Orthogonal Dmax is measured manually on DO (line with double-arrows) (36).

To assess intra-observer reproducibility, two of the three observers repeated all their measurements on the whole dataset at least 4 weeks after the original reading session.

Difference between methods was assessed by one-factor repeated-measures analysis model using PROC MIXED, with Bonferroni correction for multiple comparisons. Reproducibility was determined by intraclass correlation coefficient (ICC), reader agreement by Bland-Altman analysis

Results

For all observers, the maximal diameter measured on the axial plane overestimated the Dmax, as compared with the double-oblique method (orthogonal Dmax).

Cross-sectionally, the highest inter-observer ICCs were observed with double-oblique (orthogonal Dmax) and transverse methods (both 0.972) at baseline and the orthogonal (0.973) and sagittal MPR images at follow-up (0.977) (Table 3.1).

Measurement method	APD	TransD	AxialDmax	ShortaxisD	CoroMPRD	SagMPRD	OrthoD
ICC baseline (95% CI)	0.961 (0.935–0.978)	0.972 (0.948–0.985)	0.962 (0.923–0.981)	0.940 (0.901–0.965)	0.950 (0.917–0.972)	0.969 (0.948–0.983)	0.972 (0.943–0.986)
ICC follow-up (95% CI)	0.924 (0.877–0.956)	0.955 (0.925–0.974)	0.961 (0.932–0.978)	0.933 (0.890–0.961)	0.968 (0.947–0.982)	0.977 (0.961–0.987)	0.973 (0.954–0.985)

[a] Three observers, 40 CT examinations at baseline and FU, first reading

Table 3.1: Intraclass correlation coefficient by diameter measurement method at baseline and follow-up (102).

Longitudinally, the highest inter-observer ICCs for documenting AAA progression between baseline and follow-up were observed with the double-oblique method (orthogonal Dmax) (0.833).

All diameter measurement methods showed high intra-observer reproducibility (>0.958). Orthogonal Dmax provided excellent intra-observer reproducibility (0.969-0.985).

On the Bland-Altman analysis comparing mean error measures between the double-oblique Dmax method (orthogonal Dmax) and all other measurement methods of assessing aneurysm progression, the 95% range of agreement was always $< \pm 4.0$ mm.

Discussion

Our finding that maximal diameter in the axial plane is higher than double-oblique orthogonal D max values was consistent with prior findings in the literature (105, 106).

Overall, orthogonal Dmax measurements were among those providing the highest inter-observer reproducibility at baseline and follow-up, and excellent intra-observer reproducibility.

In the absence of an absolute gold standard, orthogonal Dmax is favored over methods because it approaches the concept of aortic centerline. It is minimally more time-consuming because it requires multiplanar reconstructions. However, unlike measurements on axial images, which overestimate the diameter, orthogonal Dmax is independent of the long-axis angle of the aneurysm relative to the axial plane.

For further details on this study, the readers are referred to the full manuscript in Appendix 2.

3.5 Clinical Validation of Software vs. Manual Dmax Measurements

In this section, we summarize the findings of the paper published by Kauffmann *et al*. (36), entitled "Clinical validation of a software for quantitative follow-up of abdominal aortic aneurysm maximal diameter and growth by CT angiography".

Introduction

In section 3.2, we described a novel semi-automated segmentation method developed at our institution. To validate the segmentation result, we must first compare it with an established Dmax measurement method. In section 3.4, we have shown that manual double-oblique Dmax was theoretically closest to reality and provided the highest overall inter- and intra-observer repeatability.

Therefore, the aim of this study was to assess the cross-sectional reproducibility and accuracy of software-determined AAA Dmax, using double-oblique MPR manual measurement as reference standard.

Materials and Methods

We performed a retrospective study on the same dataset as described in Section 3.4, which includes 40 patients with AAA > 3.5 cm who previously underwent at least 2 multidetector CTs at least 6 months apart.

All the CT examinations were processed by an experienced CT technologist using our segmentation software (Figure 3.3), blinded to the radiology report and to the results of 3 radiologists who performed the manual segmentations.

To assess intra-method reproducibility, the same technologist repeated the segmentation on the whole dataset at least 4 weeks after the original segmentation session.

Inter-observer and intra-observer reproducibility of orthogonal Dmax measurements were determined by intraclass correlation coefficient (ICC). Agreement of semi-automated orthogonal Dmax measurements with the manual double-oblique reference standard was determined by Bland-Altman analysis.

Results

Inter-observer reproducibility for manual measurements of D-max by radiologists was excellent at baseline (ICC = 0.979) and follow-up (ICC = 0.975) (Table 3.2).

Table 3.2: Inter-observer reproducibility of manual Dmax measurements (36).

Reading	Baseline		Follow-up	
	ICC (95%)	CI (two-sided)	ICC (95%)	CI (two-sided)
First	0.979	0.954–0.984	0.975	0.955–0.985
Second[a]	0.981	0.964–0.990	0.987	0.9765–0.993

[a] Radiologist 2 had not repeated the measurements twice.

Intra-observer reproducibility for Dmax measurements was excellent for software (ICC = 0.992) and for the two radiologists who performed repeated measurements (ICC = 0.985 and 0.969, respectively) (Table 3.3).

Table 3.3: Intra-observer reproducibility of software and manual Dmax measurements (36).

Observers	Baseline		Follow-up	
	ICC (95%)	CI (one-sided)	ICC (95%)	CI (one-sided)
Radiologist 1	0.985	0.974	0.984	0.973
Radiologist 3	0.969	0.948	0.979	0.965
Software	0.992	0.987	0.990	0.983

Bland-Altman analysis revealed strong agreement between semi-automated and manual Dmax measurement methods (Figure 3.8). The mean bias between the two methods was < 1 mm and the 95% range of agreement were within ± 4 mm. Using a clinically meaningful threshold of ≤ 5 mm, the software and manual measurements were within 4 mm in 40/40 instances at baseline. Stated differently, the results were always interchangeable between the two measurement methods.

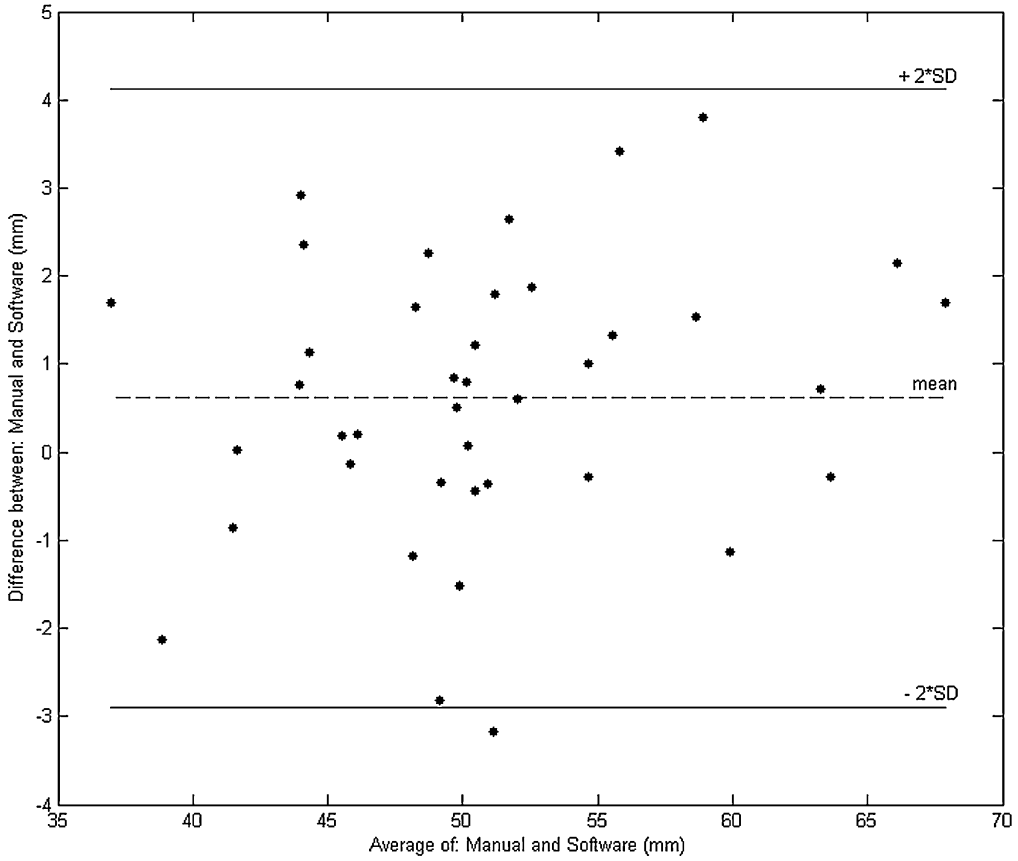

Figure 3.8: Inter-reader agreement.

Bland-Altman plot of the mean of readings 1 and 2 for software and radiologist at baseline. The average of each pair of measurements is plotted against their difference. The range of agreement (solid lines) was defined as the bias ± 2 SD, where SD is the corrected standard deviation of the differences between the two methods (36).

Discussion

Our findings, which indicated feasibility, excellent reproducibility of software-determined Dmax, and excellent agreement with manually-determined Dmax measurements, validate the use of this orthogonal Dmax measurement method for clinical use.

Since this method is delegated to a CT technologist, it has the potential to become a reproducible method for determining Dmax. In addition, since the entire AAA envelope is modeled, it opens the possibility of performing AAA volume and morphology analysis. In conclusion, our results indicated higher reproducibility for the semi-automated software than manual double-oblique method for determining orthogonal Dmax. In conclusion, we validated the use of a software method for segmenting AAAs and calculating the Dmax. Given the additional time required for segmentation, we must however demonstrate additional benefits of our software before it can be used clinically.

For further details on this study, the readers are referred to the full manuscript in Appendix 3.

3.6 Reproducibility and Accuracy of Software Dmax and Volume Growth Measurements

In this section, we summarize the findings of the paper published by Kauffmann *et al*. (30), entitled "Measurements and detection of abdominal aortic aneurysm growth: Accuracy and reproducibility of a segmentation software".

Introduction

In the setting of AAA follow-up of patients who have undergone EVAR, it has been suggested that volume changes are more sensitive than diameter changes in the detection of aneurysm growth after EVAR (29, 101). A 2% volume increase has been suggested by Bley *et al*. as a threshold for detection of endoleaks after EVAR (101).

Hence, the aim of this study was to evaluate the longitudinal inter and intra-observer reproducibility of software-determined Dmax and volume changes over time.

Materials and Methods

We performed a retrospective study of 27 patients with AAA $\geq$ 4.0 cm who previously underwent at least 2 multidetector CTs at least 4 months apart. Four observers (3 first-year medical students with no prior experience in imaging and one senior radiologist with 20 years of experience), blinded to previous radiological reports and to each other, segmented aneurysms on each of the 56 studies (2 x 27) using our software.

To evaluate longitudinal diameter and volume changes, baseline and follow-up CTs co-registration was based on mutual information and confirmed by visual inspection (Figure 3.9).

To assess intra-observer reproducibility, the senior radiologist repeated the segmentation on the whole dataset at least 4 weeks after the original segmentation session.

Intra-observer reproducibility (senior radiologist) and inter-observer (4 readers) was assessed by intraclass correlation coefficient for software-based D-max, volume, and their

growth. Agreement between untrained medical students and the senior radiologist was evaluated by Bland-Altman analysis.

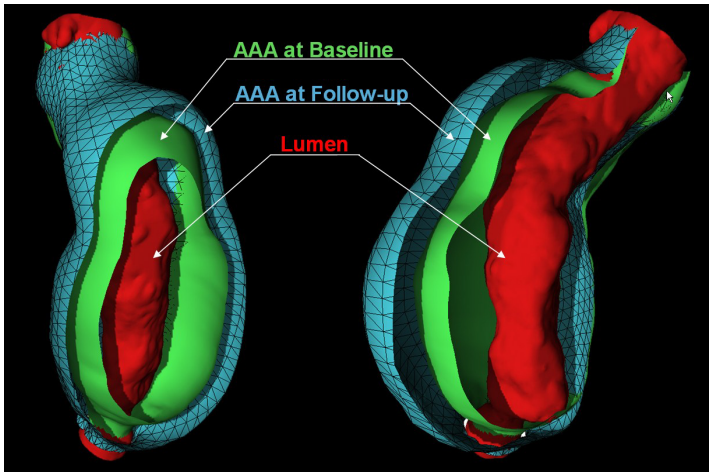

Figure 3.9: 3D representation of AAA growth over time.
Baseline and Follow-up CTA of the same patient were segmented and then co-registered. Since the two exams are co-registered, the AAA volumes can be measured on exactly the same aorta section, and Dmax and volume progression can be quantitatively evaluated (31).

Results

Intra-observer reproducibility was excellent, with ICC = 0.997 for Dmax and ICC = 1.000 for volume measurements performed by the senior radiologist. For medical students, the inter-observer reproducibility was excellent, at least ICC = 0.995 for Dmax and ICC = 0.999 for volume (Table 3.4).

Observers	Baseline	Follow-up	*D*-max			Volume		
			Absolute growth	Relative growth	Baseline	Follow-up	Absolute growth	Relative growth
Intra-observer reproducibility								
R-R	0.997 (0.991–0.999)	0.999 (>0.997)	0.991 (0.972–0.997)	0.991 (0.972–0.997)	1.000 (>0.999)	1.000 (1.000)	0.999 (>0.996)	0.995 (0.985–0.998)
Inter-observer reproducibility								
R-T1	0.989 (0.976–0.995)	0.997 (0.993–0.998)	0.968 (0.931–0.985)	0.959 (0.911–0.981)	0.999 (>0.998)	0.999 (>0.999)	0.996 (0.991–0.998)	0.989 (0.977–0.995)
R-T2	0.994 (0.988–0.997)	0.995 (0.988–0.998)	0.964 (0.922–0.983)	0.959 (0.912–0.981)	0.999 (0.998–0.999)	1.000 (>0.999)	0.998 (0.995–0.999)	0.993 (0.985–0.997)
R-T3	0.989 (0.977–0.995)	0.996 (0.992–0.998)	0.947 (0.885–0.975)	0.941 (0.873–0.973)	0.999 (0.998–1.000)	0.999 (>0.999)	0.997 (0.994–0.999)	0.994 (0.986–0.997)
All	0.995 (0.990–0.997)	0.998 (0.996–0.999)	0.976 (0.957–0.988)	0.972 (0.950–0.986)	0.999 (>0.999)	1.000 (1.000)	0.999 (0.997–0.999)	0.996 (0.993–0.998)

Table 3.4: Intra- and inter-observer reproducibility Dmax and volume growth measurements (36).

Bland-Altman analysis revealed good agreement between the medical students and the senior radiologist, for Dmax and for volume (Figure 3.10). Dmax comparison between medical students and the senior radiologist revealed an accuracy <1 mm for Dmax, < 1 mm for diameter growth, and <1% for relative diameter growth. Volume comparison between medical students and the senior radiologist revealed an accuracy <2 ml for volume, <1 ml for volume growth, and <1% for relative volume growth. Relative volume growth (17.3%) was higher than relative Dmax progression (8.0%).

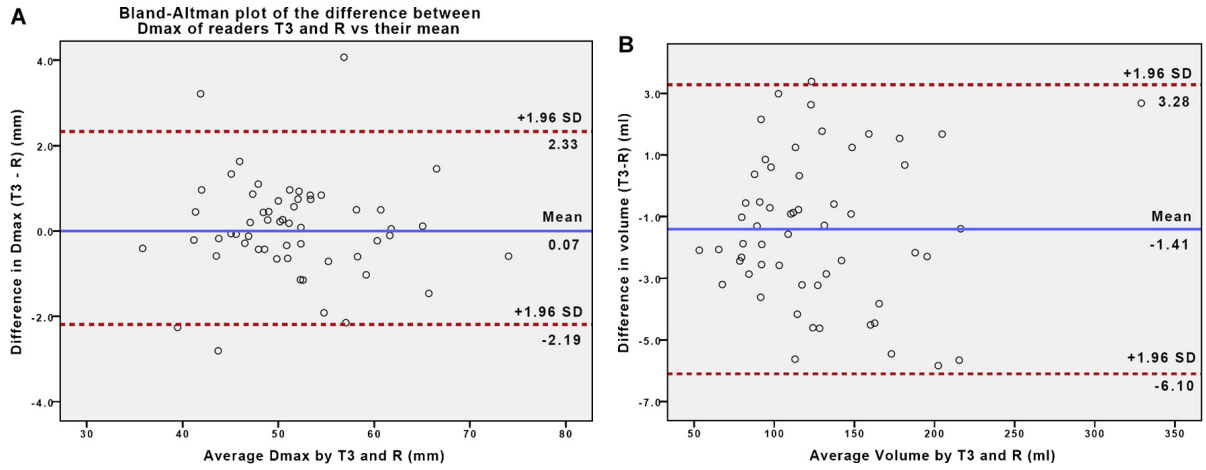

Figure 3.10: Inter-reader agreement for volume measurements.
(A) Bland–Altman plot of the difference between Dmax measurements by senior radiologist (R) and third medical student (T3) vs. their mean. (B) Bland–Altman plot of the difference between volume measurements by senior radiologist (R) and third medical student (T3) vs. their mean. Range of agreement (solid lines) was defined as the bias ± 2 SD (30).

Discussion

Our results demonstrated that AAA volume measured by a semi-automated software was highly reproducible and accurate, as shown by the excellent agreement between novice readers with little formal training and an experienced radiologist. This suggests that AAA segmentation can be delegated to CT technologists.

We have also shown that AAA segmentation for volume follow-up was more sensitive than Dmax follow-up, while providing an equivalent reproducibility. This suggests that volume measurement may improve the sensitivity for early detection of endoleaks.

For further details on this study, the readers are referred to the full manuscript in Appendix 4.

3.7 Impact of Contrast Injection and Stent-graft Implantation on Volume Reproducibility

In this section, we summarize the findings of the study performed by Morin-Roy *et al*. (104), entitled "Abdominal aortic aneurysm segmentation on CT angiography: Optimization of a semiautomated software, impact of contrast injection, and stent-graft implantation on volume measurements reproducibility".

Introduction

It is estimated that 35% of patients with AAA have co-existent renal failure (45). In these patients, an unenhanced CT must be performed because of iodinated contrast nephrotoxicity.

Unenhanced CT creates an additional challenge: low contrast between AAA thrombus and adjacent tissues (Figure 3.2). Previously, a manual segmentation technique was suggested for unenhanced CTA (107).

Previously, we validated a segmentation software with contrast-enhanced CTA (36), but not on unenhanced studies or in patients post-EVAR who require volume surveillance.

Therefore, the aim of this study was to evaluate the impact of contrast injection and stent-graft implantation on volume reproducibility.

Materials and Methods

We performed a retrospective study of 80 patients with AAA > 4.0 cm. Patients selection was designed to obtain 20 cases in each of these 4 categories: contrast-enhanced with stent-graft (C+SG+), contrast-enhanced without stent-graft (C+SG-), unenhanced with stent-graft (C-SG+), and unenhanced without stent-graft (C-SG-) (Figure 3.11). Three medical students and one senior radiologist, blinded to previous radiological reports and to each other, performed the segmentations.

To assess intra-observer reproducibility, the three students repeated the segmentation on the whole dataset at least 4 weeks after the original segmentation session.

Inter-observer and intra-observer reproducibility of Dmax measurements were determined by intraclass correlation coefficient (ICC). Agreement was determined by Bland-Altman analysis. Identification of factors that could induce systematic volume measurement variations was evaluated by linear mixed model.

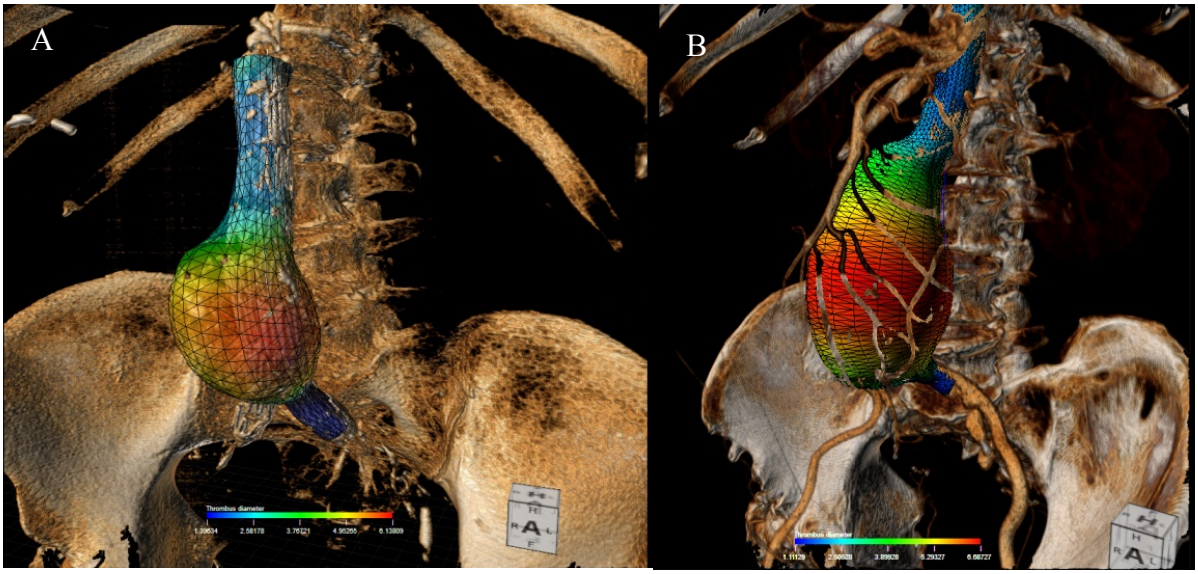

Figure 3.11: 3D renderings of AAA models.
(A) Unenhanced study with stent-graft and (B) unenhanced study without stent-graft.

Results

Inter-and intra-observer reproducibilities were excellent, with ICCs ≥ 0.99 for the four groups (C+SG+, C+SG-, S-SG+, C-SG-). Bland-Altman analysis showed good agreement between the senior radiologist and medical students, with absolute volume differences of -1.15 mL (95% confidence interval (CI): -8.66, 6.36 mL). The relative volume difference was -0.81% (95% CI: -5.74, 4.13%).

The linear mixed model did not reveal any factor (C+/C- or SG+/SG-) inducing systematic volume variations ($p = 0.4$).

Discussion

Our results demonstrated that segmentation was successful for all AAAs in each group. The reproducibility was excellent, regardless of presence/absence of contrast injection or presence/absence of stent-graft.

We have also shown that the magnitude of the volume difference between the senior radiologist and medical students remained within an acceptable range (± 5.21 mL or ± 4.9%).

Bley *et al*. (101) suggested that a volume growth of 2% or more required further investigation for an endoleak. This 2% threshold was based on the percent volume difference on repeated volumetric measurements performed by operators with varying degrees of experience in a study performed by Caldwell *et al.* (108). In the cited study, the average relative volume difference was 1.2% for the experienced reader, 3.2% for the moderately experienced reader, and 6.0% and 5.8% for the two readers with least experience.

We believe that this 2% arbitrary threshold derived from a *transversal* repeatability study cannot be extrapolated to longitudinal volumetric assessment. This threshold does not take into account the fact that measurement errors add up when comparing two examinations.

This level of precision cannot be currently obtained with our software method. Instead, we suggest using a more conservative growth threshold, such as 10% volume growth or 5 mm Dmax growth for detection of endoleak. These thresholds are justified by the 95% repeatability coefficients that we found in a *longitudinal* study, which were < 3 mm for Dmax and < 6% for relative volume growth using our software (30).

3.8 Geometrical Indices

So far, we have focused on Dmax and volume for quantification of AAA size. It is worthwhile to note that Dmax is a simple 1D measurement performed on 2D images and that volumetry requires either summation of organ contour segmented on consecutive 2D images or an advanced segmentation method based on curved multiplanar images.

Once an AAA has been segmented for volumetry calculation, there is an inherent benefit in reusing the resulting mesh to compute geometrical parameters or perform mechanical stress simulations. This may be clinically relevant to identify which AAAs pose a significant risk of rupture despite their small size.

Martufi *et al*. have proposed and evaluated a series of 1D size, 2D shape, 3D size, 3D shape, and second-order curvature-based indices to quantify AAA geometry (91). Even the authors acknowledge that "It is unlikely that any one of the proposed geometrical indices alone would be a reliable index of rupture risk or a threshold for elective repair. Rather, the complete geometry and a positive correlation of a set of indices should be considered to assess the potential for rupture."

The authors must be lauded for their thorough work and formal definitions. Rather than propose a competing system, we adopted their definitions, made minor modifications, and integrated their geometrical indices to our segmentation software.

One-dimensional indices include diameter, length, height and centricity measurements along centerline or cross sectional images to characterize neck and aortic sac geometry. 2D indices include Dmax-height ratio, Dmax-Dneck ratios, AAA height/neck ratio, bulge location, asymmetry factor, and tortuosity. 3D measurements include volume, surface and ratio of volume measurements. Tridimensional shape indices were used to estimate the shape of AAA surface and fusiform shape. Finally, second order curvature-based indices include formulas to estimate AAA curvatures (elliptic, hyperbolic, regularity). The mathematical definitions geometric indices are described in detail in the Appendix in Figure A.1 and Tables A.1 to A.5 of the Appendix.

3.9 Potential Clinical Applications of Segmentation Software

By means of our research program, we have validated our AAA segmentation software. We have demonstrated the feasibility of a semiautomated segmentation method. This method is rapid, typically requiring to 3-5 minutes to perform a process that previously took more than one hour to perform per case (94, 95).

We have shown that it is possible to segment and simultaneously display the AAA lumen, thrombus, and outer wall. It is possible to extract the orthogonal Dmax and volume from the resulting 3D model.

We validated the accuracy and reproducibility of Dmax measurements derived from AAA segmentation against a manual reference standard. We performed this validation both cross-sectionally and longitudinally.

Previously limited to the realm of research, a rapid segmentation method now makes 3D modeling a clinically feasible option for cross-sectional and longitudinal volume assessment.

This segmentation method is robust, on unenhanced or contrast-enhanced CTA, without or with stent-graft. This integrated segmentation solution allows co-registration of baseline and follow-up studies. This feature provides the ability to detect AAA growth and visually display longitudinal volume changes.

In addition to traditional Dmax and volume measurements, we recently incorporated geometric parameters that describe the AAA morphology. In the next section, we will report a pilot case-control study in which we compare the geometrical indices in cases with symptomatic or ruptured AAA and controls awaiting EVAR or open aortic repair.

4 Morphologic Evaluation of Ruptured and Unruptured AAA by 3D Modeling

4.1 Abstract

Purpose: To identify geometric indices that are associated with abdominal aortic aneurysm (AAA) rupture at computed tomography (CT).

Methods: This study had institutional board approval from the two participating universities. This retrospective case-control study involved 63 cases with ruptured or symptomatic AAA and 94 controls with asymptomatic AAA. The computed tomography of these patients with AAA were segmented under the supervision of a senior image analyst. The AAA three-dimensional (3D) models were generated and used for the calculation of 27 geometric indices divided in 5 classes: one-dimensional size indices, two- dimensional size indices, 3D size indices, 3D shape indices and second order curvature-based indices. On the basis of the results of univariate analysis, Student's t-test and Pearson's chi-square test, and multivariable sequential logistic regression analyses with a forward stepwise model selection based on likelihood ratios, a traditional model based on sex and maximal diameter (Dmax) was compared with a model that also incorporated geometric indices while adjusting for sex and Dmax. Receiver operating characteristic (ROC) curves were calculated for these two models to evaluate their classification accuracy.

Results: Univariate analysis revealed that sex ($P = 0.024$), Dmax ($P = 0.001$) and 14 other geometric indices were associated with AAA rupture at $P < 0.05$. In the multivariable analysis, adjusting for sex and Dmax, the AAA with a higher bulge location ($P = 0.020$) and higher mean averaged surface area ($P = 0.005$) were associated with AAA rupture.

With these two geometric indices, the area under the ROC curve showed a trend toward improvement from 0.674 (95% confidence interval (CI): 0.584 - 0.765) to 0.752 (95% CI: 0.673 - 0.832) ($P < 0.001$). Our predictive model showed comparable sensitivity (63.5 % versus 60.3 %) and specificity (78.7 % versus 76.6 %) with current treatment criteria based on diameter and sex at the point optimizing the Youden index (sensitivity + specificity - 1) on the ROC curve.

Conclusion: Two geometric indices derived from AAA 3D modeling were independently associated with AAA rupture. The addition of these indices in a predictive model based on current treatment criteria modestly improved the accuracy to detect aneurysm rupture. Other rheological and mechanical stress parameters may be needed to improve rupture risk prediction.

4.2 Introduction

Abdominal aortic aneurysm (AAA) affects 2% of the elderly population, and the incidence is increasing (1, 109). Rupture is the main complication of untreated AAA with 90% associated mortality (44). The main predictors of rupture risk are the maximal diameter (Dmax) and the expansion rate of the aneurysm. For instance, the annual rupture risk of 6 to 7 cm aneurysm is 10 to 20% (7). Follow up of the AAA is necessary to determine when an intervention is warranted. Based on the rupture risk, mortality rate in elective procedure, and life expectancy of the patient, the American Association for Vascular Surgery (AAVS) in association with the Society for Vascular Surgery (SVS) have issued recommendations regarding AAA treatment (6). The main indications for a procedure are Dmax ≥ 5.5 cm in men, ≥ 4.5-5.0 cm in women, rapid expansion > 1cm/year, or symptomatic AAA.

However, there is a need to revisit the maximum diameter criterion for two reasons. First, the estimated rupture risk of 4.0-4.9 cm AAA is 1.0% per year (11), but may be as high as 12.8% to 23% (10, 110). Second, recent technological advances in segmentation

methods and computer modeling have raised the possibility of patient-specific risk prediction based on AAA geometry (95, 111).

It was previously tedious to perform volumetric analysis of AAA because this required manually delineating the contours of AAA wall and thrombus on hundreds of images. To circumvent this limitation, semiautomated AAA segmentation and 3D modelization software recently developed (30, 31, 36) provide the ability to extract AAA geometric parameters from CT studies (53, 90, 91).

4.1.1 Hypothesis

We hypothesized that the knowledge of AAA geometric parameters, as defined by size and shape indices derived from AAA segmentation, would be helpful to improve the prediction of rupture risk which presently rely on maximal diameter measurement and sex. Since it would be impossible to perform a prospective observational study on AAA rupture risk, we designed a retrospective case-control study comparing ruptured or symptomatic cases with asymptomatic controls awaiting endovascular aortic repair (EVAR) or open surgical repair.

4.1.2 Aim

The purpose of this study was to identify geometric indices that are associated with abdominal aortic aneurysm (AAA) rupture at computed tomography (CT).

4.3 Materials and Methods

4.3.1 Study Design

Our study was approved by the Institutional Review Boards of the two participating hospitals, the Centre Hospitalier de l'Université de Montréal (CHUM) and McGill

University Health Centre (MUHC). Informed consent was waived for this retrospective case-control study.

4.3.2 Study Population

Subjects were eligible in this study if (a) they had an AAA, defined by a Dmax threshold equal or larger than 3.5 cm, (b) underwent a CT during their admission between January 2001 and August 2009, and (c) if the CT was available in DICOM format at one of the two participating centers. This time interval for patient selection was defined to coincide with our PACS records.

Subjects were excluded if (a) their CT had missing images, (b) the structure of the dataset prevented segmentation, or (c) previously underwent aortic open or endovascular repair or bypass surgery.

The medical archives were used to select cases whose main admission diagnosis was ruptured or symptomatic AAA. A registry was used to select controls who underwent elective EVAR or open surgical repair during the same time period. Our dataset consisted of 63 cases with ruptured or symptomatic AAA and 94 randomly selected controls to achieve a 1:1.5 ratio (Fig. 4.1). Eighty-six subjects were identified from the CHUM (33 ruptured or symptomatic/53 controls) and 71 from MUHC (30 ruptured or symptomatic/41 controls).

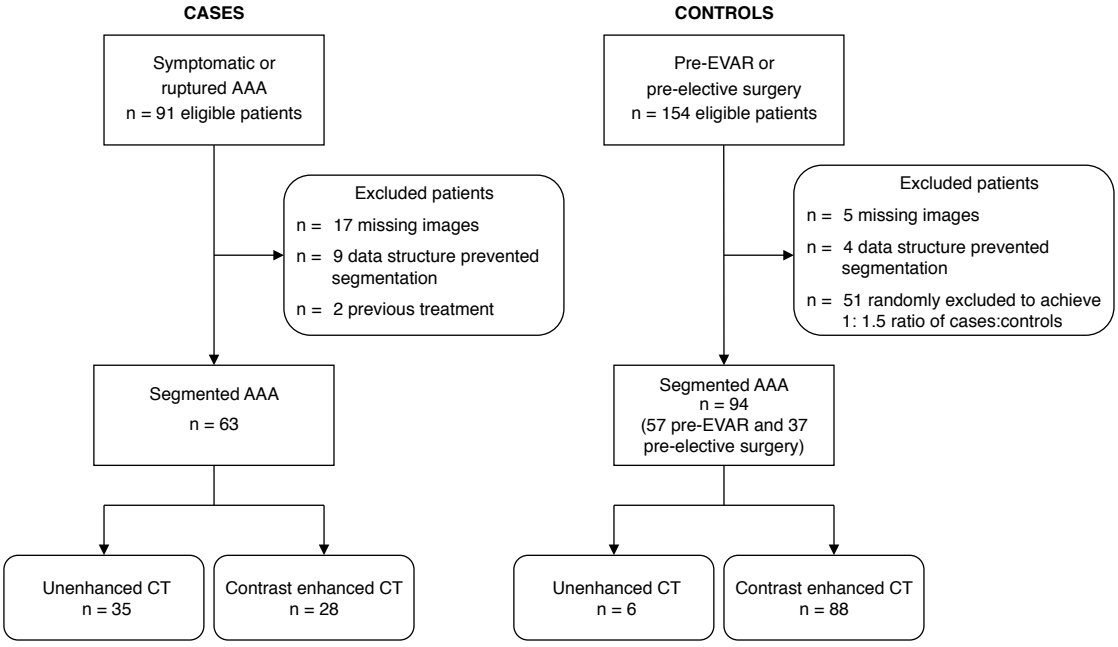

Figure 4.1: Study Flowchart.

4.3.3 Data Collection

Two of the authors (LCG and STP) reviewed the laboratory data, medical records, official surgical notes, and discharge summaries of all patients.

The American Society of Anesthesiologists (ASA) Classification System was used to describe the physical status of our cases and controls subjects. Class 1 indicates a normal healthy patient, class 2 a patient with mild systemic disease, class 3 a patient with severe systemic disease, class 4 a patient with severe systemic disease that is a constant threat to life, class 5 a moribund patient who is not expected to survive without the operation.

4.3.4 CT Imaging Techniques

Studies collected from participating institutions, or referring centers for evaluation of symptomatic AAA, were performed with one-, 4-, 16-, or 64-section CT scanners with acquisition of volumetric data from the entire abdomen and pelvis. A section thickness varied between 0.625 and 5 mm (image interval, 1.0–2.5 mm), depending on scanner type

and local scanning protocol of each hospital, was used. Rotation time varied from 0.5 to 1.0 second. Study parameters were 50–200 mA and 120 kVp. Intravenous contrast agent injection was not systematically used.

4.3.5 Segmentation Methods

Four trained operators, 3 medical students and 1 radiology resident, segmented aneurysms on 157 CT studies under the supervision of a senior image analyst. All segmentations were performed using a semiautomated software method (A3Dmax; Object Research System, Montreal, Canada) previously validated for Dmax and volume measurements (112). The main steps of our interactive method consisted of: (*a*) manual identification of AAA lumen entry at the level of the inferior renal artery at the neck of the aneurysm and exit points at the iliac bifurcation; (*b*) automatic segmentation of lumen; (*c*) automatic aneurysm wall segmentation on curved MPR based on active contour models; (*d*) manual correction of the segmentation on curved MPR and orthogonal views if needed; (*e*) automatic 3D reconstruction of the wall and centerline. For contrast-enhanced CT studies, the segmentation also included the thrombus and lumen (Fig 4.2). The segmentation algorithm is described in detail elsewhere (113).

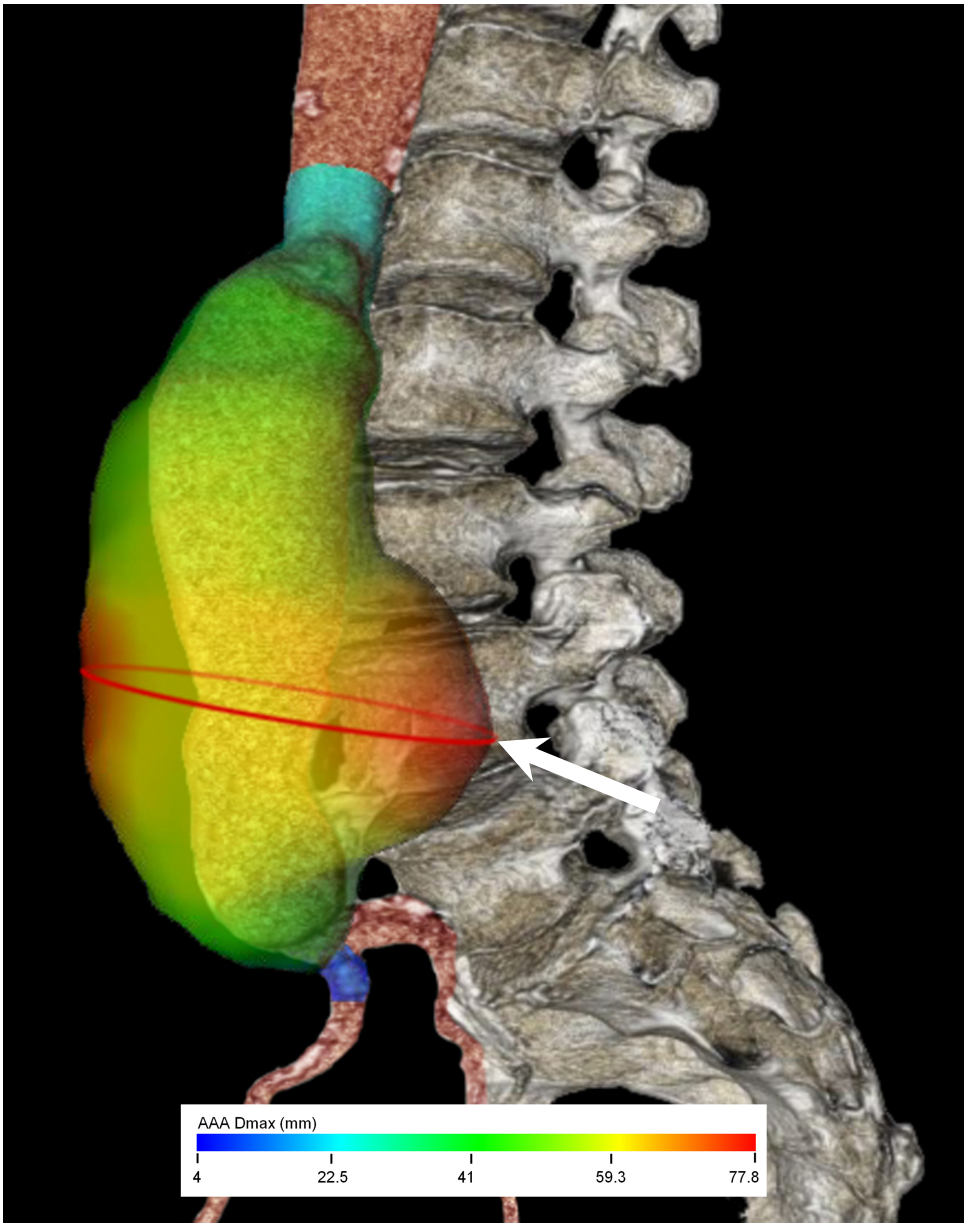

Figure 4.2: 3D volume rendering with parametric maps on model overlay based on a contrast-enhanced CT in a patient with ruptured AAA.

Different diameter values are color-coded, the smallest diameters are represented in blue and the largest in red. The bulge site (white arrow) is concordant with the location of the Dmax (78 mm), indicated by a red circle.

4.3.6 Size and Shape Indices

The analysis of segmentation meshes was performed with custom software (MatLab R2010b; MathWorks, Natick, Mass). The AAA three-dimensional (3D) models were generated and used for the calculation of 27 geometric indices divided in 5 classes: one-dimensional size indices, two- dimensional size indices, 3D size indices, 3D shape indices and second order curvature-based indices (53, 91). One dimensional indices include diameter, length, height and centricity measurements along centerline or cross sectional images to characterize neck and aortic sac geometry. 2D indices include ratio between diameters, diameter and length, heights, diameter and centricity and length and centricity. 3D measurements include volume, surface and ratio of volume measurements. Tridimensional shape indices were used to estimate the shape of AAA surface and fusiform shape. Finally, second order curvature-based indices include complex formulas to estimate AAA curvatures (elliptic, hyperbolic, regularity). The mathematical definitions and figures of geometric indices are described in detail in Appendix I.

4.3.7 Statistical analysis

Subjects.—Descriptive statistics of baseline demographic, clinical data and geometric indices were summarized as a frequency table or as mean ± SD for cases and controls.

Univariate Analysis.—The association between each clinical and geometric parameter and AAA rupture were analysed using independent Student's t-tests or Pearson's chi-square test. The adjusted odds ratio for sex and Dmax with a 95% confidence interval was also calculated.

Multivariate Analysis.—Forward stepwise multivariate logistic regression analyses based on likelihood ratios were performed to predict AAA rupture risk. A traditional model based on sex and Dmax was compared with a model also incorporating geometric indices, while adjusting for sex and Dmax to account for the confounding effects of these known rupture risk factors.

Classification Accuracy.—Receiver operating characteristic (ROC) curves were calculated for these two models to evaluate their classification accuracy. Sensitivity, specificity, with 95% confidence interval (CI) were reported to optimize the Youden index (sensitivity + specificity - 1). Statistical analysis was performed with SPSS (version 20; SPSS Inc., Chicago, IL). Differences were considered significant at the *P* value of .05.

4.4 Results

4.4.1 Clinical Characteristics

Table 4.1 summarizes the demographic and clinical characteristics of the cases and controls. In our dataset, the case subjects had a mean age at diagnostic CT of 74.0 ± 9.2 (standard deviation), and the control subjects had a mean age of 75.1 ± 8.4, with $P = 0.415$. The proportion of male was lower among the case subjects than the control subjects (73.0% vs. 87.2%, $P = 0.024$). Tobacco use was higher among the case subjects than the control subjects, with $P = 0.004$, whereas the two groups were comparable in terms of frequency of associated hypertension, diabetes, volume exhaled at end of first second of forced expiration (FEV1), and family history of AAA. The American Society of Anesthesiologists (ASA) class indicated worse patient fitness before surgery among the case subjects than the control subjects, with $P < 0.001$.

The proportion contrast-enhanced CT examinations was lower among the case subjects than the control subjects (44.4% vs. 93.6%, $P < 0.001$). The other clinical features were not significantly different.

Table 4.1: Patient characteristics in case and control groups (157 subjects)

	Cases (N= 63)	Controls (N= 94)	*P* Value
Demographic			
Age (yr)			
Mean ± standard deviation (SD)	74.0 ± 9.2	75.1 ± 8.4	0.415
Sex			
Male	46/63 (73.0%)	82/94 (87.2)	0.024
Female	17/63 (27.0%)	12/94 (12.8%)	
Weight (kg)	81.9 ± 16.2	82.9 ± 15.6	0.761
Height (cm)	171.3 ± 9.5	172.3 ± 8.6	0.673
Body mass index (kg/m2)	27.3 ± 4.3	27.5 ± 4.0	0.826
History			
Tobacco use			
None	12/48 (25.0%)	20/83 (24.1%)	0.004
Past	9/48 (18.8%)	38/83 (45.8%)	
Current < 1 pack/d	20/48 (41.7%)	22/83 (26.5%)	
Current > 1 pack/d	7/48 (14.6%)	3/83 (3.6%)	
Hypertension values			
Systolic value	125.9 ± 24.3	133.3 ± 20.3	0.162
Diastolic value	72.8 ± 17.7	76.6 ± 13.5	0.309
Hypertension status			
None	16/51 (31.3%)	16/85 (18.85%)	0.176
Controlled	13/51 (25.5%)	16/85 (18.8%)	
Controlled with 2 drugs	10/51 (19.6%)	25/85 (29.4%)	
> 2 drugs or uncontrolled	12/51 (23.5%)	28/85 (32.9%)	
Diabetes mellitus			
None	40/48 (83.3%)	70/85 (82.4%)	0.886
FEV1			
Mean ± SD	1.85 ± 0.74	1.71 ± 0.63	0.726
AAA family history			
Yes	0/2 (0%)	48/53 (90.6%)	0.649
No	2/2 (100%)	5/53 (9.4%)	
ASA Class			
Healthy	0/51 (0%)	0/84 (0%)	<0.001
Mild systemic disease	2/51 (3.9%)	24/84 (28.6%)	
Severe systemic disease	7/51 (13.7%)	54/84 (64.3%)	
Severe systemic disease that is a constant threat to life	28/51 (54.9%)	6/84 (7.1%)	
Not expected to survive without intervention	14/51 (27.5%)	0/84 (0%)	
Medication			
Beta blocker	18/51 (35.3%)	39/84 (46.4%)	0.204
Aspirin	18/51 (35.3%)	27/46 (58.7%)	0.050
Statin or Fibrate	55/84 (65.5%)	21/50 (42.0%)	0.025

Biochemical			
Total cholesterol (mmol/L)	3.64 ± 1.2	13.0 ± 53.9	0.466
LDL (mmol/L)	2.20 ± 0.89	1.94 ± 1.40	0.554
Triglycerides (mmol/L)	2.29 ± 2.82	1.16 ± 0.78	0.033
Creatinine (mmol/L)	148.16 ± 150.33	101.51 ± 59.3	0.011
Platelets (x10^9 /L)	219.5 ± 88.8	193.7 ± 60.6	0.043
CT Examinations			
CT with iodine contrast injection	28/63 (44.4%)	88/94 (93.6%)	<0.001

Note.— Numbers in parentheses are percentages.
AAA = abdominal aortic aneurysm. CT = computed tomography. FEV1 = volume exhaled at end of first second of forced expiration. *LDL* = low-density lipoprotein. SD = standard deviation.

4.4.2 Geometric Characteristics

Table 4.2: Geometric characteristics of AAA in case and control groups (157 subjects)

	Cases (N= 63)	Controls (N=94)	*P* Value
1D size indices			
Dmax (cm)	7.85 ± 2.09	6.92 ± 1.33	0.001
Proximal neck diameter (mm)	29.6 ± 15.4	25.9 ± 7.6	0.049
Distal neck diameter (mm)	34.3 ± 16.4	28.8 ± 8.4	0.006
Sac height (mm)	125.3 ± 41.7	112.2 ± 21.3	0.011
Neck height (mm)	12.9 ± 12.3	16.4 ± 13.0	0.098
Sac length (mm)	150.9 ± 46.7	135.1 ± 26.2	0.008
Neck length (mm)	16.7 ± 13.9	20.5 ± 15.3	0.115
Bulge height (mm)	72.8 ± 31.1	76.2 ± 18.1	0.546
Distance between lumen centroid and cross-section centroid (mm)	9.16 ± 7.16	9.8 ± 6.0	0.618
Euclidian distance between centroids (mm)	140.8 ± 40.4	131.6 ± 16.2	0.049
2D size indices			
Diameter-height ratio	0.64 ± 0.16	0.61 ± 0.14	0.246
Diameter max-diameter neck ratio	12.6 ± 43.9	2.9 ± 2.7	0.033
Height ratio	28.3 ± 40.2	14.8 ± 15.7	0.004
Bulge location	0.52 ± 0.16	0.59 ± 0.35	0.004
Asymmetry factor	0.88 ± 0.08	0.86 ± 0.08	0.112
Tortuosity	1.20 ± 0.09	1.18 ± 0.08	0.412
3D size indices			
Outer wall volume (cm^3)	401.6 ± 353.6	262.0 ± 148.0	0.001
Lumen volume (cm^3)	190.8 ± 157.6	130.0 ± 89.6	0.012
Thrombus volume (cm^3)	199.3 ± 222.8	132.1 ± 100.8	0.029
Wall surface area (mm^2)	28 367 ± 15 021	22 499 ± 7285	0.001
Ratio of AAA/ILT Volume	0.46 ± 0.21	0.49 ± 0.18	0.424

3D shape indices			
Isoperimetric ratio	5.62 ± 0.40	5.69 ± 0.28	0.171
Non-fusiform index	-0.15 ± 0.07	-0.15 ± 0.06	0.604
Second-order curvature-based indices			
Gaussian averaged area (10^{-2} mm^{-1})	0.14 ± 0.07	0.17 ± 0.06	0.017
Mean averaged area (10^{-2} mm^{-1})	-3.89 ± 0.68	-4.31 ± 0.53	<0.001
Gaussian averaged area L2-norm ratio (non-dimensional)	5.44 ± 2.72	5.11 ± 2.08	0.396
Mean averaged area L2-norm ratio (non-dimensional)	0.57 ± 0.12	0.58 ± 0.10	0.907

Note.–AAA = abdominal aortic aneurysm. Dmax = maximal AAA diameter. ILT = intraluminal thrombus.

4.4.3 Results of Univariate Logistic Regression Analysis

Univariate regression analysis revealed that sex ($P = 0.024$), Dmax ($P = 0.001$) and 14 other geometric indices were associated with AAA rupture at $P < 0.05$ (Table 4.2).

4.4.4 Results of Multivariable Logistic Regression Analysis

In the multivariable logistic regression analysis, adjusting for sex and Dmax, the AAA with a higher bulge location (adjusted OR: 0.044; 95% CI: 0.003, 0.608; $P = 0.020$) and higher mean averaged area (adjusted OR: 2.654; 95% CI: 1.346, 5.184; $P = 0.005$) were most strongly associated with AAA rupture (Table 4.3).

Table 4.3: Results of multivariate logistic regression analysis

Variables	OR	95% CI	*P* Value
Traditional model			
Sex	2.848	1.212, 6.694	0.016
Dmax	1.425	1.149, 1.766	0.001
Model incorporating geometric indices			
Sex	2.359	0.924, 6.021	0.073
Dmax	1.291	1.017, 1.638	0.036
Bulge location	0.044	0.003, 0.608	0.020
Mean averaged area	2.641	1.346, 5.184	0.005

Note.—CI = confidence interval. OR = odds ratio.

4.4.5 Classification Accuracy

For distinguishing case and control subjects, the traditional model reflecting current treatment criteria based on sex and Dmax only had an area under the ROC curve (AUC) of 0.674 (95% CI: 0.584 - 0.765). The best threshold point of Dmax for classification of case and control was 7.69 cm (point that maximizes the Youden index) in our study sample.

The traditional model provides a 60.3% sensitivity (95% CI: 47.2%, 72.2%) and 76.6% specificity (95% CI: 66.5%, 84.5%).

The inclusion of two geometric indices to the traditional model showed a modest improvement ($P < 0.001$) with an AUC of 0.752 (95% CI: 0.673 - 0.832) (Figure 4.3). This model provides a 63.5% sensitivity (95% CI: 50.3%, 75.0%) and 78.7% specificity (95% CI: 68.8%, 86.2%).

4.4.6 ROC Curve Analysis

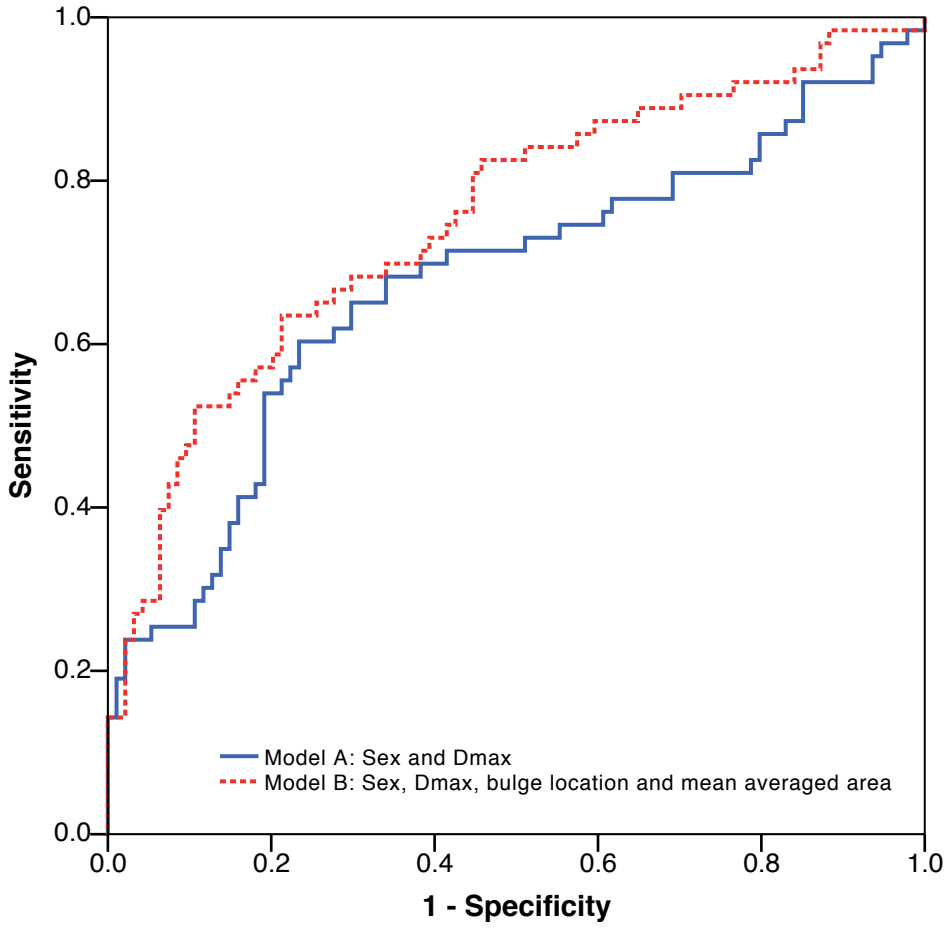

Figure 4.3: ROC analysis.

Two models for distinguishing case and control subjects based on sex and Dmax alone (model A) and based on sex, Dmax, bulge location and mean averaged area (model B). The inclusion of two geometric indices to the traditional model showed a trend toward improvement ($P < 0.001$).

4.5 Discussion

4.5.1 Main Findings

This retrospective case-control study evaluated geometric indices derived from CT segmentation that are associated with AAA rupture. The univariate analysis revealed that Dmax ($P = 0.001$) and 13 other geometric indices were associated with AAA rupture at $P <$

0.05. In the multivariable logistic regression analysis, adjusting for sex and Dmax, the AAA with a higher bulge location (P = 0.020) and higher mean averaged surface area curvature (P = 0.005) were associated with AAA rupture.

Imaging plays an important role in the screening and management of AAA (6, 114). While ultrasound is the preferred screening modality for evaluation of the aorta diameter (115), computed tomographic angiography (CTA) has emerged as the current "gold standard" in the preoperative evaluation of AAA anatomy and endovascular aortic repair (EVAR) suitability (116, 117).

The most widely used criteria to predict the risk of aneurysm rupture are the maximum diameter and sex, which are based on a cutoff values of 5.5 cm for men and 4.5 cm for women, or rapid growth of >1cm/year (6). It is clear from a population-based cohort study (7, 11) and randomized trials (5, 45) that the rupture risk increases with larger AAA diameter.

In our study sample, the traditional model based on sex and Dmax alone exhibited moderate specificity (76.6%), which is reassuring considering that mortality rate of open surgery ranges between 2 and 4% (5) and that mortality rate of EVAR, though less invasive, is still 1.7% (83). In contrast with specificity, the low sensitivity (60.3%) exhibited in the identification of AAA at risk of rupture is considered suboptimal, resulting in a considerable number of false negative classification. Therefore, newer geometric indices are needed to improve sensitivity while maintaining specificity within an acceptable range. Ultimately, this modeling could influence therapeutic decision in patients whose AAA diameter is near the 5.5 cm cutoff in men and 4.5 cm in women.

We found that a model incorporating geometric indices tend to increase the area under the receiver operating characteristics curve (AUC = 0.752) to discriminate cases from controls as compared with a traditional model reflecting current treatment criteria based on sex and Dmax alone (AUC = 0.674). However, this did not improve the accuracy in terms of sensitivity and specificity to be clinically meaningful. A substantial portion of ruptured cases were still not identified, as revealed by the low sensitivity (63.5%).

Some of the prediction inaccuracy may be an inherent limitation of rupture risk factors based solely on anatomy. This is highlighted by the small yet non-negligible annual rupture

rate of AAA < 5.0 cm, in the range of 1.0% per year (3). Accurate data on rupture risk is difficult to obtain because current clinical guidelines recommend treatment for patients with Dmax ≥ 5.5 cm in men and ≥ 4.5-5.0 cm in women (6). This is exacerbated by the fact that in the past 3 decades, few patients have been followed without intervention; hence, the true natural history of untreated AAA remains poorly defined (118).

Given the 90% mortality rate of ruptured AAA (44), there is a need to identify additional predictors of AAA rupture that would be more sensitive and patient-specific. Geometric evaluation is more sophisticated than Dmax measurement and requires AAA segmentation.

4.5.2 Interpretation of Results

Our work represents an intermediate step for predicting AAA rupture risk on a patient-specific basis (9) and builds on the formal framework of geometric indices described by Martufi *et al*. (53, 91). To our knowledge, this is the largest case-control study to date on AAA geometric indices.

Shum *et al.* (53) recently reported the results of a retrospective case-control study of 10 ruptured and 66 unruptured aneurysms. Their model, based on a decision tree, correctly predicted rupture in 86.6% of patients and was superior to a Dmax threshold of 5.0 cm which resulted in an accuracy of only 38.2%. A frequent issue with decision trees lies in the tendency to overfit the data. This may be problematic with their decision tree which contained 4 splits for only 10 ruptured cases. To highlight this issue, we cross-validated their decision tree with our own database.

With the exception of wall thickness indices and volume of intraluminal thrombus, which could not be assessed due to unenhanced CT examinations in our study, all the geometric parameters defined previously by Shum *et al.* and Martufi *et al*. were tested in our study (53, 91). Our study had several strengths. Our case-control ratio of 1: 1.5 was more balanced than their ratio of 1: 6.6 (53). In addition, the Dmax in our case and control groups (7.85 ± 2.09 cm vs. 6.92 ± 1.33 cm) were more balanced than in the study by Shum

et al. (7.84 ± 1.32 vs. 5.49 ± 1.11 cm). Finally, we reported the clinical characteristics of subjects included in our case and control groups.

Our results confirm that the addition of geometric indices to a predictive model improves the accuracy to detect aneurysm rupture. Using a multivariate logistic regression analysis instead of a decision tree, we confirmed that bulge height and surface area were independent predictive features of AAA rupture. We also confirmed that sac height, sac length, and volume were associated with rupture at univariate analysis, although they were not significant when adjusting for Dmax and sex at multivariate analysis. Unlike Shum *et al.*, we did not confirm that intra-luminal thrombus volume and tortuosity were predictors of rupture potential.

4.5.3 Clinical Implications

Our work in AAA segmentation represents a prerequisite for personalized wall stress analysis, either by finite element analysis (FEA) or fluid structure interaction modeling (119). The patient-specific AAA geometry will be needed to accurately simulate patient-specific hemodynamics, such as pressure and velocity profiles, that will be required to improve individual rupture risk prediction (9, 50, 92).

4.5.4 Limitations

There were a few limitations in our study. First, CT-scans in our case group were obtained at the moment of rupture, which may result in acute AAA deformation. The geometric indices obtained may not be perfectly representative of AAA morphology before rupture. However, we anticipate difficulties to obtain this data because few patients with large AAAs are followed without intervention (118) and those diagnosed at rupture are unlikely to have prior imaging, otherwise they would have been offered and declined treatment.

Second, only 44.4% CT-scan in the case group were contrast-enhanced. This limited the number of cases with complete lumen and thrombus segmentation. This proportion of

contrast-enhanced study was significantly lower than in the control group. However, assessment of intraluminal thrombus has limited clinical utility in ruptured cases because CT is often performed unenhanced in this clinical setting.

Third, the retrospective nature of our case-control study is susceptible to sampling bias. Geometric indices were not assessed in all patients with symptomatic or ruptured AAA, but rather those who were stable enough to undergo CT. Yet, this is an inherent logistical limitation of studies which require emergency imaging in patients with ruptured AAA (24).

4.5.6 Conclusion

In summary, our retrospective case-control study comparing ruptured and unruptured AAA suggests that several previously published geometric indices are associated with AAA rupture with 2 being independent factors after controlling for diameter and sex. However, the inclusion of these indices in the current model based on diameter and sex provide only a modest, but significant improvement in the classification accuracy of AAA with high rupture risk at CT. This improvement did not translate in better sensitivity to detect AAA rupture over Dmax measurement in a clinical setting. Addition of flow and biomechanical simulations should be investigated to improve AAA modeling.

5 Conclusion

5.1 Closing Words

AAA affects 2% of the elderly population, with an increasing incidence. Rupture is associated with a high mortality rate. Although the current indications for treatment rely mainly on maximum diameter thresholds, there is a need to revisit this size criteria due to rupture in smaller aneurysms.

The research in this dissertation emerged from a need to improve the assessment of rupture risk. Instead of a "one size fits all" approach, we investigated a patient-specific analysis of AAA geometry in the setting of a case-control study in ruptured and unruptured aneurysms.

To do so, we used the AAA segmentation software developed at our institution and that we previously validated in a series of studies. We adopted the comprehensive geometrical indices reported by Martufi *et al.* (91) for the purpose of our case-control study.

By doing this retrospective study, we realized the difficulty of obtaining imaging prior to an acute episode of AAA rupture. Few patients with ruptured AAA have prior CT scans available. This is because patients who are diagnosed with AAA are followed and eventually offered endovascular or open surgical repair, which prevent rupture. Hence, with the current standard of care, it would be very difficult to collect *longitudinal* data on the natural history of AAA morphology.

To improve our sample size, we designed this study as a collaborative work between radiologists and vascular surgeons from two university health networks affiliated to Université de Montréal and McGill University. Together, these two networks receive a large number of referrals from hospitals in the Montreal metropolitan area.

To evaluate the true predictive value of geometrical indices on the rupture risk, one would have to perform a *longitudinal* rather than a *cross-sectional* study. We found that only 5% of ruptured AAA had imaging > 1 week prior to the acute episode of rupture. This highlights the challenges of obtaining longitudinal imaging data in patients with ruptured AAA.

We anticipate that any future *prospective* study attempting to evaluate the rupture risk of AAA would have to be performed in a multicenter setting to obtain appropriate sample size. The at-risk population should ideally include patients who are not eligible to AAA repair due to medical contraindications and patients who refuse treatment, but yet accept to be followed with serial CTA.

5.2 Future Work

Our study suggests that a predictive model incorporating geometric indices provide modest, but significant, improvement in the classification accuracy of AAA with high rupture risk at CT over a traditional model reflecting current treatment criteria based on sex and Dmax alone. This improvement did not translate in better sensitivity to detect AAA rupture over Dmax measurement in a clinical setting.

The 3D models of ruptured and unruptured AAAs obtained by segmentation during this study may be used to perform biomechanical simulations. Now that we have converted a large dataset of medical images into finite element models, we may perform simulations to evaluate the impact of mural thrombus on wall stress, rupture modeling, catheter-aorta interactions, and virtual stent-graft deployment.

This is a very exciting time to be working in AAA modeling. Research in AAA patient-specific rupture risk prediction will require the collaboration of physicians and biomechanical engineers. At another level, this collaboration reflects the powerful forces at play in medical imaging: automation of segmentation, extraction of quantitative information from images, and abundance of computing power.

I hope that you enjoyed this dissertation as much as I did in its preparation. Over the course of my Master in Biomedical Research, I collected images and 3D renderings to illustrate our progress so far. I look forward to the day when I will be able to evaluate the mechanical wall stresses acting on an AAA while I am reviewing the CT of a patient at the reading console.

Bibliography

Publications by the team are in bold characters

1. Ouriel K, Green RM, Donayre C, Shortell CK, Elliott J, DeWeese JA. An evaluation of new methods of expressing aortic aneurysm size: relationship to rupture. J Vasc Surg. 1992;15(1):12-8; discussion 9-20. Epub 1992/01/01.
2. Johnston KW, Rutherford RB, Tilson MD, Shah DM, Hollier L, Stanley JC. Suggested standards for reporting on arterial aneurysms. Subcommittee on Reporting Standards for Arterial Aneurysms, Ad Hoc Committee on Reporting Standards, Society for Vascular Surgery and North American Chapter, International Society for Cardiovascular Surgery. J Vasc Surg. 1991;13(3):452-8. Epub 1991/03/01.
3. Mortality results for randomised controlled trial of early elective surgery or ultrasonographic surveillance for small abdominal aortic aneurysms. The UK Small Aneurysm Trial Participants. Lancet. 1998;352(9141):1649-55. Epub 1998/12/16.
4. Ashton HA, Buxton MJ, Day NE, Kim LG, Marteau TM, Scott RA, et al. The Multicentre Aneurysm Screening Study (MASS) into the effect of abdominal aortic aneurysm screening on mortality in men: a randomised controlled trial. Lancet. 2002;360(9345):1531-9. Epub 2002/11/22.
5. Lederle FA, Wilson SE, Johnson GR, Reinke DB, Littooy FN, Acher CW, et al. Immediate repair compared with surveillance of small abdominal aortic aneurysms. N Engl J Med. 2002;346(19):1437-44. Epub 2002/05/10.
6. Brewster DC, Cronenwett JL, Hallett JW, Jr., Johnston KW, Krupski WC, Matsumura JS. Guidelines for the treatment of abdominal aortic aneurysms. Report of a subcommittee of the Joint Council of the American Association for Vascular Surgery and Society for Vascular Surgery. J Vasc Surg. 2003;37(5):1106-17. Epub 2003/05/21.
7. Nevitt MP, Ballard DJ, Hallett JW, Jr. Prognosis of abdominal aortic aneurysms. A population-based study. N Engl J Med. 1989;321(15):1009-14. Epub 1989/10/12.

8. Lederle FA, Johnson GR, Wilson SE, Ballard DJ, Jordan WD, Jr., Blebea J, et al. Rupture rate of large abdominal aortic aneurysms in patients refusing or unfit for elective repair. JAMA. 2002;287(22):2968-72. Epub 2002/06/08.
9. Vorp DA, Vande Geest JP. Biomechanical determinants of abdominal aortic aneurysm rupture. Arterioscler Thromb Vasc Biol. 2005;25(8):1558-66. Epub 2005/08/02.
10. Darling RC, Messina CR, Brewster DC, Ottinger LW. Autopsy study of unoperated abdominal aortic aneurysms. The case for early resection. Circulation. 1977;56(3 Suppl):II161-4. Epub 1977/09/01.
11. Reed WW, Hallett JW, Jr., Damiano MA, Ballard DJ. Learning from the last ultrasound. A population-based study of patients with abdominal aortic aneurysm. Arch Intern Med. 1997;157(18):2064-8. Epub 1997/10/24 21:27.
12. Dubost C, Allary M, Oeconomos N. [Treatment of aortic aneurysms; removal of the aneurysm; re-establishment of continuity by grafts of preserved human aorta]. Mem Acad Chir (Paris). 1951;77(12-13):381-3. Epub 1951/04/11. A propos du traitement des anevrysmes de l'aorte; ablation de l'anevrysme; retablissement de la continuite par greffe d'aorte humaine conservee.
13. De Bakey ME, Cooley DA. Successful resection of aneurysm of thoracic aorta and replacement by graft. Journal of the American Medical Association. 1953;152(8):673-6. Epub 1953/06/20.
14. Cooley DA. Aortic surgery: a historical perspective. Seminars in cardiothoracic and vascular anesthesia. 2012;16(1):7-10. Epub 2012/02/14.
15. Volodos NL, Shekhanin VE, Karpovich IP, Troian VI, Gur'ev Iu A. [A self-fixing synthetic blood vessel endoprosthesis]. Vestnik khirurgii imeni I I Grekova. 1986;137(11):123-5. Epub 1986/11/01. Samofiksiruiushchiisia sinteticheskii protez dlia endoprotezirovaniia sosudov.
16. Torsello G, Osada N, Florek HJ, Horsch S, Kortmann H, Luska G, et al. Long-term outcome after Talent endograft implantation for aneurysms of the abdominal aorta: a multicenter retrospective study. J Vasc Surg. 2006;43(2):277-84; discussion 84. Epub 2006/02/16.

17. Becquemin JP, Pillet JC, Lescalie F, Sapoval M, Goueffic Y, Lermusiaux P, et al. A randomized controlled trial of endovascular aneurysm repair versus open surgery for abdominal aortic aneurysms in low- to moderate-risk patients. J Vasc Surg. 2011;53(5):1167-73 e1. Epub 2011/02/01.
18. Endovascular aneurysm repair and outcome in patients unfit for open repair of abdominal aortic aneurysm (EVAR trial 2): randomised controlled trial. Lancet. 2005;365(9478):2187-92. Epub 2005/06/28.
19. Blankensteijn JD, de Jong SE, Prinssen M, van der Ham AC, Buth J, van Sterkenburg SM, et al. Two-year outcomes after conventional or endovascular repair of abdominal aortic aneurysms. N Engl J Med. 2005;352(23):2398-405. Epub 2005/06/10.
20. De Bruin JL, Baas AF, Buth J, Prinssen M, Verhoeven EL, Cuypers PW, et al. Long-term outcome of open or endovascular repair of abdominal aortic aneurysm. N Engl J Med. 2010;362(20):1881-9. Epub 2010/05/21.
21. Greenhalgh RM, Brown LC, Powell JT, Thompson SG, Epstein D, Sculpher MJ. Endovascular versus open repair of abdominal aortic aneurysm. N Engl J Med. 2010;362(20):1863-71. Epub 2010/04/13.
22. Buth J, van Marrewijk CJ, Harris PL, Hop WC, Riambau V, Laheij RJ. Outcome of endovascular abdominal aortic aneurysm repair in patients with conditions considered unfit for an open procedure: a report on the EUROSTAR experience. J Vasc Surg. 2002;35(2):211-21. Epub 2002/02/21.
23. Yusuf SW, Whitaker SC, Chuter TA, Wenham PW, Hopkinson BR. Emergency endovascular repair of leaking aortic aneurysm. Lancet. 1994;344(8937):1645. Epub 1994/12/10.
24. Sadat U, Boyle JR, Walsh SR, Tang T, Varty K, Hayes PD. Endovascular vs open repair of acute abdominal aortic aneurysms--a systematic review and meta-analysis. J Vasc Surg. 2008;48(1):227-36. Epub 2008/02/05.
25. Iezzi R, Cotroneo AR. Endovascular repair of abdominal aortic aneurysms: CTA evaluation of contraindications. Abdom Imaging. 2006;31(6):722-31. Epub 2006/02/01.
26. Karthikesalingam A, Hinchliffe RJ, Holt PJ, Boyle JR, Loftus IM, Thompson MM. Endovascular aneurysm repair with preservation of the internal iliac artery using the

iliac branch graft device. Eur J Vasc Endovasc Surg. 2010;39(3):285-94. Epub 2009/12/08.

27. Verhoeven EL, Tielliu IF, Ferreira M, Zipfel B, Adam DJ. Thoraco-abdominal aortic aneurysm branched repair. J Cardiovasc Surg (Torino). 2010;51(2):149-55. Epub 2010/04/01.
28. Cross J, Gurusamy K, Gadhvi V, Simring D, Harris P, Ivancev K, et al. Fenestrated endovascular aneurysm repair. Br J Surg. 2012;99(2):152-9. Epub 2011/12/21.
29. Prinssen M, Verhoeven EL, Verhagen HJ, Blankensteijn JD. Decision-making in follow-up after endovascular aneurysm repair based on diameter and volume measurements: a blinded comparison. Eur J Vasc Endovasc Surg. 2003;26(2):184-7. Epub 2003/08/15.
30. **Kauffmann C, Tang A, Therasse E, Giroux MF, Elkouri S, Melanson P, et al. Measurements and detection of abdominal aortic aneurysm growth: Accuracy and reproducibility of a segmentation software. Eur J Radiol. 2012;81(8):1688-94. Epub 2011/05/24.**
31. **Kauffmann C, Tang A, Therasse E, Soulez G, editors. An hybrid CPU-GPU framework for quantitative follow-up of abdominal aortic aneurysm volume by CT angiography. 2010: SPIE.**
32. Stenbaek J, Kalin B, Swedenborg J. Growth of thrombus may be a better predictor of rupture than diameter in patients with abdominal aortic aneurysms. Eur J Vasc Endovasc Surg. 2000;20(5):466-9. Epub 2000/12/09.
33. Bluestein D, Dumont K, De Beule M, Ricotta J, Impellizzeri P, Verhegghe B, et al. Intraluminal thrombus and risk of rupture in patient specific abdominal aortic aneurysm - FSI modelling. Comput Methods Biomech Biomed Engin. 2009;12(1):73-81. Epub 2008/07/25.
34. Powell JT, Greenhalgh RM. Clinical practice. Small abdominal aortic aneurysms. N Engl J Med. 2003;348(19):1895-901. Epub 2003/05/09.
35. Cao P. Comparison of surveillance vs Aortic Endografting for Small Aneurysm Repair (CAESAR) trial: study design and progress. Eur J Vasc Endovasc Surg. 2005;30(3):245-51. Epub 2005/09/01.

36. Kauffmann C, Tang A, Dugas A, Therasse E, Oliva V, Soulez G. Clinical validation of a software for quantitative follow-up of abdominal aortic aneurysm maximal diameter and growth by CT angiography. Eur J Radiol. 2011;77(3):502-8. Epub 2009/12/08.

37. Singh K, Bonaa KH, Jacobsen BK, Bjork L, Solberg S. Prevalence of and risk factors for abdominal aortic aneurysms in a population-based study : The Tromso Study. American journal of epidemiology. 2001;154(3):236-44. Epub 2001/08/02.

38. Lederle FA, Johnson GR, Wilson SE, Chute EP, Littooy FN, Bandyk D, et al. Prevalence and associations of abdominal aortic aneurysm detected through screening. Aneurysm Detection and Management (ADAM) Veterans Affairs Cooperative Study Group. Ann Intern Med. 1997;126(6):441-9. Epub 1997/03/15.

39. Wilmink TB, Quick CR, Day NE. The association between cigarette smoking and abdominal aortic aneurysms. J Vasc Surg. 1999;30(6):1099-105. Epub 1999/12/10.

40. Izzillo R, Cassagnes L, Boutekadjirt R, Garcier JM, Cluzel P, Boyer L. [Imaging of abdominal aortic aneurysms: when, how and why?]. J Radiol. 2004;85(6 Pt 2):870-82. Epub 2004/07/10. Quand, comment et pourquoi realiser une imagerie d'un anevrisme de l'aorte abdominale?

41. Schewe CK, Schweikart HP, Hammel G, Spengel FA, Zollner N, Zoller WG. Influence of selective management on the prognosis and the risk of rupture of abdominal aortic aneurysms. The Clinical investigator. 1994;72(8):585-91. Epub 1994/08/01.

42. Brady AR, Thompson SG, Fowkes FG, Greenhalgh RM, Powell JT. Abdominal aortic aneurysm expansion: risk factors and time intervals for surveillance. Circulation. 2004;110(1):16-21. Epub 2004/06/24.

43. Vardulaki KA, Prevost TC, Walker NM, Day NE, Wilmink AB, Quick CR, et al. Growth rates and risk of rupture of abdominal aortic aneurysms. Br J Surg. 1998;85(12):1674-80. Epub 1999/01/06.

44. Patel MI, Hardman DT, Fisher CM, Appleberg M. Current views on the pathogenesis of abdominal aortic aneurysms. J Am Coll Surg. 1995;181(4):371-82. Epub 1995/10/01.

45. Brown LC, Powell JT. Risk factors for aneurysm rupture in patients kept under ultrasound surveillance. UK Small Aneurysm Trial Participants. Ann Surg. 1999;230(3):289-96; discussion 96-7. Epub 1999/09/24.

46. Powell JT, Brown LC, Greenhalgh RM, Thompson SG. The rupture rate of large abdominal aortic aneurysms: is this modified by anatomical suitability for endovascular repair? Ann Surg. 2008;247(1):173-9. Epub 2007/12/25.

47. Arita T, Matsunaga N, Takano K, Nagaoka S, Nakamura H, Katayama S, et al. Abdominal aortic aneurysm: rupture associated with the high-attenuating crescent sign. Radiology. 1997;204(3):765-8. Epub 1997/09/01.

48. Vorp DA, Lee PC, Wang DH, Makaroun MS, Nemoto EM, Ogawa S, et al. Association of intraluminal thrombus in abdominal aortic aneurysm with local hypoxia and wall weakening. J Vasc Surg. 2001;34(2):291-9. Epub 2001/08/10.

49. Kazi M, Thyberg J, Religa P, Roy J, Eriksson P, Hedin U, et al. Influence of intraluminal thrombus on structural and cellular composition of abdominal aortic aneurysm wall. J Vasc Surg. 2003;38(6):1283-92. Epub 2003/12/19.

50. Fillinger M. The long-term relationship of wall stress to the natural history of abdominal aortic aneurysms (finite element analysis and other methods). Ann N Y Acad Sci. 2006;1085:22-8. Epub 2006/12/22.

51. Vande Geest JP, Di Martino ES, Bohra A, Makaroun MS, Vorp DA. A biomechanics-based rupture potential index for abdominal aortic aneurysm risk assessment: demonstrative application. Ann N Y Acad Sci. 2006;1085:11-21. Epub 2006/12/22.

52. Wang DH, Makaroun MS, Webster MW, Vorp DA. Effect of intraluminal thrombus on wall stress in patient-specific models of abdominal aortic aneurysm. J Vasc Surg. 2002;36(3):598-604. Epub 2002/09/10.

53. Shum J, Martufi G, Di Martino E, Washington CB, Grisafi J, Muluk SC, et al. Quantitative assessment of abdominal aortic aneurysm geometry. Ann Biomed Eng. 2011;39(1):277-86. Epub 2010/10/05.

54. Lederle FA, Walker JM, Reinke DB. Selective screening for abdominal aortic aneurysms with physical examination and ultrasound. Arch Intern Med. 1988;148(8):1753-6. Epub 1988/08/01.

55. Crow P, Shaw E, Earnshaw JJ, Poskitt KR, Whyman MR, Heather BP. A single normal ultrasonographic scan at age 65 years rules out significant aneurysm disease for life in men. Br J Surg. 2001;88(7):941-4. Epub 2001/07/10.
56. Scott RA, Vardulaki KA, Walker NM, Day NE, Duffy SW, Ashton HA. The long-term benefits of a single scan for abdominal aortic aneurysm (AAA) at age 65. Eur J Vasc Endovasc Surg. 2001;21(6):535-40. Epub 2001/06/09.
57. Mastracci TM, Cina CS. Screening for abdominal aortic aneurysm in Canada: review and position statement of the Canadian Society for Vascular Surgery. J Vasc Surg. 2007;45(6):1268-76. Epub 2007/06/05.
58. Singh K, Bonaa KH, Solberg S, Sorlie DG, Bjork L. Intra- and interobserver variability in ultrasound measurements of abdominal aortic diameter. The Tromso Study. Eur J Vasc Endovasc Surg. 1998;15(6):497-504. Epub 1998/07/11.
59. Wilmink AB, Forshaw M, Quick CR, Hubbard CS, Day NE. Accuracy of serial screening for abdominal aortic aneurysms by ultrasound. Journal of medical screening. 2002;9(3):125-7. Epub 2002/10/09.
60. Elkouri S, Panneton JM, Andrews JC, Lewis BD, McKusick MA, Noel AA, et al. Computed tomography and ultrasound in follow-up of patients after endovascular repair of abdominal aortic aneurysm. Ann Vasc Surg. 2004;18(3):271-9. Epub 2004/09/10.
61. Berland LL, Silverman SG, Gore RM, Mayo-Smith WW, Megibow AJ, Yee J, et al. Managing incidental findings on abdominal CT: white paper of the ACR incidental findings committee. Journal of the American College of Radiology : JACR. 2010;7(10):754-73. Epub 2010/10/05.
62. Rakita D, Newatia A, Hines JJ, Siegel DN, Friedman B. Spectrum of CT findings in rupture and impending rupture of abdominal aortic aneurysms. Radiographics. 2007;27(2):497-507. Epub 2007/03/22.
63. Wolf F, Plank C, Beitzke D, Popovic M, Domenig CM, Weber M, et al. Prospective evaluation of high-resolution MRI using gadofosveset for stent-graft planning: comparison with CT angiography in 30 patients. AJR Am J Roentgenol. 2011;197(5):1251-7. Epub 2011/10/25.

64. Lutz AM, Willmann JK, Pfammatter T, Lachat M, Wildermuth S, Marincek B, et al. Evaluation of aortoiliac aneurysm before endovascular repair: comparison of contrast-enhanced magnetic resonance angiography with multidetector row computed tomographic angiography with an automated analysis software tool. J Vasc Surg. 2003;37(3):619-27. Epub 2003/03/06.

65. Upchurch GR, Jr., Schaub TA. Abdominal aortic aneurysm. Am Fam Physician. 2006;73(7):1198-204. Epub 2006/04/21.

66. Wakefield TW, Whitehouse WM, Jr., Wu SC, Zelenock GB, Cronenwett JL, Erlandson EE, et al. Abdominal aortic aneurysm rupture: statistical analysis of factors affecting outcome of surgical treatment. Surgery. 1982;91(5):586-96. Epub 1982/05/01.

67. Pillari G, Chang JB, Zito J, Cohen JR, Gersten K, Rizzo A, et al. Computed tomography of abdominal aortic aneurysm. An in vivo pathological report with a note on dynamic predictors. Arch Surg. 1988;123(6):727-32. Epub 1988/06/01.

68. Mower WR, Quinones WJ, Gambhir SS. Effect of intraluminal thrombus on abdominal aortic aneurysm wall stress. J Vasc Surg. 1997;26(4):602-8. Epub 1997/11/14.

69. Arko FR, Lee WA, Hill BB, Olcott Ct, Dalman RL, Harris EJ, Jr., et al. Aneurysm-related death: primary endpoint analysis for comparison of open and endovascular repair. J Vasc Surg. 2002;36(2):297-304. Epub 2002/08/10.

70. Metcalfe D, Holt PJ, Thompson MM. The management of abdominal aortic aneurysms. BMJ. 2011;342:d1384. Epub 2011/03/12.

71. Richards T, Goode SD, Hinchliffe R, Altaf N, Macsweeney S, Braithwaite B. The importance of anatomical suitability and fitness for the outcome of endovascular repair of ruptured abdominal aortic aneurysm. Eur J Vasc Endovasc Surg. 2009;38(3):285-90. Epub 2009/07/07.

72. Rose DF, Davidson IR, Hinchliffe RJ, Whitaker SC, Gregson RH, MacSweeney ST, et al. Anatomical suitability of ruptured abdominal aortic aneurysms for endovascular repair. J Endovasc Ther. 2003;10(3):453-7. Epub 2003/08/23.

73. Harris PL, Buth J, Mialhe C, Myhre HO, Norgren L. The need for clinical trials of endovascular abdominal aortic aneurysm stent-graft repair: The EUROSTAR Project.

EUROpean collaborators on Stent-graft Techniques for abdominal aortic Aneurysm Repair. Journal of endovascular surgery : the official journal of the International Society for Endovascular Surgery. 1997;4(1):72-7; discussion 8-9. Epub 1997/02/01.

74. Mayer D, Pfammatter T, Rancic Z, Hechelhammer L, Wilhelm M, Veith FJ, et al. 10 years of emergency endovascular aneurysm repair for ruptured abdominal aortoiliac aneurysms: lessons learned. Ann Surg. 2009;249(3):510-5. Epub 2009/02/28.
75. Park JH, Chung JW, Choo IW, Kim SJ, Lee JY, Han MC. Fenestrated stent-grafts for preserving visceral arterial branches in the treatment of abdominal aortic aneurysms: preliminary experience. J Vasc Interv Radiol. 1996;7(6):819-23. Epub 1996/11/01.
76. Cuypers P, Buth J, Harris PL, Gevers E, Lahey R. Realistic expectations for patients with stent-graft treatment of abdominal aortic aneurysms. Results of a European multicentre registry. Eur J Vasc Endovasc Surg. 1999;17(6):507-16. Epub 1999/06/22.
77. Wain RA, Marin ML, Ohki T, Sanchez LA, Lyon RT, Rozenblit A, et al. Endoleaks after endovascular graft treatment of aortic aneurysms: classification, risk factors, and outcome. J Vasc Surg. 1998;27(1):69-78; discussion -80. Epub 1998/02/25.
78. Zarins CK, White RA, Hodgson KJ, Schwarten D, Fogarty TJ. Endoleak as a predictor of outcome after endovascular aneurysm repair: AneuRx multicenter clinical trial. J Vasc Surg. 2000;32(1):90-107. Epub 2000/07/06.
79. Stavropoulos SW, Charagundla SR. Imaging techniques for detection and management of endoleaks after endovascular aortic aneurysm repair. Radiology. 2007;243(3):641-55. Epub 2007/05/23.
80. Prinssen M, Verhoeven EL, Buth J, Cuypers PW, van Sambeek MR, Balm R, et al. A randomized trial comparing conventional and endovascular repair of abdominal aortic aneurysms. N Engl J Med. 2004;351(16):1607-18. Epub 2004/10/16.
81. Ouriel K, Clair DG, Kent KC, Zarins CK. Endovascular repair compared with surveillance for patients with small abdominal aortic aneurysms. J Vasc Surg. 2010;51(5):1081-7. Epub 2010/03/23.
82. Cao P, De Rango P, Verzini F, Parlani G, Romano L, Cieri E. Comparison of surveillance versus aortic endografting for small aneurysm repair (CAESAR): results

from a randomised trial. Eur J Vasc Endovasc Surg. 2011;41(1):13-25. Epub 2010/09/28.

83. Greenhalgh RM, Brown LC, Kwong GP, Powell JT, Thompson SG. Comparison of endovascular aneurysm repair with open repair in patients with abdominal aortic aneurysm (EVAR trial 1), 30-day operative mortality results: randomised controlled trial. Lancet. 2004;364(9437):843-8. Epub 2004/09/08.
84. Lederle FA, Freischlag JA, Kyriakides TC, Padberg FT, Jr., Matsumura JS, Kohler TR, et al. Outcomes following endovascular vs open repair of abdominal aortic aneurysm: a randomized trial. JAMA. 2009;302(14):1535-42. Epub 2009/10/15.
85. Hinchliffe RJ, Bruijstens L, MacSweeney ST, Braithwaite BD. A randomised trial of endovascular and open surgery for ruptured abdominal aortic aneurysm - results of a pilot study and lessons learned for future studies. Eur J Vasc Endovasc Surg. 2006;32(5):506-13; discussion 14-5. Epub 2006/08/05.
86. Wolf YG, Thomas WS, Brennan FJ, Goff WG, Sise MJ, Bernstein EF. Computed tomography scanning findings associated with rapid expansion of abdominal aortic aneurysms. J Vasc Surg. 1994;20(4):529-35; discussion 35-8. Epub 1994/10/01.
87. Fillinger MF, Racusin J, Baker RK, Cronenwett JL, Teutelink A, Schermerhorn ML, et al. Anatomic characteristics of ruptured abdominal aortic aneurysm on conventional CT scans: Implications for rupture risk. J Vasc Surg. 2004;39(6):1243-52. Epub 2004/06/12.
88. Hans SS, Jareunpoon O, Balasubramaniam M, Zelenock GB. Size and location of thrombus in intact and ruptured abdominal aortic aneurysms. J Vasc Surg. 2005;41(4):584-8. Epub 2005/05/06.
89. Giannoglou G, Giannakoulas G, Soulis J, Chatzizisis Y, Perdikides T, Melas N, et al. Predicting the risk of rupture of abdominal aortic aneurysms by utilizing various geometrical parameters: revisiting the diameter criterion. Angiology. 2006;57(4):487-94. Epub 2006/10/07.
90. Pappu S, Dardik A, Tagare H, Gusberg RJ. Beyond fusiform and saccular: a novel quantitative tortuosity index may help classify aneurysm shape and predict aneurysm rupture potential. Ann Vasc Surg. 2008;22(1):88-97. Epub 2007/11/21.

91. Martufi G, Di Martino ES, Amon CH, Muluk SC, Finol EA. Three-dimensional geometrical characterization of abdominal aortic aneurysms: image-based wall thickness distribution. J Biomech Eng. 2009;131(6):061015. Epub 2009/05/20.

92. Roy D, Kauffmann C, Delorme S, Lerouge S, Cloutier G, Soulez G. A Literature Review of the Numerical Analysis of Abdominal Aortic Aneurysms Treated with Endovascular Stent-Grafts. Comput Math Methods Med. 2012. Epub Accepted, in press.

93. Raghavan ML, Webster MW, Vorp DA. Ex vivo biomechanical behavior of abdominal aortic aneurysm: assessment using a new mathematical model. Ann Biomed Eng. 1996;24(5):573-82. Epub 1996/09/01.

94. Fillinger MF, Marra SP, Raghavan ML, Kennedy FE. Prediction of rupture risk in abdominal aortic aneurysm during observation: wall stress versus diameter. J Vasc Surg. 2003;37(4):724-32. Epub 2003/03/29.

95. Fillinger MF, Raghavan ML, Marra SP, Cronenwett JL, Kennedy FE. In vivo analysis of mechanical wall stress and abdominal aortic aneurysm rupture risk. J Vasc Surg. 2002;36(3):589-97. Epub 2002/09/10.

96. Wever JJ, Blankensteijn JD, Th MMWP, Eikelboom BC. Maximal aneurysm diameter follow-up is inadequate after endovascular abdominal aortic aneurysm repair. Eur J Vasc Endovasc Surg. 2000;20(2):177-82. Epub 2000/08/16.

97. Golledge J, Wolanski P, Parr A, Buttner P. Measurement and determinants of infrarenal aortic thrombus volume. Eur Radiol. 2008;18(9):1987-94. Epub 2008/04/17.

98. van Prehn J, van der Wal MB, Vincken K, Bartels LW, Moll FL, van Herwaarden JA. Intra- and interobserver variability of aortic aneurysm volume measurement with fast CTA postprocessing software. J Endovasc Ther. 2008;15(5):504-10. Epub 2008/10/09.

99. Lee JT, Aziz IN, Lee JT, Haukoos JS, Donayre CE, Walot I, et al. Volume regression of abdominal aortic aneurysms and its relation to successful endoluminal exclusion. J Vasc Surg. 2003;38(6):1254-63. Epub 2003/12/19.

100. Fillinger M. Three-dimensional analysis of enlarging aneurysms after endovascular abdominal aortic aneurysm repair in the Gore Excluder Pivotal clinical trial. J Vasc Surg. 2006;43(5):888-95. Epub 2006/05/09.

101. Bley TA, Chase PJ, Reeder SB, Francois CJ, Shinki K, Tefera G, et al. Endovascular abdominal aortic aneurysm repair: nonenhanced volumetric CT for follow-up. Radiology. 2009;253(1):253-62. Epub 2009/08/26.

102. Dugas A, Therasse E, Kauffmann C, Tang A, Elkouri S, Nozza A, et al. Reproducibility of abdominal aortic aneurysm diameter measurement and growth evaluation on axial and multiplanar computed tomography reformations. Cardiovasc Intervent Radiol. 2012;35(4):779-87. Epub 2011/08/25.

103. Kauffmann C, inventor; Method for tracking 3D anatomical and pathological changes in tubular-shaped anatomical structures patent PCT/CA2008/000933. 2011.

104. Morin-Roy F, Kauffmann C, Hadjadj S, Thomas O, Tang A, Therasse E, et al. Abdominal Aortic Aneurysm Segmentation on CT Angiography: Optimization of a Semiautomated Software, Impact of Contrast Injection and Stent-graft Implantation on Volume Measurements Reproducibility. Radiological Society of North America Scientific Assembly and Annual Meeting Program. Oak Brook, Ill: Radiological Society of North America; 2011.

105. Wolf YG, Hill BB, Rubin GD, Fogarty TJ, Zarins CK. Rate of change in abdominal aortic aneurysm diameter after endovascular repair. J Vasc Surg. 2000;32(1):108-15. Epub 2000/07/06.

106. Sprouse LR, 2nd, Meier GH, 3rd, Parent FN, DeMasi RJ, Glickman MH, Barber GA. Is ultrasound more accurate than axial computed tomography for determination of maximal abdominal aortic aneurysm diameter? Eur J Vasc Endovasc Surg. 2004;28(1):28-35.

107. Nambi P, Sengupta R, Krajcer Z, Muthupillai R, Strickman N, Cheong BY. Non-contrast Computed Tomography is Comparable to Contrast-enhanced Computed Tomography for Aortic Volume Analysis after Endovascular Abdominal Aortic Aneurysm Repair. Eur J Vasc Endovasc Surg. Epub 2011/01/05.

108. Caldwell DP, Pulfer KA, Jaggi GR, Knuteson HL, Fine JP, Pozniak MA. Aortic aneurysm volume calculation: effect of operator experience. Abdom Imaging. 2005;30(3):259-62. Epub 2005/02/03.

109. Bengtsson H, Sonesson B, Bergqvist D. Incidence and prevalence of abdominal aortic aneurysms, estimated by necropsy studies and population screening by ultrasound. Ann N Y Acad Sci. 1996;800:1-24. Epub 1996/11/18.

110. Hall AJ, Busse EF, McCarville DJ, Burgess JJ. Aortic wall tension as a predictive factor for abdominal aortic aneurysm rupture: improving the selection of patients for abdominal aortic aneurysm repair. Ann Vasc Surg. 2000;14(2):152-7. Epub 2000/04/01.

111. Vorp DA, Raghavan ML, Webster MW. Mechanical wall stress in abdominal aortic aneurysm: influence of diameter and asymmetry. J Vasc Surg. 1998;27(4):632-9. Epub 1998/05/12.

112. Kauffmann C, Tang A, Dugas A, Therasse E, Oliva V, Soulez G. Clinical validation of a software for quantitative follow-up of abdominal aortic aneurysm maximal diameter and growth by CT angiography. Eur J Radiol. 2009. Epub 2009/12/08.

113. Kauffmann C, Tang A, Therasse E, Soulez G. An Hybrid CPU-GPU Framework for Quantitative Follow-up of Abdominal Aortic Aneurysm Volume by CT Angiography. Proceedings of the SPIE. 2010;7624:12. Epub March 9 2010.

114. Kent KC, Zwolak RM, Jaff MR, Hollenbeck ST, Thompson RW, Schermerhorn ML, et al. Screening for abdominal aortic aneurysm: a consensus statement. J Vasc Surg. 2004;39(1):267-9. Epub 2004/01/14.

115. Cosford PA, Leng GC. Screening for abdominal aortic aneurysm. Cochrane Database Syst Rev. 2007(2):CD002945. Epub 2007/04/20.

116. Hirsch AT, Haskal ZJ, Hertzer NR, Bakal CW, Creager MA, Halperin JL, et al. ACC/AHA 2005 Practice Guidelines for the management of patients with peripheral arterial disease (lower extremity, renal, mesenteric, and abdominal aortic): a collaborative report from the American Association for Vascular Surgery/Society for Vascular Surgery, Society for Cardiovascular Angiography and Interventions, Society for Vascular Medicine and Biology, Society of Interventional Radiology, and the

ACC/AHA Task Force on Practice Guidelines (Writing Committee to Develop Guidelines for the Management of Patients With Peripheral Arterial Disease): endorsed by the American Association of Cardiovascular and Pulmonary Rehabilitation; National Heart, Lung, and Blood Institute; Society for Vascular Nursing; TransAtlantic Inter-Society Consensus; and Vascular Disease Foundation. Circulation. 2006;113(11):e463-654. Epub 2006/03/22.

117. Rubin GD, Armerding MD, Dake MD, Napel S. Cost identification of abdominal aortic aneurysm imaging by using time and motion analyses. Radiology. 2000;215(1):63-70. Epub 2001/02/07.
118. Lederle FA. Risk of rupture of large abdominal aortic aneurysms. Disagreement among vascular surgeons. Arch Intern Med. 1996;156(9):1007-9. Epub 1996/05/13.
119. Di Martino ES, Bohra A, Vande Geest JP, Gupta N, Makaroun MS, Vorp DA. Biomechanical properties of ruptured versus electively repaired abdominal aortic aneurysm wall tissue. J Vasc Surg. 2006;43(3):570-6; discussion 6. Epub 2006/03/08.

Appendix

Appendix 1. Mathematical definitions of geometric indices

Summary

In this appendix, various mathematical definitions of geometric indices are presented, ranging from the simplest to more abstract measurements. The 1D indices represent lengths. The 2D indices are derived from 1D measurements. The 3D size indices, 3D shape indices and second-order curvature-based indices require AAA segmentation and calculation with a dedicated software. The figures and tables below are adapted from Martufi *et al*. (91) and Shum *et al*. (53).

The purpose of our study was to compare these geometric indices in ruptured or symptomatic with unruptured AAAs.

The 1D indices are represented in Figure A.1.

In the tables below, the following color convention is used: the geometric indices measured from lumen and thrombus mesh are highlighted in blue. The shape indices calculated from the indices in blue are highlighted in orange. Data affected by the Dmax value are highlighted in pink.

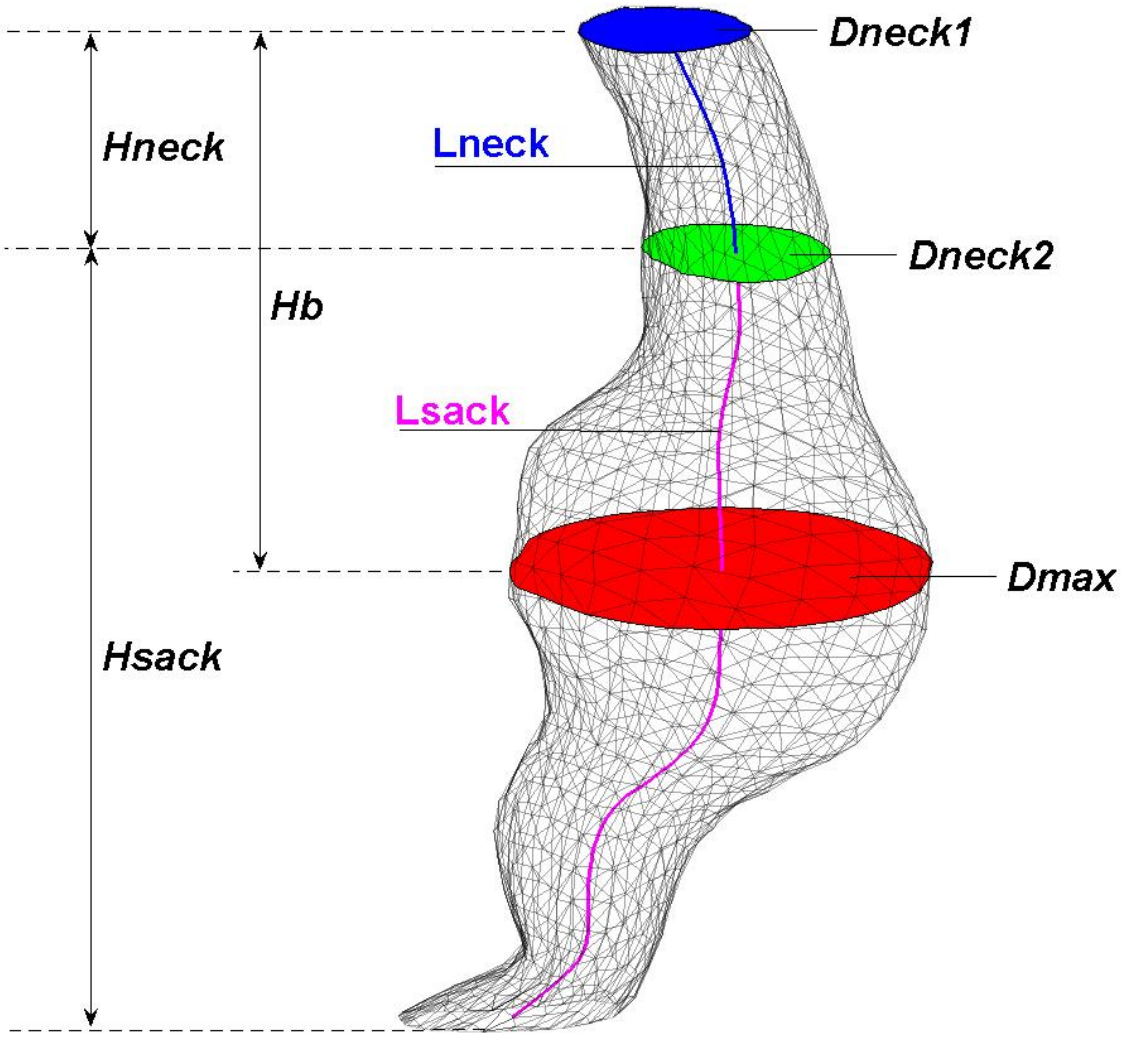

Figure A.1. Definition of 1 D geometrical indices, modified from Martufi *et al*. (91).

Table A.1: One-dimensional size indices

Variable	Units	Definition
Dmax	mm	Geometrical definition of the maximum diameter, defined as the greatest distance included in the contour
Dneck1	mm	Proximal neck diameter immediately below the renal arteries
Dneck2	mm	Distal neck diameter, defined as 20% enlargement of proximal neck, where: Neck_Area > Neck_Area1 * 1.2
Hsac	mm	Height of sac, defined as the perpendicular distance from the cross section where Dneck2 is measured to the distal end of AAA
Hneck	mm	Height of neck, defined as the perpendicular distance from the cross section where Dneck1 is measured to the cross section where Dneck2 is measured
Lsac	mm	Length of AAA sac centerline from neck2 to the distal end of AAA
Lneck	mm	Length of neck centerline between the two planes defined by neck1 and neck2
Hb	mm	Bulge height, defined as the perpendicular distance from the cross section where Dmax is measured to the cross section where Dneck1 is measured
dc	mm	Distance between the lumen centroid and the centroid of the cross section where Dmax is located
d	mm	Euclidean distance from the centroid of the cross section where Dneck1 is located to the centroid of the cross section at the AAA distal end.

Table A.2: Two-dimensional size indices

Variable	Units/type	Definition
DHr	ratio	Diameter-height ratio : DHr = Dmax / H
DDr	ratio	Diameter-diameter ratio : DDr = Dmax / Dneck1
Hr	ratio	Height ratio : Hr = H / Hneck
BL	ratio	Bulge location : BL=Hb/H
ß	ratio	Asymmetry factor : β=1−dc/Dmax
T	ratio	Tortuosity : T = (L+ Lneck) / d

Table A.3: Three-dimensional size indices

Table 3. Three-dimensional size indices		
Variable	Units/type	Definition
V	ml	Outer wall AAA volume
S	mm^2	Outer wall surface area of the AAA sac
VILT	ml	Volume of intraluminal thrombus contained within the AAA sac
γ	ratio	Ratio of AAA ILT volume defined as: γ = VILT/V

Table A.4: Three-dimensional shape indices

Variable	Units/type	Definition
IPR3D	ratio	3D isoperimetric ratio. The ratio of the luminal surface area to the volume of the sac is a quantification of the degree of folding of the surface area. $$IPR = \frac{S_L}{V^{2/3}}$$
NFI	ratio	Non fusiform index. Varies from 0 (fusiform shaped aneurysm) to 1 (deviation from fusiform). $$NFI = \frac{IPR}{IPR_{fusiform}} = \frac{\frac{S_L}{V^{2/3}}}{\frac{S_{L\,fusiform}}{V_{fusiform}^{2/3}}}$$

Table A.5: Second order curvature-based indices

Variable	Units/type	Definition
GAA	10^{-2} mm^{-1}	Gaussian averaged area curvature. A positive index indicates a surface with an elliptic region, whereas a negative index indicates a hyperbolic region. GAA depends on the shape and size of the aneurysm. $GAA = \frac{\sum_{all\ elements} K_j S_j}{\sum_{all\ elements} S_j}$
MAA	10^{-2} mm^{-1}	Mean averaged area curvature. A positive index indicates a surface with an elliptic region, whereas a negative index indicates a hyperbolic region. MAA depends on the shape and size of the aneurysm. $MAA = \frac{\sum_{all\ elements} M_j S_j}{\sum_{all\ elements} S_j}$
GLN	non-dimensional ratio	L2 norm of the Gaussian curvature. The nondimensional GLN depends on the surface shape and represents a measure of irregularities on the AAA surface. $\mathrm{GLN} = \frac{1}{4\pi}\sqrt{\sum_{\text{all elements}} S_j \cdot \sum_{\text{all elements}} (K_j^2 S_j)}$
MLN	non-dimensional ratio	L2 norm of the Mean curvature. The nondimensional MLN depends on the surface shape and represents a measure of irregularities on the AAA surface. $\mathrm{MLN} = \frac{1}{4\pi}\sqrt{\sum_{\text{all elements}} (M_j^2 S_j)}$

Appendix 2. Manuscript 1: Reproducibility of AAA diameter measurement and growth. Published in *Cardiovascular and Interventional Radiology* (102). Full text reproduced with permission from licensed content publisher (Springer) and all co-authors.

Cardiovasc Intervent Radiol
DOI 10.1007/s00270-011-0259-y

CLINICAL INVESTIGATION

Reproducibility of Abdominal Aortic Aneurysm Diameter Measurement and Growth Evaluation on Axial and Multiplanar Computed Tomography Reformations

Alexandre Dugas · Éric Therasse · Claude Kauffmann · An Tang · Stephane Elkouri · Anna Nozza · Marie-France Giroux · Vincent L. Oliva · Gilles Soulez

Received: 7 April 2011 / Accepted: 9 August 2011

Abstract
Purpose To compare different methods measuring abdominal aortic aneurysm (AAA) maximal diameter (Dmax) and its progression on multidetector computed tomography (MDCT) scan.
Materials and Methods Forty AAA patients with two MDCT scans acquired at different times (baseline and follow-up) were included. Three observers measured AAA diameters by seven different methods: on axial images (anteroposterior, transverse, maximal, and short-axis views) and on multiplanar reformation (MPR) images (coronal, sagittal, and orthogonal views). Diameter measurement and progression were compared over time for the seven methods. Reproducibility of measurement methods was assessed by intraclass correlation coefficient (ICC) and Bland–Altman analysis.
Results Dmax, as measured on axial slices at baseline and follow-up (FU) MDCTs, was greater than that measured using the orthogonal method ($p = 0.046$ for baseline and 0.028 for FU), whereas Dmax measured with the orthogonal method was greater those using all other measurement methods (p-value range: <0.0001–0.03) but anteroposterior diameter ($p = 0.18$ baseline and 0.10 FU). The greatest interobserver ICCs were obtained for the orthogonal and transverse methods (0.972) at baseline and for the orthogonal and sagittal MPR images at FU (0.973 and 0.977). Interobserver ICC of the orthogonal method to document AAA progression was greater (ICC = 0.833) than measurements taken on axial images (ICC = 0.662–0.780) and single-plane MPR images (0.772–0.817).
Conclusion AAA Dmax measured on MDCT axial slices overestimates aneurysm size. Diameter as measured by the orthogonal method is more reproducible, especially to document AAA progression.

A. Dugas · É. Therasse · C. Kauffmann · A. Tang · M.-F. Giroux · V. L. Oliva · G. Soulez (✉)
Department of Radiology, Centre Hospitalier de l'Université de Montreal (CHUM) and CHUM Research Center (CRCHUM), University of Montreal, Montreal, QC, Canada

S. Elkouri
Department of Surgery, Centre Hospitalier de l'Université de Montreal (CHUM), University of Montreal, Montreal, QC, Canada

A. Nozza
Montreal Heart Institute Coordinating Centre, Institut de Cardiologie de Montréal, Montreal, QC, Canada

Introduction

Current indications to intervene in patients with abdominal aortic aneurysm (AAA), either by the surgical or endovascular approaches, are mostly based on the AAA's maximal diameter (Dmax) [1–4]. AAA FU, before and after intervention, also relies on Dmax measurements, because treatment is based on its progression [2, 5–8]. Although reports on AAA volumetric analysis are emerging [9–17], Dmax remains the most widely accepted criterion for AAA evaluation and therapeutic management.

Previous studies have advocated different ways of measuring Dmax and its evolution by multidetector computed tomography (MDCT). Although some investigators have suggested Dmax assessment on axial slices (axialDmax) [3, 18], others have proposed the measurement of the diameter perpendicular to axialDmax (shortaxisD) [19–22], anteroposterior diameter (APD) [23–25], transverse diameter (transD) [24], and diameter perpendicular to the

Published online: 24 August 2011

estimated central line on axial slices [26]. Finally, several researchers have recommended the measurement of diameter perpendicular to the aneurysm's central line (orthogonal) on multiplanar reformation (MPR [orthoD]) [6, 16, 27, 28]. Investigations reporting on orthoD have either used single-plane reformation [24], used specialized software [16, 27] or not precisely described the method of plane selection [6, 19]. Moreover, debates based on reproducibility concerns persist [26, 28]. The two main issues involved in selecting the best measurement method are its reproducibility and theoretical "truthfulness" in the absence of a "gold standard" [29].

It has been recognized and supported by ultrasound data [18, 27, 30] that axialDmax tends to overestimate real diameters, especially in the presence of tortuous aorta, because the axial plane is one perpendicular to the patient's craniocaudal axis but not necessarily perpendicular to the long axis of the aorta [29–33]. This explains why ultrasound shows better correlation with orthoD measurements on MDCT when they are taken perpendicular to the central line [27]. However, ultrasound can be less reproducible, especially for patient FU [29–32].

With widely available MPR images on MDCT workstations, a double-oblique plane perpendicular to the central axis of the aneurysm can be easily generated to calculate orthoD. However, because this method involves more manipulations, reproducibility may be decreased [24].

According to the Society of Vascular Surgery guidelines [28], the aneurysm diameter should be measured perpendicular to the centerline of the aneurysm or, as a second-best choice if multiplanar reconstruction is not available, perpendicular to the maximum ellipse on axial computed tomography (CT). However, despite variable approaches recommended in the literature, no study has specifically evaluated the reproducibility of all of these different approaches of diameter measurement to estimate AAA progression.

The purpose of the present investigation was to assess and compare the intraobserver and interobserver reproducibility of all approaches reported previously for AAA Dmax measurement on MDCT axial slices and on single- and double-oblique MPR images. The secondary objective was to evaluate the reproducibility of these different methods in the assessment of diameter progression over time.

Materials and Methods

Study Design and Patient Selection

We performed a retrospective study of 40 patients with AAA examined by MDCT. Patients were selected from the radiological information system if they had an untreated (endovascular or surgical) AAA with a diameter >3.5 cm and at least two MDCT examinations available on the local picture archiving and communication (PACS) system with a minimum 6-month interval between the two examinations. These patients were then contacted by a research nurse. Approval of radiological imaging was obtained through written patient consent. The Institutional Review Board approved this Health Insurance Portability and Accountability Act-compliant research project. If a patient had >2 MDCT examinations, the most remote and most recent pretreatment examinations were selected. In total, 80 MDCT examinations were analyzed.

MDCT Protocols

All 80 examinations were undertaken on 4 different MDCT scanners (Somatom Sensation 4, 16, and 64; Siemens, Erlangen, Germany; Lightspeed 16; General Electric, Milwaukee, WI). The scanning parameters were as follows: pitch 1 to 1.5, slice thickness 1–2 mm, collimation 0.75–1.5, and field of view ranging from 240 to 320. Intravenous contrast was injected at 3–5 ml/s for a total of 80–120 ml. Bolus-tracking technique was used for all examinations.

Measurement Methods

Three observers (one senior resident and two vascular interventional radiologists with >10 years of experience), who were blinded to previous radiological reports, independently measured aneurysm Dmax on each of the 80 examinations using seven different methods. All diameters were measured from the aneurysms' outside to outside wall using electronic callipers with zooming function (liberally performed) and, when judged to be pertinent, on the same workstation (Impax version 5.2; Agfa, Mortsel, Belgium).

The first four diameters were measured on original axial slices. By scrolling through the axial images, each observer selected the slice on which he thought the largest diameter was present, as would be performed clinically. After slice selection, the following diameters were measured: (1) from anterior to posterior wall (APD), (2) from right to left lateral wall (transD), (3) maximal diameter in any direction (axialDmax) and (4) perpendicular to axialDmax (short-axisD) (Fig. 1).

Afterward, MPR images (reconstructed with a slice thickness of 1–3 mm) were processed from axial images with workstation MPR software (Impax version 5.2). Dmax perpendicular to the long axis of the aneurysm was measured on two single-plane MPR images: coronal (CoroMPRD) and sagittal planes (SagMPRD) (Fig. 2).

Finally, the last diameter was measured on a double-oblique reformation by establishing a plane perpendicular to the largest portion of the aneurysm, first on sagittal MPR images, then on coronal MPR images, creating a "modified axial" plane perpendicular to the long axis of the aneurysm

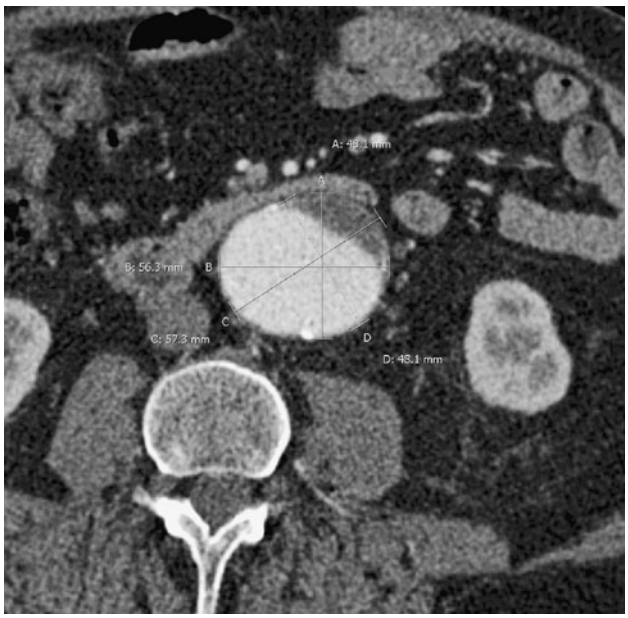

Fig. 1 CT scan acquisition in a 77-year-old man with an AAA. After selection of the axial slice displaying the largest diameter, the radiologist measured the following diameters: *A* APD, *B* TransD, *C* AxialDmax, and *D* ShortaxisD

in two orthogonal planes (i.e., double-oblique). Aneurysm maximum diameter (in any axis) of that orthogonal plane was then measured (Fig. 3), thus constituting orthoD.

To obtain intraobserver reproducibility, two of the three observers (one junior and one senior), who were blinded to the radiological report and to their first set of measurements, independently measured every diameter (seven different methods on 80 examinations) a second time with a minimal 4-week interval according to the same protocol described previously.

The time required to measure orthoD was recorded on that second set of values. The calculated time include the time needed to create the double-oblique reformation from the axial source images, measure Dmax, and store it in the PACS system.

Data Analysis

Patient Demographics and Aneurysm Characteristics

Descriptive statistics of patient baseline demographics, the interval between the two MDCT scans and mean AAA diameters (averaging all values; 40 examinations, three observers, and seven different methods) at baseline and FU, were calculated with SDs. For each type of method, the measurements of the first reading from the three observers were averaged for each patient. A one-factor (type of method) repeated-measures analysis model using PROC MIXED was then used to assess differences among the methods. The *p*-values from the SAS procedure were adjusted using Bonferroni method to correct for multiple comparisons. This was performed separately for both the baseline and FU examinations. For each observer, the measurements of the first reading from all of the seven methods were averaged for each patient. Again, a one-factor (observer) repeated-measures analysis model using PROC MIXED was used to assess differences among the three observers for both the baseline and FU examination

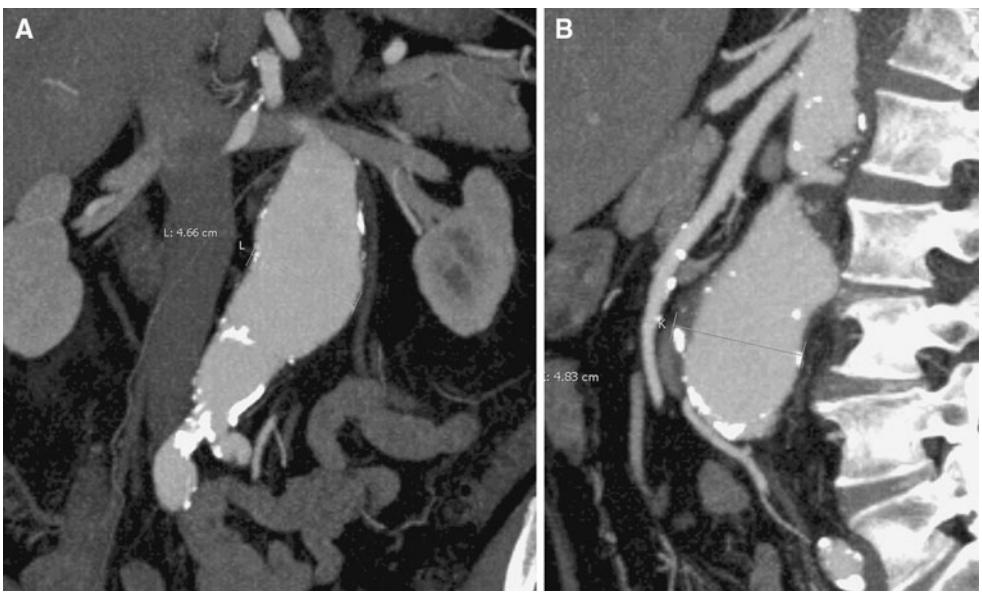

Fig. 2 Same patient shown in Fig. 1. Measurement of Dmax on single-plane MPR images. **A** Dmax measured on CoroMPRD. **B** Dmax measured on SagMPRD

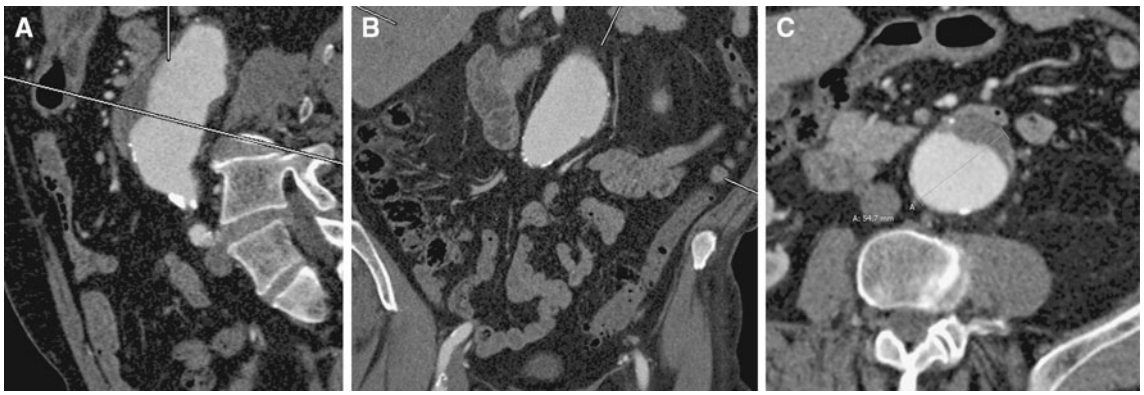

Fig. 3 Same patient shown in Fig. 1. Creation of double-oblique MPR images (orthogonal plane) and measurement of orthoD. **A** First, a plane perpendicular to the long axis of the largest portion of the AAA is created on sagittal MPR images. **B** Then a plane perpendicular to the long axis of the largest portion of the AAA is created on coronal MPR images. **C** Finally, Dmax is measured on the orthogonal plane created from the two previous steps (orthoD)

separately. In addition, for the first reading, to assess discordant differences <5 mm among the seven methods for both the baseline and FU scans combined ($n = 80$ scans) was determined using McNemar's test. All analyses were performed with SAS version 9.2 (SAS, Cary, NC), and p value <0.05 was considered statistically significant.

Intraobserver and Interobserver Reproducibility

Interobserver (three readers) and intraobserver (two readers) reproducibility was assessed by intraclass coefficient (ICC) for all seven methods. ICC between the three observers when evaluating aneurysm diameter progression (between baseline and FU MDCTs) was also measured for all seven methods.

Interobserver Discordance by Measurement Method and by Threshold-of-Measurement Discordance for all Examinations

Interobserver reproducibility was also assessed by looking at absolute differences between measurements as performed previously in other studies [18, 19, 25, 27, 32, 33]. Absolute differences, recorded as being <5 or ≥5 mm and <10 or ≥10 mm, were calculated by taking into account all three observers. That is, to be recorded as <5 mm, differences between maximal and minimal values out of the three values available for the three observers for a particular examination and a single method (3 observers) had to be <5 mm. This concept was applied to all seven methods, computing all 80 examinations (baseline and FU) by each method.

Finally, Bland–Altman analysis was undertaken to assess mean errors for the different methods of diameter measurement (all observers together) compared with the orthoD approach to estimate aneurysm progression between baseline and FU. Range of agreement was defined as bias ±2 SDs, where SDs was the corrected SDs of differences between the two methods.

Results

Patient Demographics and Aneurysm Characteristics

Forty patients (33 men and 7 women) with a mean age of 72 years (range 49–86) were studied. The average interval between baseline and FU MDCTs was 16 ± 8 months (range 8–42). Considering all measurement methods and observers, average diameter was 49.2 ± 6.9 mm (range 31.6–74.1) at baseline and 53.2 ± 8.4 mm (range 31.3–77.4) at FU ($p < 10^{-6}$).

Descriptive Analysis of the Different Measurement Methods

Average measurements (40 patients) taken during the first reading session are listed in Table 1 by observer and measurement method for baseline and FU. The means of all diameters measured (40 patients and seven diameter measurement methods) at baseline and FU were, respectively, 49.4 ± 7.0 and 53.4 ± 8.5 mm for observer 1, 49.0 ± 6.8 and 53.2 ± 8.5 mm for observer 2, and 49.1 ± 6.8 and 53.1 ± 8.2 mm for observer 3. The means of all diameters generated by observer 1 were significantly larger than by observers 2 ($p < 0.008$) and 3 ($p = 0.05$) at baseline, but no difference was observed at FU.

For all observers, the largest diameter evaluation was obtained with axialDmax followed by orthoD. AxialDmax yielded diameters significantly larger than orthoD for baseline and FU ($p = 0.046$ and 0.028 respectively), whereas orthoD was significantly larger than all other

Table 1 Mean diameters by measurement method and by observers[a]

Measurement method (mm)	APD	TransD	AxialDmax	ShortaxisD	CoroMPRD	SagMPRD	OrthoD
Observer 1 (baseline examination)	48.5 ± 6.4	50.1 ± 7.0	52.4 ± 7.0	46.8 ± 6.3	49.3 ± 7.0	48.0 ± 6.6	51.2 ± 7.4
Observer 1 (FU examination)	52.4 ± 8.4	53.8 ± 8.4	56.4 ± 8.4	50.3 ± 7.9	53.4 ± 8.4	52.5 ± 8.4	55.2 ± 8.4
Observer 2 (baseline examination)	48.4 ± 6.4	49.3 ± 6.9	51.0 ± 6.9	47.0 ± 6.2	48.8 ± 6.5	48.4 ± 6.8	50.1 ± 7.4
Observer 2 (FU examination)	52.8 ± 8.9	53.3 ± 8.5	55.4 ± 8.5	51.2 ± 8.5	53.1 ± 8.1	52.1 ± 8.5	54.3 ± 8.7
Observer 3 (baseline examination)	48.5 ± 6.6	49.3 ± 6.6	51.6 ± 6.8	46.7 ± 6.0	48.6 ± 6.5	47.8 ± 7.0	51.2 ± 7.5
Observer 3 (FU examination)	52.0 ± 8.2	53.1 ± 7.9	55.4 ± 8.2	51.1 ± 7.6	53.2 ± 8.3	51.8 ± 8.5	54.9 ± 8.7
Average of 3 observers (baseline examination)	48.5 ± 6.4	49.6 ± 6.8	51.7 ± 6.9	46.8 ± 6.1	48.9 ± 6.6	48.1 ± 6.8	50.8 ± 7.4
Average of 3 observers (FU examination)	52.4 ± 8.3	53.4 ± 8.2	55.8 ± 8.3	50.9 ± 7.8	53.2 ± 8.2	52.1 ± 8.4	54.8 ± 8.5

[a] Forty patients, baseline and FU examinations, first reading

measurements (p range < 0.0001 and 0.03) except APD ($p = 0.18$ at baseline and 0.10 at FU).

Interobserver Reproducibility of Baseline and Follow-Up Examinations

ICCs on interobserver agreement for baseline and FU examinations are listed by measurement method in Table 2. Interobserver ICC was high for all methods, ranging from 0.924 to 0.977. The highest interobserver ICC was obtained with orthoD and transD (0.972) at baseline and orthoD and sagMPRD at FU (0.973 and 0.977, respectively).

Intraobserver Reproducibility of Baseline and Follow-Up Examinations

Intraobserver reproducibility was assessed for every method, and the ICCs are reported in Table 3. All methods showed high intraobserver reproducibility ($p > 0.95$). The intraobserver ICC of orthoD measurements was consistently in the upper range (0.979–0.985) except for the baseline measurements of observer 3, which were in the mid-range (0.969).

Interobserver Discordance by Measurement Method and by Threshold-of-Measurement Discordance for all Examinations (Baseline and Follow-Up)

Interobserver discordance (absolute difference between the highest and lowest AAA measurements of the three observers for a particular examination and a single method) is detailed by threshold-of-measurement discordance in Table 4. Discordance between the three observers never exceeded 10 mm for any of the methods using MPR images (coroMPRD, sagMPRD, orthoD). The smallest discordance with this model was obtained with orthoD, with

Table 2 Interobserver correlation coefficient by measurement method[a]

Measurement method	APD	TransD	AxialDmax	ShortaxisD	CoroMPRD	SagMPRD	OrthoD
ICC baseline (95% CI)	0.961 (0.935–0.978)	0.972 (0.948–0.985)	0.962 (0.923–0.981)	0.940 (0.901–0.965)	0.950 (0.917–0.972)	0.969 (0.948–0.983)	0.972 (0.943–0.986)
ICC follow-up (95% CI)	0.924 (0.877–0.956)	0.955 (0.925–0.974)	0.961 (0.932–0.978)	0.933 (0.890–0.961)	0.968 (0.947–0.982)	0.977 (0.961–0.987)	0.973 (0.954–0.985)

[a] Three observers, 40 CT examinations at baseline and FU, first reading

Table 3 Intraobserver correlation coefficient by measurement method at baseline and FU[a]

Measurement method	APD	TransD	AxialDmax	ShortaxisD	CoroMPRD	SagMPRD	OrthoD
Observer 1 ICC baseline examination (95% CI)	0.967 (0.944)	0.958 (0.929)	0.982 (0.969)	0.967 (0.945)	0.955 (0.924)	0.976 (0.960)	0.985 (0.974)
Observer 1 ICC follow-up examination (95% CI)	0.981 (0.968)	0.989 (0.981)	0.981 (0.968)	0.983 (0.972)	0.975 (0.958)	0.966 (0.942)	0.984 (0.973)
Observer 3 ICC baseline examination (95% CI)	0.978 (0.962)	0.975 (0.958)	0.976 (0.960)	0.953 (0.922)	0.966 (0.943)	0.960 (0.933)	0.969 (0.949)
Observer 3 ICC follow-up examination (95% CI)	0.980 (0.966)	0.977 (0.962)	0.971 (0.952)	0.971 (0.951)	0.967 (0.945)	0.986 (0.976)	0.979 (0.965)

[a] Two observers, 40 CT examinations, first and second readings

Table 4 Interobserver discordance by measurement method and by threshold-of-measurement discordance[a,b]

Measurement method (mm)	APD	TransD	AxialDmax	ShortaxisD	CoroMPRD	SagMPRD	OrthoD
Interobserver difference <5 mm	72 (90)	74 (92.5)	75 (93.75)	70 (87.5)	73 (91.25)	76 (95)	77 (96.25)
Interobserver difference 5–9.9 mm	5 (6.25)	5 (6.25)	4 (5)	9 (11.25)	7 (8.75)	4 (5)	3 (3.75)
Interobserver difference ≥10 mm	3 (3.75)	1 (1.25)	1 (1.25)	1 (1.25)	–	–	–

[a] Eighty CT examinations: 40 baseline and 40 FU

[b] Values are presented as frequencies (percentages)

differences between the three observers being <5 mm in 96.25% and 5–10 mm in 3.75% of examinations. In comparison, the proportion of discordant measurements >5 mm for the six other methods ranged from 5 to 12.5%. The difference in proportion of discordance >5 mm was significant only between the orthoD and shortaxisD methods ($p = 0.035$).

Interobserver Reproducibility of AAA Progression Between Baseline and Follow-Up Examinations

As listed in Table 5, lower values of interobserver ICCs were observed for all measurement methods to document AAA progression compared with baseline or FU diameter measurements. The highest ICC was obtained with orthoD (ICC = 0.833). Lower values were recorded for all measurements taken on axial images (range 0.662–0.780), whereas CoroMPRD and SagMPRD values ranged between 0.772 and 0.817.

Bland–Altman Analysis Comparing DODmax and Other Measurement Methods to Evaluate AAA Progression

Bland–Altman analysis of the comparison between orthoD and other measurement methods of assessing AAA progression between baseline and FU is listed in Table 6. When compared with orthoD, slightly lower AAA progression was observed with APD, transD, and shortaxisD measurements and greater progression with axialDmax, sagMPRD, and coroMPRD measurements, with the latter showing the largest increase in size. However, on Bland–Altman analysis, the 95% CI of mean error for all observers between orthoD and the other methods of documenting AAA progression was always <4 mm. The average time to measure orthoD was 1 min 40 s (range 1–3 min).

Table 6 Bland–Altman analysis comparing mean error between orthoD and all other measurements methods of assessing aneurysm progression[a]

Measurement method	Mean error (mm)	SD (mm)	95% CI (mm)
OrthoD/APD	0.09	1.19	−2.24 to 2.43
OrthoD/TransD	0.13	1.82	−3.45 to 3.70
OrthoD/AxialDmax	−0.09	0.91	−1.88 to 1.70
OrthoD/ShortaxisD	0.06	1.38	−2.75 to 2.64
OrthoD/CoroMPRD	−0.32	1.88	−3.99 to 3.36
OrthoD/SagMPRD	−0.01	1.065	−2.10 to 2.08

[a] All observers

Discussion

As reported previously, we noted that axialDmax leads to larger diameter values compared with orthoD [6, 27]. OrthoD was also significantly greater than all other remaining diameter-measurement methods except APD. In the absence of an absolute gold standard, orthoD measured in a plane perpendicular to the central axis of the aneurysm yields the measure closest to reality because it is independent of the angle of the aneurysm axis relative to the MDCT axial slice. Because orthoD measurement involves more manipulations, it was discouraged by Abada et al. [24]. In their study, they observed slightly better reproducibility of APD and transD measurements compared with CoroD and SagD measurements [24].

The measurements technique of the seven methods under evaluation in our study was well standardized, resulting in high interobserver agreement for all of them at baseline and FU (ICC > 0.92). Standardization of measurement techniques on the workstation has been shown to be an important factor for improvement of reproducibility [20, 26].

Table 5 Intraclass interobserver correlation coefficient by method to evaluate AAA progression[a]

Measurement method	APD	TransD	AxialDmax	ShortaxisD	CoroMPRD	SagMPRD	OrthoD
ICC (95% CI)	0.662 (0.507–0.789)	0.773 (0.653–0.863)	0.780 (0.664–0.868)	0.738 (0.606–0.841)	0.772 (0.652–0.863)	0.817 (0.715–0.891)	0.833 (0.739–0.901)

[a] Forty patients, 80 CT examinations, three observers, first reading

In our investigation, however, orthoD measurement was among the methods demonstrating the highest interobserver and intraobserver reproducibility for baseline study and among the greatest for FU study. It presented the lowest proportion of discordance >5 mm (3.75%) between observers, whereas this proportion was significantly greater at 12.5% when using the shortaxisD method, which has been proposed by several investigators [19–21]. Dillavou et al. reported high interobserver reproducibility of orthoD (ICC = 0.95), which was superior to manual measurement with shortaxisD (ICC = 0.90). However, their method of determining orthoD was not clearly defined [19].

Other investigators have measured orthoD by manually constructing a median centerline through the lumen and assessing transverse aortic diameter in a plane perpendicular to it [6, 34]. With this approach, Wever et al. [34] obtained a good interobserver repeatability coefficient (3.9 mm) and acceptable mean error (1.61 ± 2 mm) with this method.

Advanced postprocessing software can now easily and automatically generate the central line from the enhanced aortic lumen [16]. However, this central line can be different from the real AAA central line, especially if the thrombus is asymmetrical. Basically, all commercially available software conceived to generate reformation from luminal central line were validated to calculate lumen vessel stenosis and not the maximal diameter of an aneurysm surrounded by a thrombus. To automatically generate a true AAA central line calculated from the aneurysm wall, segmentation of the thrombus and the external wall of the AAA is necessary. Because surrounding structures (psoas,

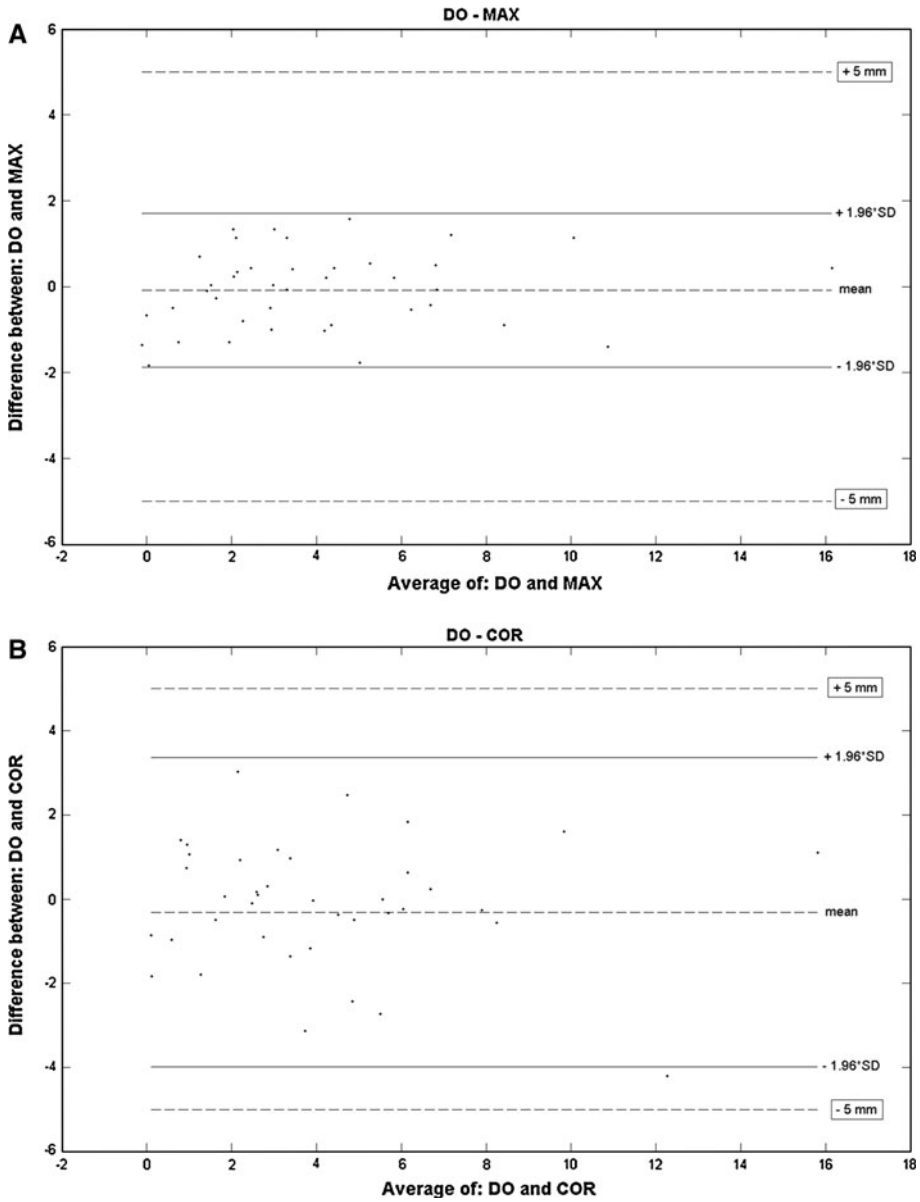

Fig. 4 Bland–Altman analysis plotting differences in Dmax between the orthoD and six other methods of documenting AAA progression between baseline and follow-up examinations. **A** The best agreement was observed between orthoD and AxialDmax. **B** The worst agreement was observed between orthoD and CoroMPRD

inferior vena cava, and duodenum) display the same density as the aortic thrombus and wall, this is not an easy task [35]. We recently validated semiautomatic software allowing aortic segmentation of the different AAA components with an average time of 3 min [36]. Using the same database, orthoD measured by this software presented a good correlation with the manual orthoD method with a mean absolute difference of 1.1 ± 0.9 mm and error always <5 mm [36], confirming that manual measurement of orthoD using the double-oblique method is close to true orthogonal diameter computed with a validated software.

In our study, the reproducibility of all methods to assess Dmax progression during FU was lower than baseline and FU measurements. Because Dmax assessment computes the difference between two measurements, the combined variability of the baseline and FU diameter measurement explains its greater variability. Hence, the reproducibility of Dmax progression is important in clinical practice because diameter progression is a criteria for therapeutic management before surgical or endovascular aortic aneurysm repair (EVAR) and after EVAR. In this setting, the orthoD method presented the best interobserver reproducibility in assessing Dmax progression. It is interesting that estimation of AAA progression based on axial slice measurements was less reproducible than measurements taken on MPR or double-oblique images. It is probably easier to perform consecutive measurements at baseline and FU examinations in the same portion of the AAA on MPR images in a longitudinal aneurysm axis. SagMPRD showed high reproducibility, being the second most reproducible method to assess AAA growth. However because it does not reflect exactly the growth of the true maximum diameter, it is not advisable to rely on this method.

Finally, when comparing Dmax progression, as assessed by orthoD, with the six other methods by Bland-Altman analysis, small differences were seen, except for Coro-MPRD, which tended to show slightly larger AAA growth. The best agreement for orthoD was obtained with AxialDmax (Table 6; Fig. 4). OrthoD could be easily processed on any standard PACS workstation with an average required time of 1 min 40 s (range 1–3 min) in our hands. Hence, it is easy to integrate into clinical workflow.

The main limitation of our study is the absence of an absolute gold standard. That being said, measurement reproducibility is the main concern, especially when endovascular specialists must assess diameter variation between two consecutive examinations.

Conclusion

AAA diameter should not be measured as Dmax on the axial plane because this measurement depends on the angle of aneurysm axis relative to the axial CT slice, often resulting in aneurysm size overestimation. Measurements should be taken on a plane orthogonal to the aneurysm's central axis. The orthoD method, based on a modified axial plane perpendicular to orthogonal, coronal, and sagittal MPR images on a standard PACS workstation, yields measurements that are highly reproducible for evaluating AAA diameter and its growth over time.

Acknowledgments This work was supported by a clinical research scholarship (to G. S.) from Fonds de la Recherche en Santé du Québec; an operating grant from the Ministère du Développement Économique, de L'innovation et de L'exportation du Québec (Grant No. PSVT3-12792); and the Canadian Head of Academic Radiologist.

Conflict of interest None.

References

1. Nevitt MP, Ballard DJ, Hallett JW Jr (1989) Prognosis of abdominal aortic aneurysms. A population-based study. N Engl J Med 321:1009–1014
2. Katz DA, Littenberg B, Cronenwett JL (1992) Management of small abdominal aortic aneurysms. Early surgery vs watchful waiting. JAMA 268:2678–2686
3. The UK Small Aneurysm Trial Participants (1988) Mortality results for randomised controlled trial of early elective surgery or ultrasonographic surveillance for small abdominal aortic aneurysms. Lancet 352:1649–1655
4. Brewster DC, Cronenwett JL, Hallett JW Jr, Johnston KW, Krupski WC, Matsumura JS (2003) Guidelines for the treatment of abdominal aortic aneurysms. Report of a subcommittee of the Joint Council of the American Association for Vascular Surgery and Society for Vascular Surgery. J Vasc Surg 37:1106–1117
5. Brady AR, Thompson SG, Fowkes FG, Greenhalgh RM, Powell JT (2004) Abdominal aortic aneurysm expansion: risk factors and time intervals for surveillance. Circulation 110:16–21
6. Wolf YG, Hill BB, Rubin GD, Fogarty TJ, Zarins CK (2000) Rate of change in abdominal aortic aneurysm diameter after endovascular repair. J Vasc Surg 32:108–115
7. Hackmann AE, Rubin BG, Sanchez LA, Geraghty PA, Thompson RW, Curci JA (2008) A randomized, placebo-controlled trial of doxycycline after endoluminal aneurysm repair. J Vasc Surg 48: 519–526 (discussion 526)
8. Gadowski GR, Pilcher DB, Ricci MA (1994) Abdominal aortic aneurysm expansion rate: effect of size and beta-adrenergic blockade. J Vasc Surg 19:727–731
9. Hatakeyama T, Shigematsu H, Muto T (2001) Risk factors for rupture of abdominal aortic aneurysm based on three-dimensional study. J Vasc Surg 33:453–461
10. Kritpracha B, Beebe HG, Comerota AJ (2004) Aortic diameter is an insensitive measurement of early aneurysm expansion after endografting. J Endovasc Ther 11:184–190
11. van Prehn J, van der Wal MB, Vincken K, Bartels LW, Moll FL, van Herwaarden JA (2008) Intra- and interobserver variability of aortic aneurysm volume measurement with fast CTA postprocessing software. J Endovasc Ther 15:504–510
12. Wever JJ, Blankensteijn JD, Th MMWP, Eikelboom BC (2000) Maximal aneurysm diameter follow-up is inadequate after endovascular abdominal aortic aneurysm repair. Eur J Vasc Endovasc Surg 20:177–182

13. Wolf YG, Tillich M, Lee WA, Fogarty TJ, Zarins CK, Rubin GD (2002) Changes in aneurysm volume after endovascular repair of abdominal aortic aneurysm. J Vasc Surg 36:305–309
14. Bley TA, Chase PJ, Reeder SB et al (2009) Endovascular abdominal aortic aneurysm repair: nonenhanced volumetric CT for follow-up. Radiology 253(1):253–262
15. Bargellini I, Cioni R, Petruzzi P et al (2005) Endovascular repair of abdominal aortic aneurysms: analysis of aneurysm volumetric changes at mid-term follow-up. Cardiovasc Intervent Radiol 28: 426–433
16. White RA, Donayre CE, Walot I, Woody J, Kim N, Kopchok GE (2001) Computed tomography assessment of abdominal aortic aneurysm morphology after endograft exclusion. J Vasc Surg 33(Suppl 2):S1–S10
17. van Keulen JW, van Prehn J, Prokop M, Moll FL, van Herwaarden JA (2009) Potential value of aneurysm sac volume measurements in addition to diameter measurements after endovascular aneurysm repair. J Endovasc Ther 16:506–513
18. Lederle FA, Wilson SE, Johnson GR et al (1995) Variability in measurement of abdominal aortic aneurysms. Abdominal Aortic Aneurysm Detection and Management Veterans Administration Cooperative Study Group. J Vasc Surg 21:945–952
19. Dillavou ED, Buck DG, Muluk SC, Makaroun MS (2003) Two-dimensional versus three-dimensional CT scan for aortic measurement. J Endovasc Ther 10:531–538
20. Aarts NJ, Schurink GW, Schultze Kool LJ et al (1999) Abdominal aortic aneurysm measurements for endovascular repair: Intra- and interobserver variability of CT measurements. Eur J Vasc Endovasc Surg 18:475–480
21. Matsumura JS, Pearce WH, McCarthy WJ, Yao JS (1997) Reduction in aortic aneurysm size: early results after endovascular graft placement. EVT Investigators. J Vasc Surg 25:113–123
22. Rhee RY, Eskandari MK, Zajko AB, Makaroun MS (2000) Long-term fate of the aneurysmal sac after endoluminal exclusion of abdominal aortic aneurysms. J Vasc Surg 32:689–696
23. Wanhainen A, Bergqvist D, Bjorck M (2002) Measuring the abdominal aorta with ultrasonography and computed tomography—difference and variability. Eur J Vasc Endovasc Surg 24: 428–434
24. Abada HT, Sapoval MR, Paul JF, de Maertelaer V, Mousseaux E, Gaux JC (2003) Aneurysmal sizing after endovascular repair in patients with abdominal aortic aneurysm: interobserver variability of various measurement protocols and its clinical relevance. Eur Radiol 13:2699–2704
25. Singh K, Jacobsen BK, Solberg S et al (2003) Intra- and interobserver variability in the measurements of abdominal aortic and common iliac artery diameter with computed tomography. The Tromso Study. Eur J Vasc Endovasc Surg 25:399–407
26. Cayne NS, Veith FJ, Lipsitz EC et al (2004) Variability of maximal aortic aneurysm diameter measurements on CT scan: significance and methods to minimize. J Vasc Surg 39:811–815
27. Sprouse LR II, Meier GH III, Parent FN, DeMasi RJ, Glickman MH, Barber GA (2004) Is ultrasound more accurate than axial computed tomography for determination of maximal abdominal aortic aneurysm diameter? Eur J Vasc Endovasc Surg 28:28–35
28. Chaikof EL, Blankensteijn JD, Harris PL et al (2002) Reporting standards for endovascular aortic aneurysm repair. J Vasc Surg 35:1048–1060
29. Elkouri S, Panneton JM, Andrews JC et al (2004) Computed tomography and ultrasound in follow-up of patients after endovascular repair of abdominal aortic aneurysm. Ann Vasc Surg 18:271–279
30. Sprouse LR II, Meier GH III, Lesar CJ et al (2003) Comparison of abdominal aortic aneurysm diameter measurements obtained with ultrasound and computed tomography: is there a difference? J Vasc Surg 38:466–471 (discussion 471–462)
31. Bargellini I, Cioni R, Napoli V et al (2009) Ultrasonographic surveillance with selective CTA after endovascular repair of abdominal aortic aneurysm. J Endovasc Ther 16:93–104
32. Singh K, Jacobsen BK, Solberg S, Kumar S, Arnesen E (2004) The difference between ultrasound and computed tomography (CT) measurements of aortic diameter increases with aortic diameter: analysis of axial images of abdominal aortic and common iliac artery diameter in normal and aneurysmal aortas. The Tromso Study, 1994–1995. Eur J Vasc Endovasc Surg 28: 158–167
33. Jaakkola P, Hippelainen M, Farin P, Rytkonen H, Kainulainen S, Partanen K (1996) Interobserver variability in measuring the dimensions of the abdominal aorta: comparison of ultrasound and computed tomography. Eur J Vasc Endovasc Surg 12:230–237
34. Wever JJ, Blankensteijn JD, van Rijn JC, Broeders IA, Eikelboom BC, Mali WP (2000) Inter- and intraobserver variability of CT measurements obtained after endovascular repair of abdominal aortic aneurysms. AJR Am J Roentgenol 175:1279–1282
35. Olabarriaga SD, Rouet JM, Fradkin M, Breeuwer M, Niessen WJ (2005) Segmentation of thrombus in abdominal aortic aneurysms from CTA with nonparametric statistical grey level appearance modeling. IEEE Trans Med Imaging 24:477–485
36. Kauffmann C, Tang A, Dugas A, Therasse E, Oliva V, Soulez G (2009) Clinical validation of a software for quantitative follow-up of abdominal aortic aneurysm maximal diameter and growth by CT angiography. Eur J Radiol 77(3):502–508

Appendix 3. Manuscript 2: Clinical validation of a software for quantitative follow-up of AAA maximal diameter and growth by CTA.

Published in *European Journal of Radiology* (36). Full text reproduced with permission from licensed content publisher (Elsevier) and all co-authors.

European Journal of Radiology 77 (2011) 502–508

Contents lists available at ScienceDirect

European Journal of Radiology

journal homepage: www.elsevier.com/locate/ejrad

Clinical validation of a software for quantitative follow-up of abdominal aortic aneurysm maximal diameter and growth by CT angiography

Claude Kauffmann[a,*], An Tang[b,1], Alexandre Dugas[a,2], Éric Therasse[c,3], Vincent Oliva[b,4], Gilles Soulez[b,5]

[a] Department of Medical Imaging, Hôpital Notre-Dame, Centre Hospitalier Universitaire de Montréal, 1560 Sherbrooke Est, Montréal, Québec, Canada H2L 4M1
[b] Department of Medical Imaging, University of Montreal, Hôpital Saint-Luc, Centre Hospitalier Universitaire de Montréal, 1058 rue Saint-Denis, Montréal, Québec, Canada H2X 3J4
[c] Department of Medical Imaging, University of Montreal, Hôpital Hôtel-Dieu, Centre Hospitalier Universitaire de Montréal, 3840 rue Saint-Urbain, Montréal, Québec, Canada H2W 1T8

ARTICLE INFO

Article history:
Received 11 May 2009
Received in revised form 21 July 2009
Accepted 22 July 2009

Keywords:
Abdominal aortic aneurysm
Quantitative analysis
D-max follow-up
3D segmentation
CTA

ABSTRACT

Purpose: To compare the reproducibility and accuracy of abdominal aortic aneurysm (AAA) maximal diameter (D-max) measurements using segmentation software, with manual measurement on double-oblique MPR as a reference standard.
Materials and methods: The local Ethics Committee approved this study and waived informed consent. Forty patients (33 men, 7 women; mean age, 72 years, range, 49–86 years) had previously undergone two CT angiography (CTA) studies within 16 ± 8 months for follow-up of AAA ≥35 mm without previous treatment. The 80 studies were segmented twice using the software to calculate reproducibility of automatic D-max calculation on 3D models. Three radiologists reviewed the 80 studies and manually measured D-max on double-oblique MPR projections. Intra-observer and inter-observer reproducibility were calculated by intraclass correlation coefficient (ICC). Systematic errors were evaluated by linear regression and Bland–Altman analyses. Differences in D-max growth were analyzed with a paired Student's *t*-test.
Results: The ICC for intra-observer reproducibility of D-max measurement was 0.992 (≥0.987) for the software and 0.985 (≥0.974) and 0.969 (≥0.948) for two radiologists. Inter-observer reproducibility was 0.979 (0.954–0.984) for the three radiologists. Mean absolute difference between semi-automated and manual D-max measurements was estimated at 1.1 ± 0.9 mm and never exceeded 5 mm.
Conclusion: Semi-automated software measurement of AAA D-max is reproducible, accurate, and requires minimal operator intervention.

1. Introduction

Abdominal aortic aneurysm (AAA) therapeutic management, either surgical or endovascular and follow-up, currently rely on measurement of the maximal diameter (D-max) [1,2]. While AAA volumetric analysis is an area of active research, D-max remains a widely accepted clinical tool [3,4]. Although ultrasound is a radiation-free, widely available modality for D-max screening and follow-up, it is not as accurate as computed tomographic (CT) angiography for measurement of aneurysm diameter [5,6]. Because of its volumetric acquisition mode suitable for multiplanar and three-dimensional reconstructions of complex anatomy, as well as ability to distinguish between lumen and thrombus, there is an inherent benefit to use CT angiography for modeling of aneurysms. In addition to standard measurements of diameter, length and angulation [7] used for patient selection before EVAR, three-dimensional reconstructions allows the study of thrombus volume [8] and predictors of risk rupture such as expansion rate of aneurysmal volume [3].

Validation of a novel segmentation method requires comparison against established D-max measurement standards. A recent study [9] directly compared different methods of AAA D-max measurement and has shown that the manual double-oblique MPR method is theoretically closest to reality and provides the lowest inter- and intra-observer variability and is theoretically closer to reality than axial and orthogonal multiplanar reformations, which

0720-048X/$ – see front matter © 2009 Elsevier Ireland Ltd. All rights reserved.
doi:10.1016/j.ejrad.2009.07.027

both tend to overestimate the real diameter perpendicular to the centerline.

An ideal software method is commonly associated with automated segmentation. However, fully automated segmentation of AAA generally fails because of low contrast between thrombus and surrounding structures such as psoas, bowel loops or unopacified inferior vena cava. With this approach, the solution is to correct segmentation errors on several hundred slices, a tedious and time-consuming task, incompatible with clinical workflow. For these reasons, a semi-automated or supervised method is more appropriate in clinical practice because segmentation errors can be avoided by introducing user input at specific steps during the segmentation process. Conceptual image understanding is used to initialize algorithmic tasks by the computer. The success of this approach lies in the complementarity between operator and machine tasks.

While published studies have addressed some issues, such as a proof-of-concept of automated D-max calculation [10] or aneurysm volume calculation [11–14], to our knowledge, no clinical validation of an integral solution has been reported for D-max measurement obtained from complete segmentation of AAA wall, lumen, thrombus and calcification.

Thus, the purpose of our study was to develop a semi-automated software for AAA segmentation on MDCT examinations and assess its reproducibility and accuracy to determine AAA maximal diameter and its progression in comparison with manual maximal diameter measurements on double-oblique MPR as the reference standard.

2. Materials and methods

2.1. Patients

Institutional review board approved this Health Insurance Portability and Accountability Act (HIPAA) compliant study. We performed a retrospective study of 40 patients with abdominal aortic aneurysm (AAA) followed by multi-detector computed tomography (MCDT). Patients were selected from the radiological information system. These patients were contacted by a research nurse and approval for the use of radiological imaging was obtained through patient's written consent. Between 2004 and 2006, 40 patients with AAA more than 35 mm, having at least two MDCT studies available on the local PACS with a minimal 6-month interval between exams were enrolled. If a patient had had more than two MDCT studies, the most remote and most recent exams were selected. A total of 80 exams were therefore analyzed in this study.

2.2. MDCT protocol

All 80 examinations were performed on 4 multi-detector CT scanners (Somatom Sensation 4, 16, 64, Siemens, Erlangen, Germany; Lightspeed 16, GE, Milwaukee, WI). The scanning parameters were the following: pitch 1–1.5, slice thickness 1–4 mm, collimation 0.75 and field of view 240–320. 79/80 exams were performed with a non-ionic contrast agent (iodine concentration 320–350 mg/ml) injected through an antecubital vein at 3–5 ml/s for total of 80–120 ml. The timing of acquisition was determined by an automatic bolus trigger positioned at the level of the thoraco-abdominal aorta.

2.3. Software measurement method

A software was written in *Interactive Data Language* (IDL) and C++ language to extract and quantify the volumetric component of AAA, distinguishing between lumen, thrombus, wall and calcifications. The task of the user is to interact with the software in order to segment the boundaries of the aneurysm on longitudinal reformations in a semi-automated process (Figs. 1 and 2). The proposed method has been previously reported in detail and consists of the following: (1) user identification of AAA lumen entry and exit points; (2) software calculation of 3D lumen; (3) creation of a curved-MPR following a luminal path with minimization of curvature; (4) automated aneurysm wall segmentation on 4–8 radial MPR reformations along the path axis initialized by the operator with an active contour based process; and (5) interactive contour editing on the same radial MPR reformations may be performed by the user, if needed. Once the segmentation was approved by the user, (6) a centerline based on the outer wall of the AAA and a 3D mathematical model of the AAA with distinct display for the thrombus and lumen were reconstructed and automatic calculation of D-max perpendicular to the new central line was processed. All CT examinations were anonymized and processed by an experimented CT technologist blinded to the radiology report. The time required to run this entire process (AAA segmentation and D-max calculation) on an IBM PC Pentium 4, CPU: 3.4 GHz, 2 Gb RAM, was recorded.

2.4. Manual measurement method

Axial images and multiplanar reformations (MPR) of the axial images were rendered and evaluated independently by two senior vascular and interventional radiologists and one junior staff, blinded to radiological reports. All diameters were measured from the aneurysm outside wall, using electronic calipers, with zooming and windowing liberally performed when judged pertinent on the same workstation (Impax, version 5.2; Agfa, Mortsel, Belgium).

The maximal diameter (D-max) was measured on a double-oblique reformation (DO) by determining a plane perpendicular to the aneurysm and the line of flow on the sagittal MPR, then on the coronal MPR, thus creating a "modified axial" plane. Maximal diameter of the aneurysm on this double-oblique plane was then measured (Fig. 3).

2.5. Repeat measurement and duration

In order to calculate intra-observer reproducibility of both methods, the same technologist and two of the three radiologists (one senior and one junior radiologist), all blinded to the results of the first reading session, independently repeated the D-max measurements on the 80 exams by the software and manual DO methods, respectively. Repeated readings were done with a 4-week minimal interval, using an identical protocol. The time required to measure the D-max manually was recorded during the second reading session.

2.6. Statistical analysis

2.6.1. Patient demographics

Descriptive statistics of patient baseline demographics, interval between D-max at baseline and follow-up, mean AAA D-max (all observers and two different methods) at baseline and follow-up were calculated.

2.6.2. Intra-observer and inter-observer reproducibility

The level of agreement for D-max between repeated measurements (reading sessions 1 and 2) by software method and by manual DO method was calculated by estimation of intra-observer intraclass correlation (ICC). The agreement between radiologists was also estimated by the inter-observer ICC for sessions 1 and 2. Values of up to 0.40 were considered to indicate positive but poor agreement; 0.41–0.60 good agreement; 0.61–0.80 very good agreement; and greater than 0.80 excellent agreement [15].

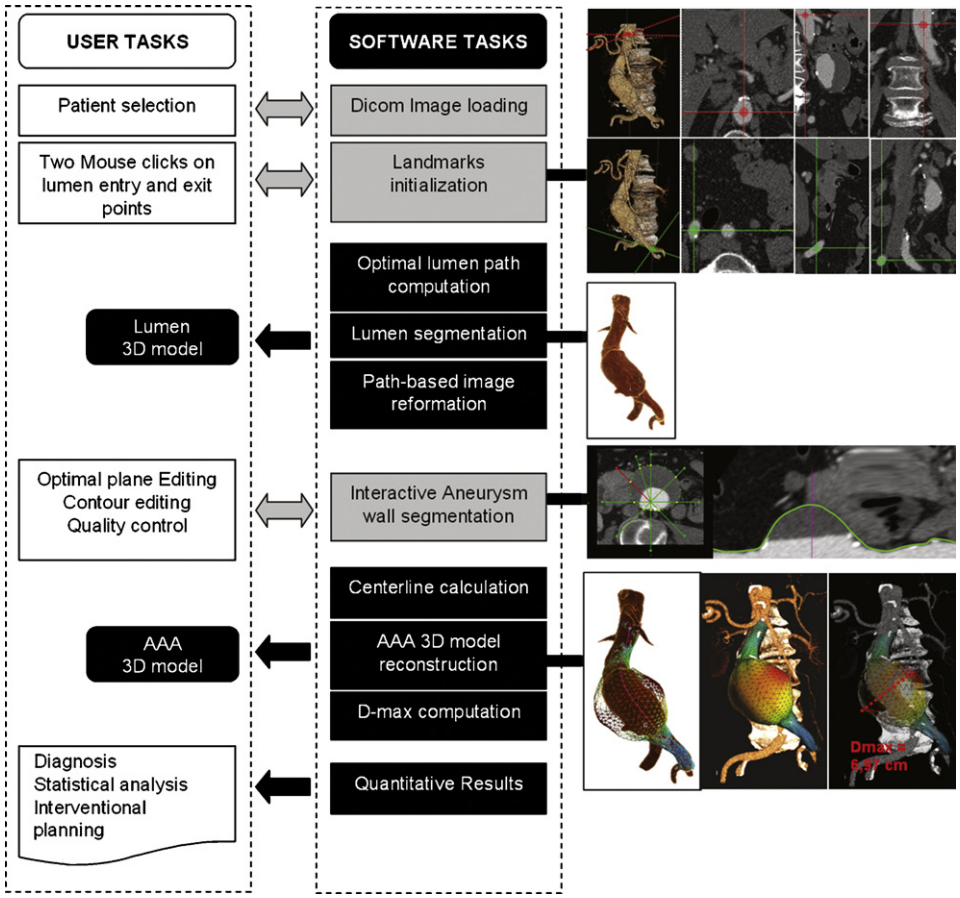

Fig. 1. Overview of software interaction. User tasks, software tasks and graphic display are illustrated in the left, middle and right column, respectively.

2.6.3. Validity

For the validity analysis, linear regression and Bland–Altman analysis were used to assess agreement between the two (software and manual DO) methods of measurement. Linear regression analysis was performed separately for measurement taken on baseline and follow-up examinations. Means of the two readings (sessions 1 and 2) were calculated for the software and for each of the two radiologists (1 and 3). The 95% CI for the slope and intercept are reported. If the slope of the line is close to unity and the intercept close to zero, this implies that the two methods of measuring D-max

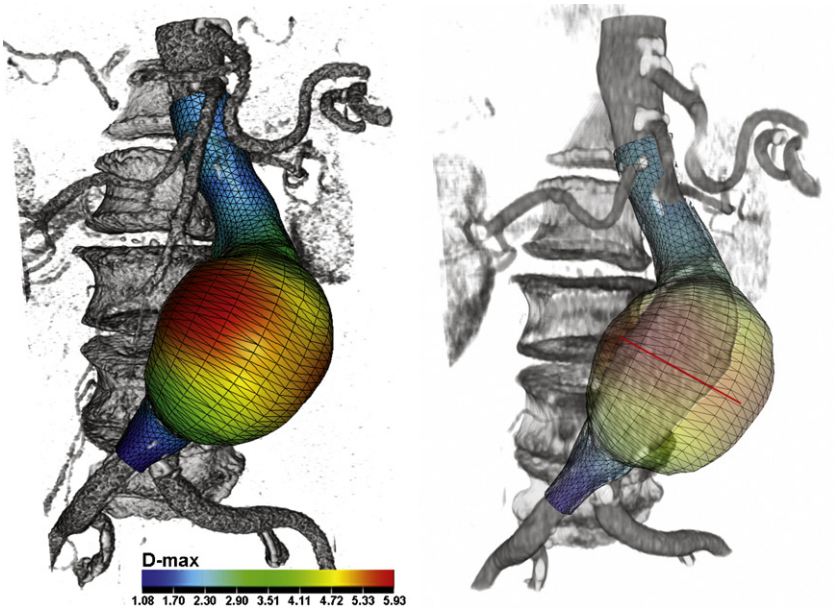

Fig. 2. Abdominal aortic aneurysm in a 79-year-old female. Left picture shows 3D volume rendering displays with 3D AAA model overlay. Different diameter values are color-coded, the smallest diameters are represented in blue and the largest in red. The automatically calculated D-max is displayed in the right picture by the red line.

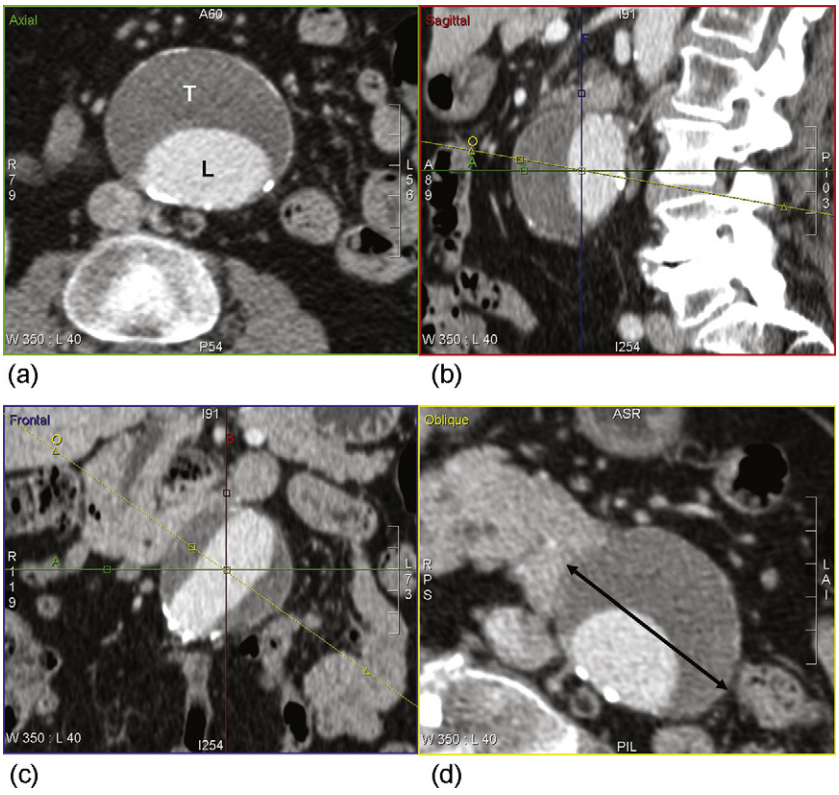

Fig. 3. Sequential approach to double-oblique (DO) reformation method illustrated in a 79-year-old female. (a) Axial contrast-enhanced CT in arterial phase shows abdominal aortic aneurysm. Lumen (L) is opacified by IV contrast. Large mural thrombus (T) fills part of the aneurysm. (b) and (c) MPR views of the aneurysm. Red line represents sagittal plane (b); blue line, coronal plane, green line, axial plane and yellow line, the user-defined DO plane (d), which is perpendicular to aneurysm wall in sagittal and coronal planes. D-max is measured manually on DO (line with double-arrows).

are in agreement. In conjunction with regression, Bland–Altman [16] range of agreement was also reported to support the conclusion of linear regression. The range of agreement was defined as the bias ± 2 SD, where SD is the corrected standard deviation of the differences between the two methods.

2.6.4. Responsiveness

To assess the responsiveness of the software method, that is, the ability to detect changes over time, a paired Student's *t*-test was used to compare D-max measurements taken at baseline with these taken at follow-up.

2.6.5. Measurement time

Descriptive statistics of measurement time by manual and semi-automated methods were calculated. The statistical analysis was performed by using a software package (SAS 9.1 for Windows).

3. Results

3.1. Patient demographics

Forty patients (33 men, 7 women; mean age, 72 years, range, 49–86 years) were included in our study. The interval between the two MDCTs at baseline and follow-up was 16 ± 8 months (mean ± SD), range 8–42 months. No patient was excluded from software segmentation for technical reasons.

The AAA diameters at baseline and follow-up are summarized in Table 1. Regardless of the measurement method and observer, the smallest aneurysm had a D-max of 35.8 mm and the largest 76.8 mm.

Table 1
Maximal AAA diameter at baseline and follow-up MDCT.

	Baseline		Follow-up	
	Mean ± SD (mm)	Range (mm)	Mean ± SD (mm)	Range (mm)
First reading				
Radiologist 1	51.2 ± 7.4	37.7–69.9	55.2 ± 8.4	42.2–74.9
Radiologist 2	50.1 ± 7.4	37.0–69.0	54.3 ± 8.7	39.0–75.0
Radiologist 3	51.2 ± 7.5	37.0–71.2	54.9 ± 8.7	38.1–75.7
Software	50.6 ± 6.9	36.4–67.2	54.8 ± 7.9	42.3–76.8
Second reading				
Radiologist 1	51.2 ± 7.1	37.1–67.6	55.4 ± 8.7	39.0–75.1
Radiologist 2	–	–	–	–
Radiologist 3	50.9 ± 7.3	36.3–69.1	55.2 ± 8.5	38.9–75.2
Software	50.5 ± 6.9	35.8–66.9	55.0 ± 8.3	41.5–76.4

3.2. Reliability

Intra-observer reproducibility's for D-max measurement were excellent for the software and the two radiologists (1 and 3) with repeated measurements by manual double-oblique MPR method: 0.992 (≥0.987), 0.985 (≥0.974) and 0.969 (≥0.948), respectively (Table 2). It was significantly higher for the software

Table 2
Intra-observer reproducibility of software and manual D-max measurements.

Observers	Baseline		Follow-up	
	ICC (95%)	CI (one-sided)	ICC (95%)	CI (one-sided)
Radiologist 1	0.985	0.974	0.984	0.973
Radiologist 3	0.969	0.948	0.979	0.965
Software	0.992	0.987	0.990	0.983

Table 3
Inter-observer reproducibility of manual D-max measurements.

Reading	Baseline		Follow-up	
	ICC (95%)	CI (two-sided)	ICC (95%)	CI (two-sided)
First	0.979	0.954–0.984	0.975	0.955–0.985
Second[a]	0.981	0.964–0.990	0.987	0.9765–0.993

[a] Radiologist 2 had not repeated the measurements twice.

when compared to observer 3 ($P < 0.05$). The D-max difference between the first and second reading sessions was not significant: -0.12 ± 0.86 mm ($P > 0.38$) for baseline examinations and 0.22 ± 1.14 mm ($P > 0.23$) for follow-up examinations.

Inter-observer reproducibility (Table 3) for manual measurement of D-max by radiologists was excellent: 0.979 (0.954–0.984) at baseline and 0.975 (0.955–0.985) at follow-up.

3.3. Assessing agreement between the two methods

The slope and intercept for the regression model between software and manual measurements indicate that the estimates of the slope and intercept are very close to unity and zero. For the analysis of the mean of readings 1 and 2 between software and radiologist #1 at baseline (Fig. 4), the intercept was −0.490 (95% CI −4.303–3.322) and slope equal to 1.022 (95% CI 0.947–1.097).

In a supportive manner, using a clinically meaningful limit of ≤5 mm, software user and radiologist #1 were within 4 mm in 40/40 instances, or interchangeable, 100% of the time for the mean of all reading on baseline (Fig. 5).

Similar results were obtained for all other analysis with the exception of the follow-up scan of radiologist #3. Although the scatter plot of the two measurements line up closely to the line of identity, only 92.5% (37/40) of the differences between the two methods were within the defined limit of agreement of 4 mm. However, there was no difference of more than 5 mm.

3.4. Responsiveness

Statistically significant D-max growth between baseline and follow-up examinations of 4.2 ± 3.2 mm (first reading session) and 4.5 ± 3.5 mm (second reading session) ($P < 0.0001$), respectively, were observed.

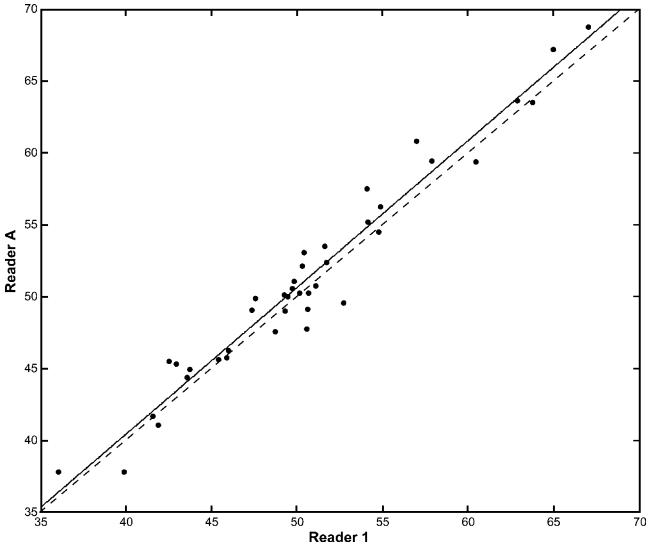

Fig. 4. Regression model between software and manual: mean of readings 1 and 2 between software (reader A) and radiologist #1 at baseline.

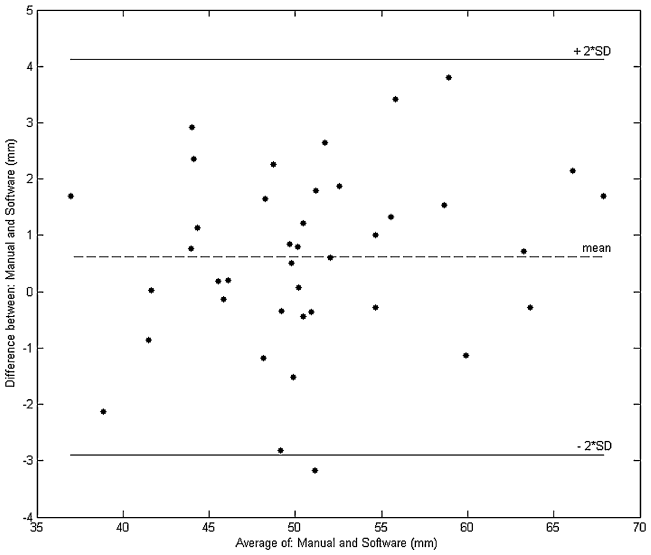

Fig. 5. Bland–Altman plot of the mean of readings 1 and 2 for software and radiologist #1 at baseline. The average of each pair of measurements is plotted against their difference. The range of agreement (solid lines) was defined as the bias ± 2 SD, where SD is the corrected standard deviation of the differences between the two methods.

3.5. Measurement time

Average measurement time was 104.7 ± 24.9 s for the manual method limited to double-oblique D-max and 175.2 ± 100.9 s for the semi-automated method, including the entire AAA segmentation, of which D-max was calculated for clinical validation.

4. Discussion

The purpose of this study was to demonstrate that reproducible quantitative follow-up of AAA D-max by MDCT can be efficiently addressed by a software with minimal human intervention, limited to correction of the AAA segmentation generated by the software, only when needed. In contrast to prior methods for AAA segmentation at CT angiography, our method is the first one that clinically validates automated D-max calculation following complete wall, lumen and thrombus segmentation. The high reproducibility of the semi-automated method combined to its accuracy (1 mm mean error difference with manual measurements), makes this method valid for clinical use. The absence of measurement error higher than 5 mm and the ability to detect a 5 mm growth between studies with 100% confidence are important criteria to assume that clinical decision made by the semi-automated method are sound. Since it can be run by a CT technologist, it could assist a radiologist or a vascular surgeon in determining D-max and its progression over time in a reproducible way. Manual comparison of D-max between multiple studies can be tedious. Significant variability of D-max measurement has been reported previously with variation of more than 5 mm in 17% of patients [5]. Without standardization of the measuring process, Cayne et al. reported a mean variation between observers of 4 ± 5.1 mm [17]. In the same study, after standardization, a mean variability of 2.8 ± 4.4 mm was still observed [5,17]. Furthermore, multiple approaches have been proposed when measuring D-max manually. Some investigators recommend measurement of antero-posterior and transverse diameter on axial images [18], others have reported lower variability when measuring shorter axis on axial images [19]. Finally, lower variability and better inter-observer correlation were found with a standardized approach and a measurement perpendicular to the central line [9,17]. The semi-automated approach proposed in our

study provides a highly reproducible D-max [9] measurement on a double-oblique plane perpendicular to the central line and prevent variation due to the methodology used by the radiologist or its interpretation.

To our knowledge, only one study [10] automatically calculated a D-max from AAA segmentation. In that study automated D-max computation and manual D-max measurements were performed in the same image plane (selected by automatic curved-MPR or manual double-oblique reformation) were compared. The D-max difference between the two methods was 0.342 ± 0.245 cm. However, since the study was limited to 4 patients, no valid statistical conclusion could be made.

The main limitation of AAA segmentation is the segmentation of the peripheral thrombus whose density is close to surrounding structures. Several segmentation methods based on exclusive or hybrid combinations of level-sets, geometric deformable models, active contours or active shape models [11,12,14] have been described for AAA segmentation. The performance of these algorithms depends on the parameter settings obtained empirically. These algorithms either perform 2D (slice-by-slice) or 3D AAA segmentation. The output is AAA global volume which is compared to AAA volume obtained by manual slice-by-slice aneurysm delineation. Since D-max measurement is the recognized gold standard for AAA diagnosis, treatment and follow-up, the validation of our software was based on D-max measurement. Additional evaluation and validation of volume measurement will be performed in subsequent studies.

Use of minimal curvature path-based image reformation, and in particular for selection of radial planes along the path axis, was a straightforward and highly reproducible method. Its intra-observer reproducibility was better than manual measurements. The correction process by interactive contour editing is also original. This feature could explain the robustness and accuracy of this method compared to manual measurements. No published work details solutions to correct the segmentation results if the process failed, a potentially disruptive outcome in clinical workflow.

Double-oblique measurement was chosen as a reference because we have previously found it was more reproducible than measurements taken on axial slices [9]. Furthermore, this measurement is closer to reality than axial measurements that can be influenced by the obliquity of the aorta [9]. In our study, a small but noticeable reproducibility improvement between the semi-automated method and the double-oblique MPR manual measurements was observed.

Development of this AAA segmentation software opens the door to additional research implications. Conceptually, automated D-max measurement requires 3D modeling of AAA. The resulting model can subsequently be analyzed for volume analysis and follow-up, topology, shape asymmetry and tissue anisotropy. By extension, these additional tools may be used for wall stress and rupture risk assessment not afforded by manual D-max.

This study had several limitations. The software segmentation time appears longer than the manual double-oblique MPR method. However, the additional processing time is fully justified since the software allowed complete 3D modeling of the AAA, of which D-max calculation was performed primarily for clinical validation. Since the software can be operated by the CT technologist, it will not involve physician time. Furthermore, the primary focus of our study was to show the feasibility and accuracy of a semi-automated segmentation and no effort was made to optimize the source code or exploit state-of-the-art workstation. We believe it can be shortened within the time of a manual measurement after optimization.

We did not include any patient after EVAR and included only one unenhanced studies. We need to validate in the future the accuracy of the software in the follow-up of patient after EVAR and also investigate on a larger population if it will give the same reliability in unenhanced studies.

5. Conclusion

Validation of this software to measure AAA maximal diameter showed higher intra-observer reproducibility than manual measurements. While this improvement was statistically significant, it might not be clinically significant. The main benefit of this automated method lies in the possibility of delegating the segmentation process, thus saving precious time for the radiologist.

Compared to manual measurements a very good accuracy was obtained for baseline and follow-up measurements and estimation of D-max growth. Since no error of more than 5 mm between both manual and software methods was observed, this algorithm is sufficiently robust to be used in various AAA morphology. This alleviates the uncertainty related to identification of the maximal diameter with conventional manual methods by providing a standardized method and would be of tremendous use to readers with less experience.

Since D-max measurement is the recognized gold standard for AAA diagnosis, treatment and follow-up, the validation of our software was based on D-max measurement. Additional evaluation and validation of volume measurement will be performed in subsequent studies.

Acknowledgements

This work was supported by a clinical research scholarship (to G.S.) from Fonds de la recherche en santé du Québec (FRSQ).

References

[1] Nevitt MP, Ballard DJ, Hallett JW. Prognosis of abdominal aortic aneurysms. A population-based study. New Engl J Med 1989;321(15):1009–14.
[2] Brewster DC, Cronenwett JL, Hallett Jr JW, et al. Guidelines for the treatment of abdominal aortic aneurysms. Report of a subcommittee of the Joint Council of the American Association for Vascular Surgery and Society for Vascular Surgery. J Vasc Surg 2003;37(5):1106–17.
[3] Hatakeyama T, Shigematsu H, Muto T. Risk factors for rupture of abdominal aortic aneurysm based on three-dimensional study. J Vasc Surg 2001;33(3):453–61.
[4] Lutz AM, Willmann JK, Pfammatter T, et al. Evaluation of aortoiliac aneurysm before endovascular repair: comparison of contrast-enhanced magnetic resonance angiography with multidetector row computed tomographic angiography with an automated analysis software tool. J Vasc Surg 2003;37(3):619–27.
[5] Lederle FA, Wilson SE, Johnson GR, et al. Variability in measurement of abdominal aortic aneurysms. Abdominal Aortic Aneurysm Detection and Management Veterans Administration Cooperative Study Group. J Vasc Surg 1995;21(6):945–52.
[6] Wilmink AB, Forshaw M, Quick CR, et al. Accuracy of serial screening for abdominal aortic aneurysms by ultrasound. J Med Screen 2002;9(3):25–7.
[7] de Gracia MM, Rodriguez-Vigil B, Garzon-Moll G, et al. Correlation between the measurement of transverse diameter in the proximal neck on computed tomography and on aortography before endovascular treatment of infrarenal aortic aneurysm. Ann Vasc Surg 2006;20(4):8–95.
[8] Golledge J, Wolanski P, Parr A, et al. Measurement and determinants of infrarenal aortic thrombus volume. Eur Radiol 15 2008.
[9] Dugas A, Therasse E, Oliva V, et al. Abdominal aortic aneurysm follow-up with MDCT: reproducibility of maximal diameter measurement. In: Radiological Society of North America Scientific Assembly and Annual Meeting Program. Oak Brook, IL: Radiological Society of North America; 2007. pp. 632–633.
[10] Bodur O, Grady L, Stillman A, et al. Semi-automatic aortic aneurysm analysis. In: Manduca A, Hu X, editors. Medical imaging 2007: physiology, function, and structure from medical images. 2007.
[11] Das B, Mallya Y, Srikanth S, et al. Aortic thrombus segmentation using narrow band active contour model. Conf Proc IEEE Eng Med Biol Soc 2006;1:408–11.
[12] Olabarriaga SD, Rouet JM, Fradkin M, et al. Segmentation of thrombus in abdominal aortic aneurysms from CTA with nonparametric statistical grey level appearance modeling. IEEE Trans Med Imaging 2005;24(4):477–85.

[13] Subasic M, Loncaric S, Sorantin E. Model-based quantitative AAA image analysis using a priori knowledge. Comput Methods Programs Biomed 2005;80(2):103–14.
[14] Zhuge F, Rubin GD, Sun S, et al. An abdominal aortic aneurysm segmentation method: level set with region and statistical information. Med Phys 2006;33(5):1440–53.
[15] Landis JR, Koch GG. The measurement of observer agreement for categorical data. Biometrics 1977;33(1):159–74.
[16] Bland JM, Altman DG. Statistical methods for assessing agreement between two methods of clinical measurement. Lancet 1986;1(8476):307–10.
[17] Cayne NS, Veith FJ, Lipsitz EC, et al. Variability of maximal aortic aneurysm diameter measurements on CT scan: significance and methods to minimize. J Vasc Surg 2004;39(4):811–5.
[18] Abada HT, Sapoval MR, Paul JF, et al. Aneurysmal sizing after endovascular repair in patients with abdominal aortic aneurysm: interobserver variability of various measurement protocols and its clinical relevance. Eur Radiol 2003;13(12):2699–704.
[19] Dillavou ED, Buck DG, Muluk SC, et al. Two-dimensional versus three-dimensional CT scan for aortic measurement. J Endovasc Ther 2003;10(3):531–8.

Appendix 4. Manuscript 3: Measurements and detection of abdominal aortic aneurysm growth: Accuracy and reproducibility of a segmentation software.

Published in *European Journal of Radiology* (30). Full text reproduced with permission from licensed content publisher (Elsevier) and all co-authors.

European Journal of Radiology 81 (2012) 1688–1694

Contents lists available at ScienceDirect

European Journal of Radiology

journal homepage: www.elsevier.com/locate/ejrad

Measurements and detection of abdominal aortic aneurysm growth: Accuracy and reproducibility of a segmentation software

Claude Kauffmann[a,1], An Tang[a,2], Éric Therasse[a,3], Marie-France Giroux[a,4], Stephane Elkouri[b,5], Philippe Melanson[a,4], Bertrand Melanson[a,4], Vincent L. Oliva[a,4], Gilles Soulez[a,*]

[a] Department of Radiology, Centre Hospitalier Universitaire de Montréal (CHUM) and CHUM Research Center (CRCHUM), University of Montreal, 1560 Sherbrooke Est, H2L 4M1 Montréal, Québec, Canada

[b] Department of Surgery, Centre Hospitalier Universitaire de Montréal (CHUM) and CHUM Research Center (CRCHUM), University of Montreal, 1560 Sherbrooke Est, H2L 4M1 Montréal, Québec, Canada

ARTICLE INFO

Article history:
Received 18 November 2010
Received in revised form 7 April 2011
Accepted 13 April 2011

Keywords:
AAA
CTA
Abdominal aortic aneurism
3D segmentation
Follow-up
D-max and volume growth

ABSTRACT

Purpose: To validate the reproducibility and accuracy of a software dedicated to measure abdominal aortic aneurysm (AAA) diameter, volume and growth over time.

Materials and methods: A software enabling AAA segmentation, diameter and volume measurement on computed tomography angiography (CTA) was tested. Validation was conducted in 28 patients with an AAA having 2 consecutive CTA examinations. The segmentation was performed twice by a senior radiologist and once by 3 medical students on all 56 CTAs. Intra and inter-observer reproducibility of *D*-max and volumes values were calculated by intraclass correlation coefficient (ICC). Systematic errors were evaluated by Bland–Altman analysis. Differences in *D*-max and volume growth were compared with paired Student's *t*-tests.

Results: Mean *D*-max and volume were 49.6 ± 6.2 mm and 117.2 ± 36.2 ml for baseline and 53.6 ± 7.9 mm and 139.6 ± 56.3 ml for follow-up studies. Volume growth (17.3%) was higher than *D*-max progression (8.0%) between baseline and follow-up examinations ($p < .0001$). For the senior radiologist, intra-observer ICC of *D*-max and volume measurements were respectively estimated at 0.997 (≥0.991) and 1.000 (≥0.999). Overall inter-observer ICC of *D*-max and volume measurements were respectively estimated at 0.995 (0.990–0.997) and 0.999 (>0.999). Bland–Altman analysis showed excellent inter-reader agreement with a repeatability coefficient <3 mm for *D*-max, <7% for relative *D*-max growth, <6 ml for volume and <6% for relative volume growth.

Conclusion: Software AAA volume measurements were more sensitive than AAA *D*-max to detect AAA growth while providing an equivalent and high reproducibility.

1. Introduction

Abdominal aortic aneurysm (AAA) treatment, either by surgical or endovascular approach, currently rely on the maximal diameter (*D*-max) of the aneurysm [1–4]. AAA *D*-max change over time, whether before or after intervention, also determine the need for further treatment [5,6].

Several studies have advocated volume rather than diameter measurement for AAA follow-up, because volume changes reflect AAA growth in all directions irrespective of *D*-max changes whereas, by definition, *D*-max ignores cranio-caudal expansion [7–11].

In the setting of AAA follow-up of patients undergoing endovascular repair (EVAR), volumetric changes are also considered to be more sensitive than diameter measurement in the detection of changes in aneurysm size after EVAR [11,12]. Volumetric analysis has also revealed size changes discordant with *D*-max in 14–19% of cases [9]. The variability of aortic volume measurement by manual segmentation correlates to level of experience of readers, being less than 2% for a well-trained technologist and up to 6% for readers with lesser experience [13]. A 2% volume increase has recently been suggested as a threshold for identification of endoleaks after EVAR,

0720-048X/$ – see front matter © 2011 Elsevier Ireland Ltd. All rights reserved.
doi:10.1016/j.ejrad.2011.04.044

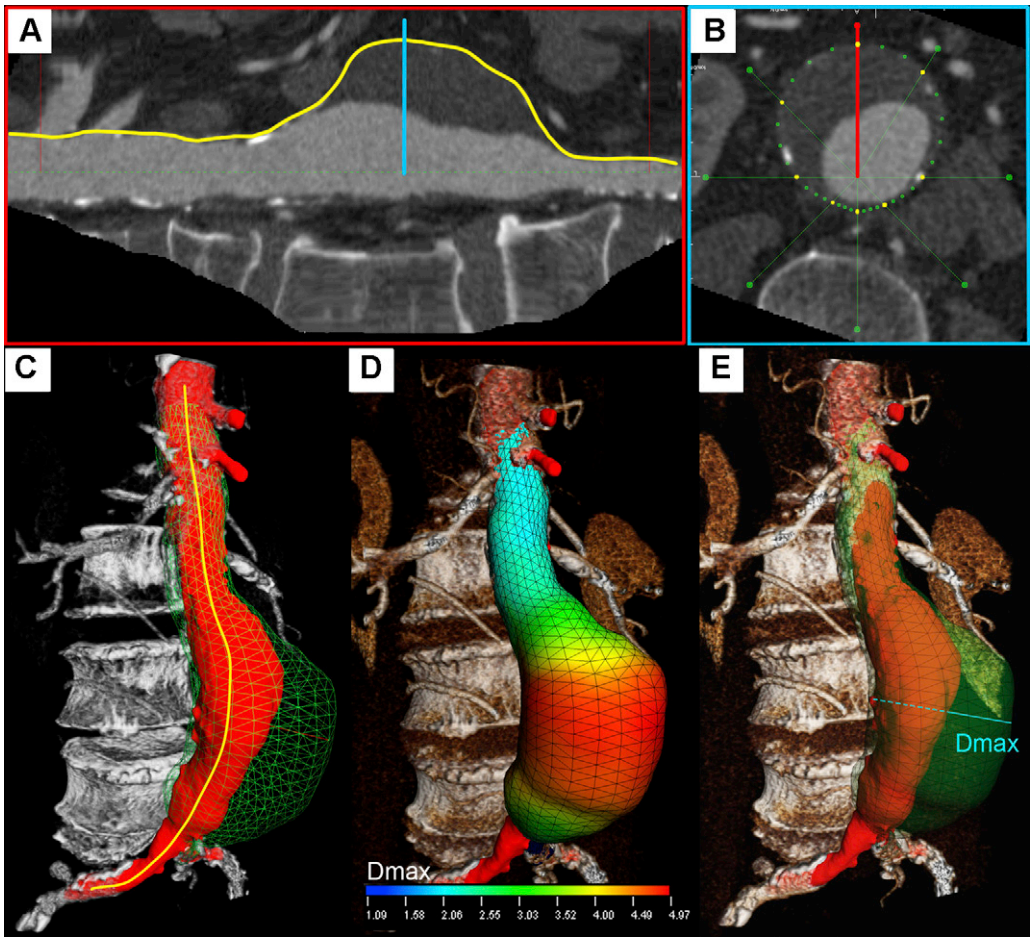

Fig. 1. AAA model in a 72-year-old man with a *D*-max of 6.97 cm. (A) Stretched longitudinal view of the path-based image. This path may be edited, if needed. The blue line represents the corresponding axial view. (B) Axial view shows AAA optimized path obtained by automated segmentation of aneurysm wall. The green lines represent the radial planes that can be edited in the orthogonal views. The red line represent the active stretched longitudinal view. (C) AAA surface model with optimized path (yellow line), lumen (red) and outer-wall mesh (green) of the AAA. (D) *D*-max values are color-coded at each location: the smallest diameters are represented in blue and the largest in red. E. The automatically calculated *D*-max is highlighted by the blue dashed line.

whereas no endoleak were observed when a volume decrease of more than 3% was observed [11]. Accurate AAA assessment will also become increasingly important to evaluate response to pharmacological therapies for small AAAs [14].

Despite theoretical advantages, AAA volumetry largely remains in the realm of research because segmentation methods are time-consuming and tedious post-processing may take up to 45 min [15]. Furthermore, current methods do not allow 3D-3D image registration between baseline and follow-up studies.

We have conceived and developed a semi-automated software enabling fast AAA segmentation and 3D modeling. This software was validated for the measurement of *D*-max measurement and showed an excellent accuracy and reproducibility [16].

To our knowledge, most of the studies investigating the potential of volumetric analysis for AAA follow-up used manual segmentation which is a tedious process. The aim of this study was to evaluate the ability of a semi-automated segmentation combined with 3D-3D registration between baseline and follow-up examinations to enable fast volumetric follow-up by operators with minimal training. While most previous studies on volumetric analysis of AAA have focused on changes after EVAR, we selected untreated patients to evaluate the software's ability to detect growth. More specifically, we evaluated the intra and inter-observer reproducibility and assessed the accuracy of this software to measure aneurysm diameter, volume and growth over time on CT angiography examinations.

2. Materials and methods

2.1. Study design and patient selection

We performed a retrospective study on 28 consecutive patients with abdominal aortic aneurysm (AAA) followed by multi-detector computed tomography (MCDT) before any treatment. Patients were selected from the radiological information system, if they had an AAA equal or larger than 4.0 cm and at least 2 MDCT studies available on the local PACS with a minimum of 4 month interval between two studies between 2007 and 2009. Selected patients were then contacted by a research nurse and their approval for the use of radiological imaging was obtained by written consent. Institutional Review Board approved this Health Insurance Portability and Accountability Act (HIPAA) compliant research project. If a patient had more than two MDCT studies, the most remote and most recent examinations were selected. A total of 56 MDCT studies were therefore analyzed.

2.2. MDCT protocols

The 56 examinations were performed on 4 different multi-detector CTs (Somatom Sensation 4, 16, 64, Siemens, Erlangen, Germany; Lightspeed 16, GE, Milwaukee, Wis). The scanning parameters were the following: pitch 1–1.5, slice thickness 1–2 mm, collimation 0.75–1.5 and field of view 240–320.

Intravenous contrast media was given in all studies with at 3–5 ml/sec, for a total of 80–120 ml.

2.3. Measurement methods

Four observers, 1 experienced senior radiologist with 20 years of experience in vascular imaging who represented the reference standard (R) and 3 first-year medical students with no prior experience in imaging (T1, T2, T3), all blinded to previous radiological reports, independently segmented aneurysms on each of the 56 studies. The medical students had 5 days of training to manipulate the software and learn the CT anatomy of AAA with serial feedback sessions from the senior radiologist using a separate 20 AAA patient CTA database. Hence, they were considered to have no particular expertise.

All segmentations were performed using a semi-automated software method (A3Dmax; Object Research System, Montreal, Canada) previously validated for *D*-max measurements [16]. The segmentation algorithm is described in detail elsewhere [17]. The main steps of our interactive method consisted of: (1) user identification of AAA lumen entry and exit points (2) software calculation of 3D lumen, (3) creation of a curved-MPR following a luminal path with minimization of curvature, (4) automated aneurysm wall segmentation on 4–8 radial MPR reformations along the path axis initialized by the operator with an active contour based process and (5) interactive contour editing on the same radial MPR reformations may be performed by the user, if needed. Once the segmentation was approved by the user, (6) a centerline based on the outer wall of the AAA and a 3D mathematical model of the AAA with distinct display for the thrombus and lumen were reconstructed and automatic calculation of *D*-max perpendicular to the new central line was processed. Finally, (7) manual markers were positioned at the level of the inferior renal artery at the neck of the aneurysm and aorto–iliac bifurcation (separation of common iliac arteries) to delineate AAA upper and lower limit planes for volume calculation (Fig. 1). The senior radiologist performed segmentations twice, on two separate sessions, at least one month apart. The first segmentation session was performed as a reference standard by reviewing the accuracy of the segmentation on all MPR views and doing any necessary correction to reach the same quality as a manual segmentation. The second segmentation session was performed to measure intra-observer reproducibility and record segmentation time. Segmentations were performed only once by unsupervised medical students to calculate inter-observer reproducibility.

Once the baseline and follow-up CT studies were segmented, those examinations were co-registered to allow longitudinal diameter and volume comparison. A 3D-3D registration process based on mutual information allowed superposition of baseline and follow-up CTs with minimal entropy [18,19]. Quality control of the registration was determined by visual inspection. Following the registration, the proximal and distal landmarks positioned at baseline were automatically localized on the follow-up examination. Three-dimensional rendering of the AAA outer wall on the baseline and follow-up examination reveals shape and volume change over time for every patient (Fig. 2).

Fig. 2. Three-dimensional mesh rendering of AAA lumen (red) and outer wall at baseline (green) and 3 years follow-up (blue) in 69-year-old man. The *D*-max was 58.5 mm at baseline and 74.3 mm at follow-up (27% relative growth). The volume was 202.9 ml at baseline and 327.3 ml at follow-up (61% relative growth). 3D-3D co-registration of baseline and follow-up examinations allow instantaneous volume comparison on the same dataset.

2.4. Statistical analyses

2.4.1. Patient demographics and aneurysm characteristics

Descriptive statistics of patient baseline demographics, interval between 2 MDCTs and mean AAA *D*-max at baseline and follow-up were calculated, with standard deviations. Paired Student's *t*-tests were used to compare the *D*-max and volume obtained by medical students (T1, T2, T3) with the senior radiologist (R) (Fig. 3).

2.4.2. D-max and volume growth

D-max growth was compared in absolute difference (mm) and in relative difference (%) of baseline value. Relative *D*-max changes were calculated using the following formula: $[(D_2 - D_1)/D_1 \times 100]$. Volume growth was also compared in absolute difference (ml) and in relative difference (%) of baseline value. Relative volume changes were calculated using the following formula: $[(V_2 - V_1)/V_1 \times 100]$. Paired Student's *t*-tests were used to compare absolute differences in *D*-max and volume growth between baseline and follow-up examinations.

2.4.3. Intra-observer and inter-observer reproducibility

Inter-observer (4 readers) and intra-observer reproducibility (senior radiologist) was assessed by the intraclass correlation coefficient (ICC) for *D*-max, volume calculation and their progression between examinations obtained by repeated segmentation for each reader.

2.4.4. Assessing agreement between readers

Bland–Altman analysis was performed to determine the agreement measurements by the senior radiologist (reference standard) and three unsupervised medical students. The bias was calculated as the average difference between the results of pairs of observers and the limits of agreement as the bias ± two standard deviations. The repeatability coefficient $CR = 1.96 \times \sqrt{\sum (d_2 - d_1)^2/(n-1)}$ [20] was also calculated to compare our performance with previous studies using manual segmentation.

2.4.5. Assessing growth significance

The significance of individual size changes was classified based on the repeatability coefficient.

Differences were considered significant at $p < 0.05$. Statistical analyses were performed using the SPSS software, version 18.0 (SPSS Inc., Chicago, IL).

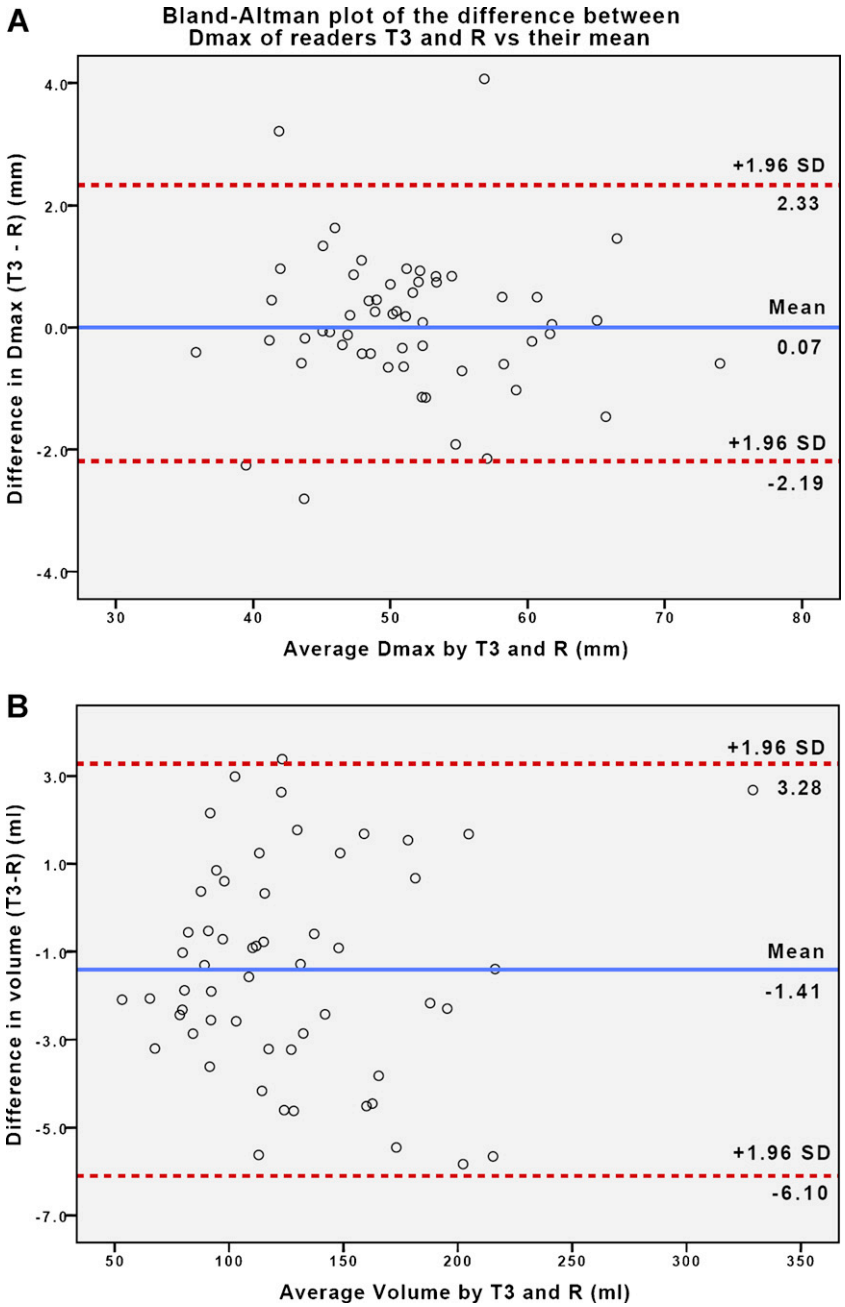

Fig. 3. (A) Bland–Altman plot of the difference between *D*-max measurements by senior radiologist (R) and third medical student (T3) vs their mean. (B) Bland–Altman plot of the difference between volume measurements by senior radiologist (R) and third medical student (T3) vs their mean. Range of agreement (solid lines) was defined as the bias ± 2 SD.

3. Results

3.1. Patient demographics and aneurysm characteristics

Twenty-eight patients, 24 men, 4 women, with a mean age of 71 years, (range 49–83 years) were included in this study. The average interval between the baseline and follow-up MDCT was 17.5 ± 7.9 months (range 5–36 months). Considering all observers, the average *D*-max value was 49.6 ± 6.2 mm at baseline and 53.6 ± 7.9 mm at follow-up; the average volume was 117.2 ± 36.2 ml at baseline and 139.6 ± 56.3 ml at follow-up (Table 1).

D-max growth between baseline and follow-up examinations was 4.0 ± 3.8 mm in absolute difference ($p < 0.0001$), which corresponds to 8.0%. In contrast, volume growth between baseline and follow-up examinations was 22.5 ± 25.2 mL in absolute difference ($p < 0.0001$), which corresponds to 17.3%. Volume progression was significantly higher than diameter progression in percentage ($p < 0.0001$).

3.2. Intra-observer and inter-observer reproducibility

For R (reference standard), intra-observer reproducibility was excellent: ICC = 0.997 (≥0.991) for *D*-max and ICC = 1.000 (≥0.999) for volume measurements. For T1, T2 and T3, overall inter-observer reproducibility was also excellent, at least ICC = 0.995 (0.900–0.997) for *D*-max and ICC = 0.999 (>0.998) for volume (Table 2).

Table 1
D-max and volume measurements for all observers.

Observers	Baseline	p^a	Follow-up	p^a	Absolute growth	p^a	Relative growth (%)	p^a	p^b
D-max (mm)									
R	49.4 ± 6.3	–	53.4 ± 8.0	–	3.9 ± 3.8	–	7.9 ± 7.1	–	
T1	49.7 ± 6.1	0.222	53.8 ± 8.2	0.025	4.0 ± 4.1	0.702	8.0 ± 7.9	0.853	
T2	49.5 ± 6.1	0.486	53.9 ± 8.0	0.027	4.3 ± 3.6	0.147	8.6 ± 6.8	0.189	
T3	49.6 ± 6.4	0.487	53.3 ± 7.9	0.831	3.7 ± 4.0	0.520	7.5 ± 7.7	0.557	
All readers	49.6 ± 6.2	–	53.6 ± 7.9	–	4.0 ± 3.8	–	8.0 ± 7.3	–	<0.0001
Volume (ml)									
R	117.2 ± 36.6	–	139.4 ± 57.1	–	22.2 ± 25.8	–	17.0 ± 14.6	–	
T1	117.6 ± 36.4	0.452	140.7 ± 57.2	0.015	23.2 ± 25.8	0.118	17.7 ± 14.4	0.193	
T2	117.9 ± 36.9	0.136	140.4 ± 56.9	0.012	22.5 ± 25.0	0.474	17.3 ± 13.7	0.546	
T3	115.9 ± 36.8	0.002	137.9 ± 57.1	0.007	22.1 ± 25.5	0.860	17.2 ± 14.2	0.694	
All readers	117.2 ± 36.2	–	139.6 ± 56.3	–	22.5 ± 25.2	–	17.3 ± 14.0	–	

Note: Data are mean ± standard deviation.
[a] Paired *t*-tests between readers T1, T2, T3 and R.
[b] Paired *t*-test for relative growth evaluated by *D*-max vs volume.

Table 2
Intra- and inter-observer reproducibility of *D*-max and volume measurements.

Observers	Baseline	Follow-up	*D*-max			Volume		
			Absolute growth	Relative growth	Baseline	Follow-up	Absolute growth	Relative growth
Intra-observer reproducibility								
R-R	0.997 (0.991–0.999)	0.999 (>0.997)	0.991 (0.972–0.997)	0.991 (0.972–0.997)	1.000 (>0.999)	1.000 (1.000)	0.999 (>0.996)	0.995 (0.985–0.998)
Inter-observer reproducibility								
R-T1	0.989 (0.976–0.995)	0.997 (0.993–0.998)	0.968 (0.931–0.985)	0.959 (0.911–0.981)	0.999 (>0.998)	0.999 (>0.999)	0.996 (0.991–0.998)	0.989 (0.977–0.995)
R-T2	0.994 (0.988–0.997)	0.995 (0.988–0.998)	0.964 (0.922–0.983)	0.959 (0.912–0.981)	0.999 (0.998–0.999)	1.000 (>0.999)	0.998 (0.995–0.999)	0.993 (0.985–0.997)
R-T3	0.989 (0.977–0.995)	0.996 (0.992–0.998)	0.947 (0.885–0.975)	0.941 (0.873–0.973)	0.999 (0.998–1.000)	0.999 (>0.999)	0.997 (0.994–0.999)	0.994 (0.986–0.997)
All	0.995 (0.990–0.997)	0.998 (0.996–0.999)	0.976 (0.957–0.988)	0.972 (0.950–0.986)	0.999 (>0.999)	1.000 (1.000)	0.999 (0.997–0.999)	0.996 (0.993–0.998)

3.3. Agreement between readers

Bland–Altman analysis showed good agreement between *D*-max measured by R and T1, T2, T3 (Table 3). *D*-max comparison between readers with least experience (T1, T2 or T3 and most experienced reader (R) revealed accuracy <1 mm for *D*-max, <1 mm for diameter growth and <1% for relative growth. The repeatability coefficient remained <3 mm for *D*-max, <4 mm for absolute *D*-max growth and <7% for relative *D*-max growth for all readers.

Bland–Altman analysis was also excellent for volume measured by R and T1, T2 and T3 (Table 3). Volume comparison between readers with least experience and most experienced reader revealed accuracy <2 ml for volume, <1 ml for volume growth and <1% for relative volume growth. The repeatability coefficient remained <6 ml for volume, <7 ml for absolute volume growth and <6% for relative volume growth for all readers.

Differences between the experienced vascular and interventional radiologist (R) and the novice operators reached statistically significant levels for certain pairs: T1 and T2 slightly overestimated *D*-max and volume at follow-up compared to R, while T3 slightly overestimated volume at baseline and follow-up compared to R (Table 1). However, this bias was consistent at baseline and follow-up and was not significant on growth.

3.4. D-max and volume growth precision

Using absolute growth, 22 patients had volumetric increase above the 95% limits of agreement (4.3 ml) whereas 18 patients had diameter increase above the 95% limits of agreement (1.6 mm). Thus, 4/28 (14.3%) of patients had discordance between volumetric and diameter changes during follow-up.

In contrast, using relative growth calculated in percentage, 22 patients had volumetric increase above the 95% limits of agreement (4.4%) whereas 21 patients had diameter increase above the 95% limits of agreement (2.2%). Thus, 1/18 (3.6%) of patients had discordance between volumetric and diameter changes during follow-up.

3.5. Time required for segmentation

The average time to segment the AAA was 227.3 ± 70.5 s.

4. Discussion

Because of its volumetric acquisition mode suitable for multi-planar and three-dimensional reconstructions of complex anatomy, there is an inherent benefit to use CT rather than ultrasound for comparison between baseline and follow-up AAA examinations. While volumetric changes have been considered more sensitive than diameter changes in detection of AAA growth [12,21–26], volumetry has largely remained in the research domain because segmentation methods are time-consuming and do not allow co-registration of interval studies.

A previous study on the effect of operator experience on AAA volume calculation revealed a learning curve: readers with little experience demonstrated higher volume differences and intra-observer variability than experienced readers. Using a manual segmentation method on a commercially available volumetric software, the average intra-observer percent volume differences ranged between 1.2% and 6.0% for the most to least experienced readers [13]. Our semi-automated method performs at least as well as the previous manual approach with a percent volume difference of 0.96% ± 0.73% for the reference reader.

Table 3
Bland–Altman analysis of reader agreement for *D*-max and volume.

Observers	*D*-max				Volume			
	Baseline (mm)	Follow-up (mm)	Absolute growth (mm)	Relative growth (%)	Baseline (ml)	Follow-up (ml)	Absolute growth (ml)	Relative growth (%)
R-R	−0.06 ± 1.47 (−1.53, 1.40)	0.20 ± 1.05 (−0.84, 1.25)	0.25 ± 1.65 (−1.40, 1.89)	0.20 ± 2.18 (−1.98, 2.38)	0.29 ± 2.53 (−2.25, 2.82)	0.74 ± 3.01 (−2.27, 3.75)	0.54 ± 4.28 (−3.74, 4.81)	0.71 ± 4.34 (−3.63, 5.05)
T1-R	0.31 ± 2.57 (−2.26, 2.88)	0.41 ± 1.80 (−1.39, 2.21)	0.10 ± 2.72 (−2.62, 2.83)	0.11 ± 5.84 (−5.74, 5.95)	0.33 ± 4.49 (−4.16, 4.82)	1.33 ± 5.29 (−3.96, 6.61)	0.99 ± 6.41 (−5.41, 7.41)	0.75 ± 5.86 (−5.11, 6.61)
T2-R	0.12 ± 1.85 (−1.73, 1.98)	0.51 ± 2.28 (−1.77, 2.80)	0.39 ± 2.70 (−2.31, 3.08)	0.70 ± 5.40 (−4.69, 6.10)	0.70 ± 4.77 (−4.06, 5.48)	1.04 ± 3.98 (−2.94, 5.02)	0.33 ± 4.75 (−4.41, 5.08)	0.27 ± 4.66 (−4.38, 4.94)
T3-R	0.17 ± 2.57 (−2.40, 2.75)	−0.04 ± 1.92 (−1.96, 1.88)	−0.21 ± 3.42 (−3.63 to 3.20)	−0.39 ± 6.80 (−7.19, 6.41)	−1.37 ± 4.22 (−5.59, 2.85)	−1.46 ± 5.20 (−6.66, 3.74)	−0.09 ± 5.34 (−5.43, 5.24)	0.17 ±4.47 (-4.29, 4.64)

Note: Results reported as bias ± repeatability coefficient (1.96 SD); (95% limits of agreement interval).

Wever et al. used a manual segmentation method based on density threshold and found intra-observer and inter-observer repeatability coefficients for volume of 5.6 ml and 10.3 ml, respectively [27]. More recently, Van Prehn et al. used a semi-automated volumetry method and found intra-observer and inter-observer repeatability coefficients of 7.8 ml and 10.8 ml, respectively [28]. Our semi-automated segmentation method compares favorably to these prior results: relying on an active contour model provides reproducible measurements with intra-observer and inter-observer repeatability coefficients of 3.0 ml and 5.3 ml for volume measurements.

Our study demonstrates that volume measurement is highly reproducible as shown by the high ICC values observed in our series. It is accurate as shown by the small difference between the reference volume calculated by the senior radiologist and the medical student. Since the mean AAA growth in volume was higher than diameter growth, we can also conclude that volume measurement are more sensitive to detect AAA growth. Since volume could be followed with high intra and inter-observer reproducibility, this method allowed growth detection in 4 (14.3%) additional patients.

More importantly, we found no statistically significant differences in diameter and volume measurements across operators with different levels of experience. This is an important finding since reproducible measurements can be obtained by low-level operators with little formal training. These findings suggest that AAA segmentation with automated software reduces the learning-curve effect and can be delegated to CT technologists. With advances in image analysis automation, certain tasks may be delegated to CT technicians without requiring dedicated laboratories with specialized personnel.

This segmentation method is highly reproducible and accurate, with a <1 mm error difference for *D*-max and <6 ml error difference for volume between low experience operator and an experienced radiologist. The absence of measurement error greater than 6 mm or 7 ml, the ability to detect 8 ml growth between studies with 100% confidence and the rapid segmentation time are important for clinical acceptance of this segmentation method. Using the registration tool between two CT datasets, it could assist a radiologist in determining volume progression and visualizing shape change over time.

Our observations are similar to a recent study comparing volume and diameter measurements in small AAA, using axial and orthogonal diameters perpendicular to the lumen axis [29]. However, the smaller diameter at baseline in their study, with a median of 41.0 mm (range: 33.0–45.8 mm), may account for the smaller orthogonal diameter increase (1.2 mm) and volume increase (4.9 ml) observed over a similar interval of 14 months. Despite larger aneurysms, our better agreement may be explained by improved reproducibility with the automated software method.

Highly reproducible results with this automated method may be explained by: (a) mutual registration of baseline and follow-up studies to minimize error on AAA volume growth estimation, (b) a validation process that allows correction of the automated segmentation on longitudinal and axial MPR views when needed and (c) a short segmentation time which prevents operator fatigue and errors.

Segmentation time with this software is rapid (3.0 min ± 1.1 min), an improvement over previous reported times in similar studies: up to 45 min [9,15] or less than 20 min [11]. Recently, the average time for volume measurement with a fast semi-automatic method was 15 min [28]. This improvement is crucial, since time consuming methods preclude volumetry use in routine clinical practice [8].

Increased accuracy and reproducibility using a rapid and automated segmentation method has important implications. Trials are currently underway to assess whether medical management, including control of blood pressure with ACEi, smoking cessation, statins, anti-platelet agents, antibiotics and matrix metalloproteinase (MMP) inhibitors will also slow aneurysm growth [14].

Most studies comparing volume and diameter changes in patients with AAA included patients after endovascular repair [9,12,25,27,30]. We expect similar results in a setting of EVAR follow-up. If similar reproducibility can be attained, automation of the segmentation process would facilitate volume follow-up.

We advocate the use of both absolute and relative changes in reporting measurement sensitivity. Reporting AAA growth or decrease in *D*-max (mm) and volume (ml) will facilitate comparison between patient population, segmentation methods and studies. Percentage values are more intuitive for the volumetric analysis.

The main limitation of our study is the absence of an absolute gold standard for the aneurysm sac volume. However, the correction process performed during the first reading of the senior radiologist is similar to a manual segmentation. Moreover, we have previously validated *D*-max measurement obtained with this software by using manual measurements by three vascular and interventional radiologists as reference standard and found higher intra-observer reproducibility than manual measurements, with an accuracy within 1.1 mm on average [16]. We did not include any patient with unenhanced studies. In the future, we intend to validate the accuracy and reproducibility of this segmentation method in unenhanced studies.

The retrospective design of our study limits generalization of our results. Prospective studies on larger populations will be needed to determine the clinical impact of volumetric studies.

5. Conclusion

We conclude that AAA segmentation for volume follow-up is more sensitive than *D*-max follow-up, while providing an equivalent reproducibility. Clinical validation showed a high accuracy and reproducibility of *D*-max and volume measurements when operated by a reader with minimal training. Volume measurement

can be used in addition to maximal diameter to refine AAA follow-up.

Acknowledgements

This work was supported by a clinical research scholarship (to GS) from Fonds de la recherche en santé du Québec (FRSQ) and an operating grant from the Ministère du développement économique, de l'innovation et de l'exportation du Québec (MDEIE) and the Canadian Head of Academic Radiologist (CHAR).

References

[1] Mortality results for randomised controlled trial of early elective surgery or ultrasonographic surveillance for small abdominal aortic aneurysms. The UK small aneurysm trial participants. Lancet 1998;352:1649–55.
[2] Brewster DC, Cronenwett JL, Hallett Jr JW, Johnston KW, Krupski WC, Matsumura JS. Guidelines for the treatment of abdominal aortic aneurysms. Report of a subcommittee of the Joint Council of the American Association for Vascular Surgery and Society for Vascular Surgery. J Vasc Surg 2003;37:1106–17.
[3] Katz DA, Littenberg B, Cronenwett JL. Management of small abdominal aortic aneurysms. Early surgery vs watchful waiting. JAMA 1992;268:2678–86.
[4] Nevitt MP, Ballard DJ, Hallett Jr JW. Prognosis of abdominal aortic aneurysms. A population-based study. N Engl J Med 1989;321:1009–14.
[5] Brady AR, Thompson SG, Fowkes FG, Greenhalgh RM, Powell JT. Abdominal aortic aneurysm expansion: risk factors and time intervals for surveillance. Circulation 2004;110:16–21.
[6] Wolf YG, Hill BB, Rubin GD, Fogarty TJ, Zarins CK. Rate of change in abdominal aortic aneurysm diameter after endovascular repair. J Vasc Surg 2000;32:108–15.
[7] Czermak BV, Fraedrich G, Schocke MF, et al. Serial CT volume measurements after endovascular aortic aneurysm repair. J Endovasc Ther 2001;8:380–9.
[8] Parr A, Jayaratne C, Buttner P, Golledge J. Comparison of volume and diameter measurement in assessing small abdominal aortic aneurysm expansion examined using computed tomographic angiography. Eur J Radiol 2010.
[9] Wever JJ, Blankensteijn JD, Th MMWP, Eikelboom BC. Maximal aneurysm diameter follow-up is inadequate after endovascular abdominal aortic aneurysm repair. Eur J Vasc Endovasc Surg 2000;20:177–82.
[10] White RA, Donayre CE, Walot I, Woody J, Kim N, Kopchok GE. Computed tomography assessment of abdominal aortic aneurysm morphology after endograft exclusion. J Vasc Surg 2001;33:S1–10.
[11] Bley TA, Chase PJ, Reeder SB, et al. Endovascular abdominal aortic aneurysm repair: nonenhanced volumetric CT for follow-up. Radiology 2009;253:253–62.
[12] Prinssen M, Verhoeven EL, Verhagen HJ, Blankensteijn JD. Decision-making in follow-up after endovascular aneurysm repair based on diameter and volume measurements: a blinded comparison. Eur J Vasc Endovasc Surg 2003;26:184–7.
[13] Caldwell DP, Pulfer KA, Jaggi GR, Knuteson HL, Fine JP, Pozniak MA. Aortic aneurysm volume calculation: effect of operator experience. Abdom Imaging 2005;30:259–62.
[14] Golledge J, Powell JT. Medical management of abdominal aortic aneurysm. Eur J Vasc Endovasc Surg 2007;34:267–73.
[15] Golledge J, Wolanski P, Parr A, Buttner P. Measurement and determinants of infrarenal aortic thrombus volume. Eur Radiol 2008;18:1987–94.
[16] Kauffmann C, Tang A, Dugas A, Therasse E, Oliva V, Soulez G. Clinical validation of a software for quantitative follow-up of abdominal aortic aneurysm maximal diameter and growth by CT angiography. Eur J Radiol 2009.
[17] Kauffmann C, Tang A, Therasse E, Soulez G. An hybrid CPU-GPU framework for quantitative follow-up of abdominal aortic aneurysm volume by CT angiography. Proceedings of the SPIE 2010;7624:12.
[18] Viola P, Wells WM. Alignment by maximization of mutual information. In: Grimson E, Shafer S, Blake A, Sugihara K, editors. International Conference on Computer Vision. Los Alamitos, CA: IEEE Computer Society Press; 1995. p. 16–23.
[19] Collignon A, Maes F, Delaere D, Vandermeulen D, Suetens P, Marchal G. Automated multimodality image registration based on information theory. In: Bizais Y, Barillot C, Di Paola R, editors. Information Processing in Medical Imaging. Dordrecht: Kluwer Academic Publishers; 1995. p. 263–74.
[20] Bland JM, Altman DG. Statistical methods for assessing agreement between two methods of clinical measurement. Lancet 1986;1:307–10.
[21] Bley TA, Chase PJ, Reeder SB, et al. Endovascular abdominal aortic aneurysm repair: nonenhanced volumetric CT for follow-up. Radiology 2009.
[22] Dias NV, Riva L, Ivancev K, Resch T, Sonesson B, Malina M. Is there a benefit of frequent CT follow-up after EVAR? Eur J Vasc Endovasc Surg 2009;37:425–30.
[23] Kritpracha B, Beebe HG, Comerota AJ. Aortic diameter is an insensitive measurement of early aneurysm expansion after endografting. J Endovasc Ther 2004;11:184–90.
[24] Lee JT, Aziz IN, Haukoos JS, et al. Volume regression of abdominal aortic aneurysms and its relation to successful endoluminal exclusion. J Vasc Surg 2003;38:1254–63.
[25] van Keulen JW, van Prehn J, Prokop M, Moll FL, van Herwaarden JA. Potential value of aneurysm sac volume measurements in addition to diameter measurements after endovascular aneurysm repair. J Endovasc Ther 2009;16:506–13.
[26] Wolf YG, Tillich M, Lee WA, Fogarty TJ, Zarins CK, Rubin GD. Changes in aneurysm volume after endovascular repair of abdominal aortic aneurysm. J Vasc Surg 2002;36:305–9.
[27] Wever JJ, Blankensteijn JD, van Rijn JC, Broeders IA, Eikelboom BC, Mali WP. Inter- and intraobserver variability of CT measurements obtained after endovascular repair of abdominal aortic aneurysms. AJR Am J Roentgenol 2000;175:1279–82.
[28] van Prehn J, van der Wal MB, Vincken K, Bartels LW, Moll FL, van Herwaarden JA. Intra- and interobserver variability of aortic aneurysm volume measurement with fast CTA postprocessing software. J Endovasc Ther 2008;15:504–10.
[29] Parr A, Jayaratne C, Buttner P, Golledge J. Comparison of volume and diameter measurement in assessing small abdominal aortic aneurysm expansion examined using computed tomographic angiography. Eur J Radiol 2010, [Epub ahead of print].
[30] Bargellini I, Cioni R, Petruzzi P, et al. Endovascular repair of abdominal aortic aneurysms: analysis of aneurysm volumetric changes at mid-term follow-up. Cardiovasc Intervent Radiol 2005;28:426–33.